The Thesis Committee for Nurtac Erturk
Certifies that this is the approved version of the following thesis:

Comparison of Direct-S Modes Produced by Different Source Types

APPROVED BY
SUPERVISING COMMITTEE:

Supervisor:

Bob A. Hardage

Clark R. Wilson

Sean Gulick

Comparison of Direct-S Modes Produced by Different Source Types

by

Nurtac Erturk, B.Sc.

Thesis

Presented to the Faculty of the Graduate School of

The University of Texas at Austin

in Partial Fulfillment

of the Requirements

for the Degree of

Master of Science in Geological Sciences

The University of Texas at Austin

August, 2014

Dedication

There is no doubt in my mind that without support of my family I could not have completed this difficult process. I would like to dedicate this master thesis my wife, Gulsah Erturk, who followed me halfway around the world in the pursuit of our dream.

Acknowledgements

I would like to express the deepest appreciation to my supervisor Dr. Bob Hardage for giving so freely of his time, guidance and knowledge. Without his guidance and persistent help this master thesis would not have been possible.

I would like to my committee members, Professor Clark Wilson for providing valuable geophysical insights and Professor Sean Gulick for providing an opportunity to have a perfect field experience. In addition, a special thank you to Paul Murray and Engin Alkan, who helped me to efficiently work on MATLAB EGL-tool. Also I am very grateful to Turkish Petroleum Corporation for financial support during my graduate education. Also many thank you to the all of the faculty, staff and students of the Jackson School for their part creating such a wonderful atmosphere for education and discovery.

I would like to thank sponsors of the Exploration Geophysics Lab (EGL), Bureau of Economic Geology, the University of Texas at Austin, for providing the seismic data and guidance during this project.

Abstract

Comparison of Direct-S Modes Produced by Different Source Types

Nurtac Erturk, MSGeoSci

The University of Texas at Austin, 2014

Supervisor: Bob A. Hardage

Compressional and shear body waves generated by a seismic source can be analyzed using vertical seismic profiling (VSP) data-acquisition procedures. If a goal of exploration geophysics is to study the physics and exploration applications of shear waves, it is important to know how much S-wave energy a source puts into the earth. To maximize S-wave created by a source, considerable effort has been expended to create surface sources that apply horizontally directed impulses to the earth (horizontal vibrators and horizontal impacts). In my project, radial shear (SR) and transverse shear (ST) waves generated by different types of sources and recorded by multicomponent receivers in a VSP well are examined and compared. The research question is 'can a vertical-impact source create shear wave energy equivalent to the S-wave energy produced by standard horizontal-force shear-wave sources?'

To quantify the energy of shear-wave modes produced by different kinds of seismic sources, a VSP field test program was conducted at the Devine Test Site owned by The University of Texas at Austin. In the VSP data acquisition phase, the orientation

of horizontal geophones is unknown because a borehole geophone rotates as it is lowered into a well, causing the horizontal geophones at each receiver station to be oriented in different azimuths. To study body waves, it is essential that all geophones in a vertical VSP array be oriented in a consistent azimuth. I mathematically rotated multi-component VSP sensors systems to change them from the inconsistent orientation they had at the time of data recording to a user-defined consistent-azimuth coordinate system. This rotation allowed ST and SR wave modes to be identified. After geophone rotation, direct-S wavelet amplitudes were analyzed in 90-ms windows starting at the first-break times of each arriving mode.

Analysis of the rotated data showed that SR energy created by a vertical-impact source, a shot-hole explosive, and an inclined-impact source differ only slightly, and that there is essentially no difference in ST energy among these sources. Also, the signal frequency of SR and ST wave modes produced by horizontal-force shear wave sources are essentially the same as the frequency of SR and ST wave modes generated by a vertical-impact source. These test data show that vertical and horizontal vibrator sources produce shear wave modes having amplitudes 1000 times stronger than the other energy sources we tested. Considering the cost of using inclined-impact sources which is relatively expensive compared to using a vertical-impact source, and the difficulty of applying inclined-impacts in some land conditions, it is possible to obtain direct-S data of the same quality by using only a vertical-impact source or a shot-hole explosive. The arguments given above demonstrate that it is not necessary to use inclined-impact sources or horizontal vibrators to produce shear-wave data. S-wave data of the same quality produced by a horizontal-force source are provided by simple vertical-impact sources and shot-hole explosives.

Table of Contents

List of Tables

List of Figures

Chapter 1: Introduction and Background

1.1. VECTOR AND SCALAR SOURCES

Much seismic data, particularly marine data, have been acquired without taking into account the direction of particle displacement associated with a seismic wave. In order to interpret scalar-based data, it is not essential to know the direction of particle displacement. However, in multicomponent seismic technology, we must know the direction of particle displacement for each wave mode in order to process and interpret multicomponent data.

Interpretation of recorded signal consists mainly in the observation of travel times by taking into account the kinematical aspect of data. However, travel times do not give unique evidence of fracture orientation. In the 1980's the oil, gas, and coal mining industry became interested in extracting more information about the lithology of the subsurface in reservoir studies for hydrocarbons and in basin analysis. As a result of these studies, it was found that the polarization and splitting of shear waves provides important information about the structure of hydrocarbon reservoirs.

Generally, shear waves are more sensitive than compressional waves to the internal fabric of a formation, which is described by stiffness parameters and geometrical distributions of micro-cracks and pores. On the other hand, the velocities of shear waves are not, in general, as sensitive to pore-fill as are P-waves so the combination of P-waves and S-waves is a valuable tool for discriminating between true and false "hot spots" in reservoirs filled with gas. Also, in subsurface conditions in which the pore pressure of a geologic formation exceeds, or is less than, the effective formation pressure, compressional and shear waves behave with different sensitivities. For these reasons, the combined use of compressional and shear waves can be a tool for discriminating between

gas-bearing formations and overpressured zones. Thus, the use of shear waves together with compressional waves can be a great auxiliary tool for reservoir geophysicists and also for drilling engineers.

In the 1980's shear waves were a developed exploration tool but they were not used frequently. This limitation was because shear wave data were more expensive to acquire and some S-wave sources caused more surface damage than corresponding compressional wave sources. Fertig and Krajewski (1989) showed that it is possible to use P-wave sources as primary or secondary sources for generating shear waves when the acquisition was two-component recording. The use of vertical vibrators for the production of converted S-waves in the subsurface and their possible generation of S-waves in the immediate surroundings of a source station are explained in their study. The conversion of P-waves to S-waves requires no special field technique, and even an explosion not far below the earth surface can produce S-waves by mode conversion in the neighborhood of a source. However, these S-waves are SV-waves, whereas pure S-waves are generated by S-wave vibrators.

Conducting a multicomponent seismic survey for the purpose of creating all possible wave modes requires the use of sources that create displacement vectors oriented in three orthogonal directions. Such sources are called vector sources (Figure 1.1). Both the direction and magnitude of particle displacement must be measured for a vector seismic source. In contrast, only the magnitude of particle displacement is measured for a scalar source.

Full vector illumination of a geologic target requires that three vector wavefields be created. One wavefield has a displacement vector directed normal to its wavefront (indicated as wave mode c in Figure 1.1). The other two wavefields have orthogonal displacement vectors that are tangent to their wavefronts. Longitudinal waves (P-waves)

are generated by the displacement vector which is perpendicular to its wavefronts, and shear wave (S-waves) are produced by displacement vectors that are tangent to their wavefront (Hardage et al., 2011).

1.2. WAVE MODES

Seismic waves generated by vector sources propagate independently as a compressional mode, P, and as two shear modes, SV and SH, in a simple homogeneous earth. Particle motion related to conventional P-wave propagation is oriented in the direction of propagation in an isotropic medium. In contrast, particle motion for a shear wave is oriented normal to direction of propagation in the same medium. Particle motion of an S-wave is usually represented by segregating the particle motion into two perpendicular directions in the plane that is normal to the beam direction (Tatham and McCormack, 1991). These directions are labelled ‘a’ and ‘b’ in Figure 1.1.

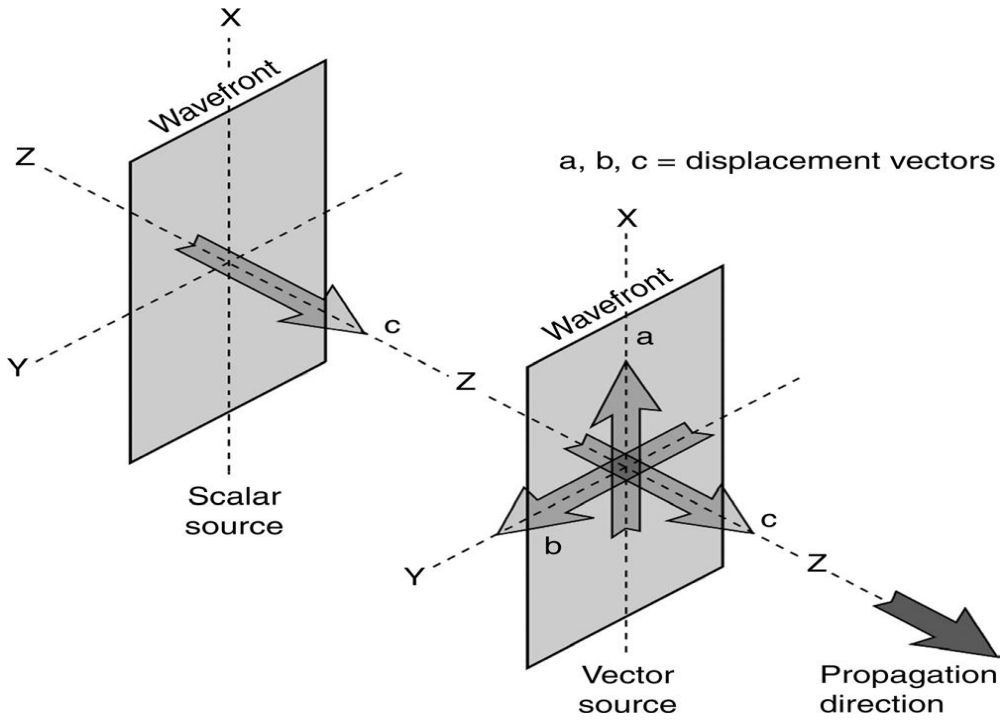

Figure 1.1: Differences between vector and scalar seismic sources (From Hardage et al., 2011).

Figure 1.2 shows how full-elastic multicomponent seismic wavefield components propagate in a homogenous isotropic earth. For P-wave propagation, the particle displacement vector is oriented in the same direction as the ray path. A source and a receiver identify a vertical plane that passes through both source and receiver positions. In Figure 1.2, this vertical plane passes through coordinate axis Z labeled on the figure. In a homogenous medium, a compressional particle displacement vector lies in this vertical plane.

For S-wave propagation, the polarization of a wave is dictated by the orientation of the source displacement vector. In Figure 1.2, an SH wave source creates a horizontal impulse in the X plane that is normal to the line direction between source and receiver. Similarly, an S displacement in the vertical Z plane creates SV shear data.

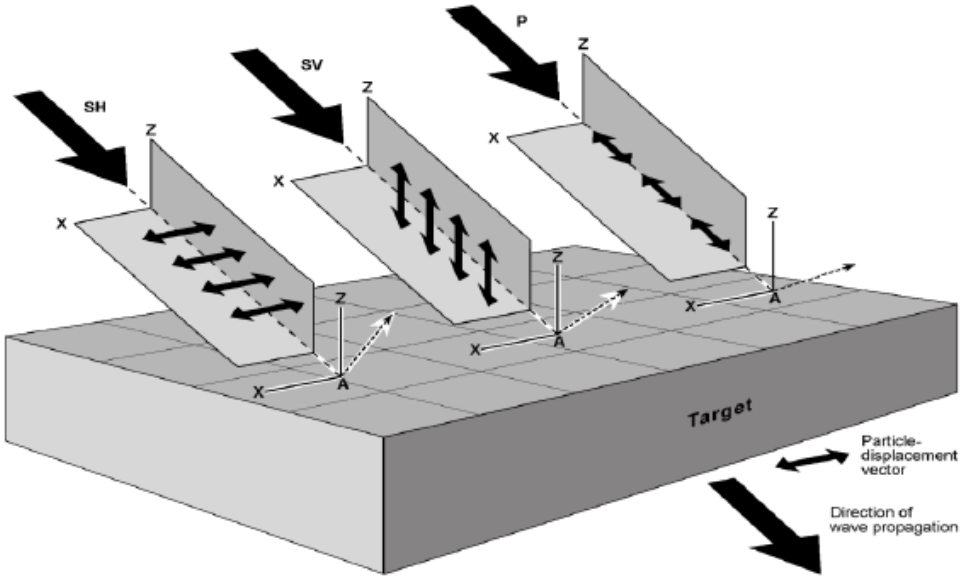

Figure 1.2: A full-elastic, multicomponent wavefield travelling in a homogeneous Earth consist of a compressional mode P and two shear modes, SV and SH. (Modified from Hardage et al., 2011).

Each mode of an elastic wavefield propagates with a different velocity while travelling though the subsurface and each mode causes deformation in a different direction as it propagates. Shear waves with vertical displacements (SV) and with horizontal displacement (SH) have propagation velocities that differ by only a few percent. However both shear velocities (V_s) are considerably less than P-wave velocity (V_p). The velocity ratio V_p / V_s may vary from a value of 50 or more for deep-water, unconsolidated, near-seafloor sediment to a value of almost 1.5 for dense, well-consolidated rocks.

Considering a vertical plane passing through a source station and an observation point is useful for understanding differences between SH and SV shear modes in a homogeneous media (Figure 1.3). While SV vector movement takes place in this vertical

plane, SH vector movement is perpendicular to the plane. Each source-receiver pair generates such a vertical plane, called a sagittal plane, which passes through the coordinates of the source station, the receiver station, and a reflection point.

Physical properties of rocks are the same, regardless of the direction of the measurement, for an isotropic medium. However, for anisotropic material, rock properties change with the direction in which they are measured. Different elastic constants come into play when the earth is distorted normal to its bedding planes versus being moved parallel to those planes, or when an earth medium is forced to displace normal to fractures versus parallel to fractures. For a long time, seismic data used in oil and gas exploration have been limited to P-wave modes that have been used as scalar data. Even when P-wave data are examined as vector data, the particle displacement vector is sensitive to elastic constants in only one direction which does not give a full sensation of earth fabric.

An advantage of using multicomponent technology is that each wave mode senses the elastic constants of the subsurface in three orthogonal directions (Figure 1.2). Therefore, unique earth information, like direction-dependent information about elastic constants, pore geometry, cementation, lateral alterations in rock and fluid types are detected by P, SH and SV wave modes as they travel from a source point to a receiver point.

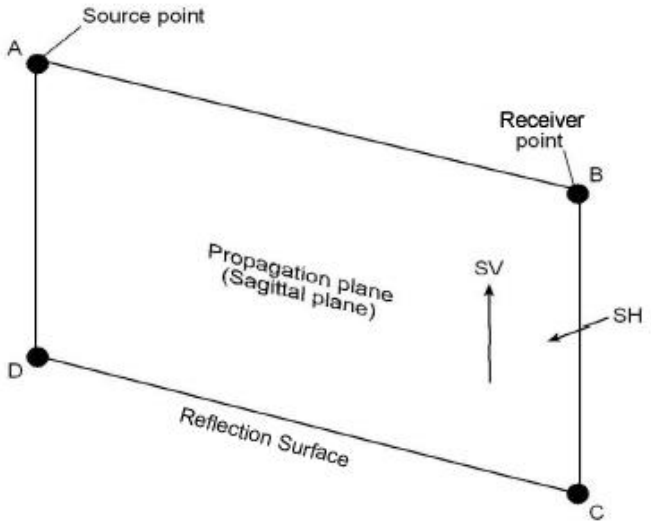

Figure 1.3: Difference between SH and SV shear wave displacements for a homogeneous media.(Modified from Hardage et al., 2011).

Some scientists prefer to use the terms radial shear (SR) and transverse shear (ST) or fast-S and slow-S when discussing shear wave propagation in stratified medium and restrict the terms SV and SH to S-wave propagation in homogeneous media, or to S-wave modes that travel only in symmetry axis planes.

1.3. WAVE MODE VELOCITIES

Behavior of S-wave modes was extended from a homogenous subsurface to stratified media by Levin (1979, 1980). Levin found that SH and SV modes travelling thorough a layered media exhibit velocity behavior as demonstrated on Figure 1.4. Figure 1.4 shows a wave velocity surface for a transversely isotropic solid composed of alternating layers of sandstone and shale. These results show that horizontal and vertical P-wave velocities differ. This phenomenon explains why interval velocities computed in a VSP study differ from interval velocities acquired using stacking velocities and Dix formula in which velocities are closely related to the horizontal velocity (Tatham and

McCormack, 1991). A key point seen from Figure 1.4 is at all take-off angles from the source except for true vertical and one angle where SH and SV wavefronts intersect, SV and SH modes propagate with different velocities. The SH mode has faster velocity at shallow take-off angles from a source point.

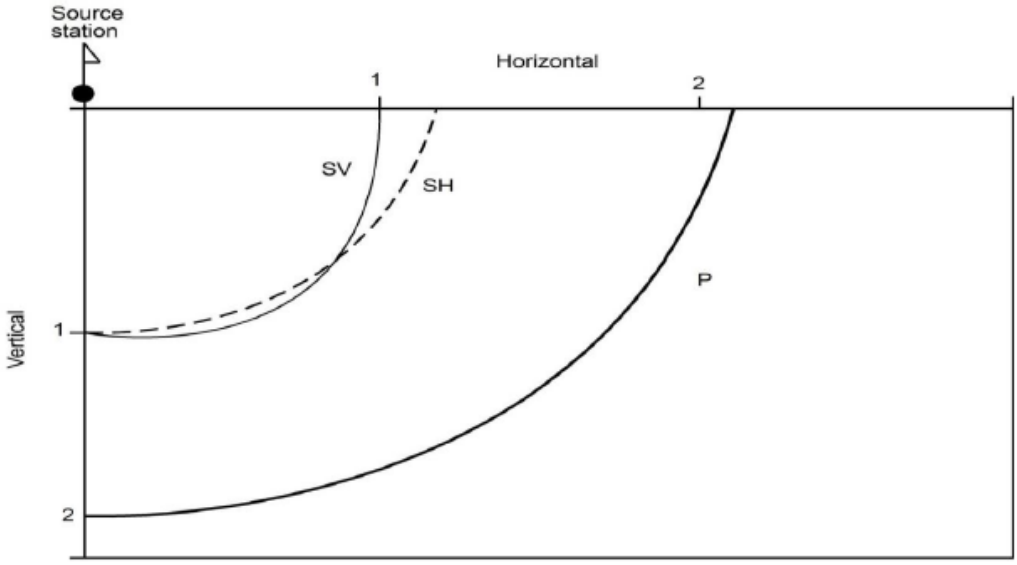

Figure 1.4: P-wave, SV-wave, and SH wave velocity behavior for elastic wave propagation in horizontally stratified media. (from Levin 1979, 1980).

1.4. STUDYING WAVE MODES WITH VSP TECHNIQUES

Azimuth orientations of X, Y horizontal geophones in a vertical receiver well vary at each station because sensors are deployed on a cable which rotates as it spools off a cable holder. Consequently, when sensors attain different deployment depths, horizontal geophones have rotated by varying amounts from station to station. These differences in geophone orientation produce phase shifts and amplitude variations in VSP data. These effects make it impossible to study P and S wave mode properties in raw, unprocessed VSP data. In order to describe downgoing and upgoing P and S modes, receivers must be oriented mathematically to uniform azimuths and to appropriate

inclinations. This orientation and rotation processing will be explained in detail in Chapter 3.

Transformation of borehole receivers from their in situ orientations to a data space where receivers are aligned to emphasize P, radial-shear (SR) and transverse shear (ST) events has been done for many years by the VSP industry (DiSiena, et. al., 1981; Hardage, 2000). On Figure 1.5, transformation of receivers from X, Y, Z coordinate space to P, SR, ST data space is illustrated graphically. In this approach, the first arrival of a P-wave is analyzed at each receiver station to identify azimuth rotation angles θ and inclination angles ϕ that, when applied to the 3C sensors, will cause every sensor to be aligned with the downgoing P-wave displacement vector oriented along ray path RS. This mathematical rotation causes a second sensor to be oriented with radial shear displacement vector SR, and a third sensor to be oriented with transverse displacement vector ST (Figure 1.5).

In order to quantify the energy of compressional-wave and shear-wave modes produced by different kinds of vertical-force seismic sources, a field test program was conducted at the Devine Test Site owned by The University of Texas at Austin. This test area is called the Devine Test Site because of its proximity to the community of Devine, Texas (Figure 1.6). The Devine Test Site was constructed by Standard Oil of Ohio (Sohio) in the 1980's and was used to develop crosswell seismic and electromagnetic profiling technologies. After Sohio was acquired by British Petroleum (BP), the test site was transferred to The University of Texas at Austin. An aerial photo showing the distribution of test wells 4, 2, and 9 on the test site is shown in Figure 1.7. The location of the well in which a receiver array was deployed is labeled by solid circle 4 on Figure 1.7. All wells are 3000 ft (914-m) deep.

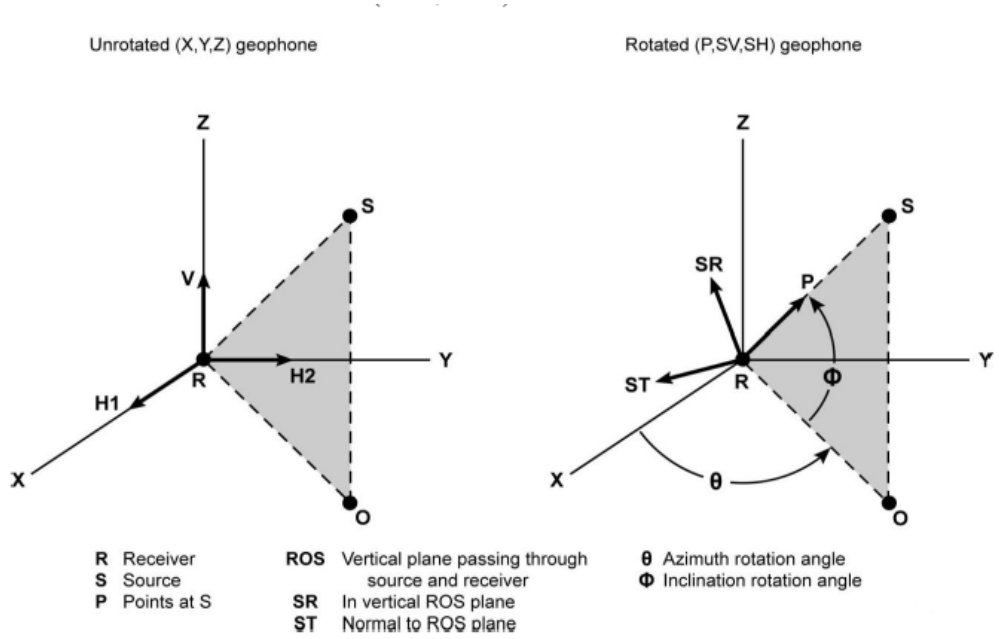

Figure 1.5: Reorientation of X, Y, Z receivers to P, SR, ST receivers (from Hardage et. al., 2011).

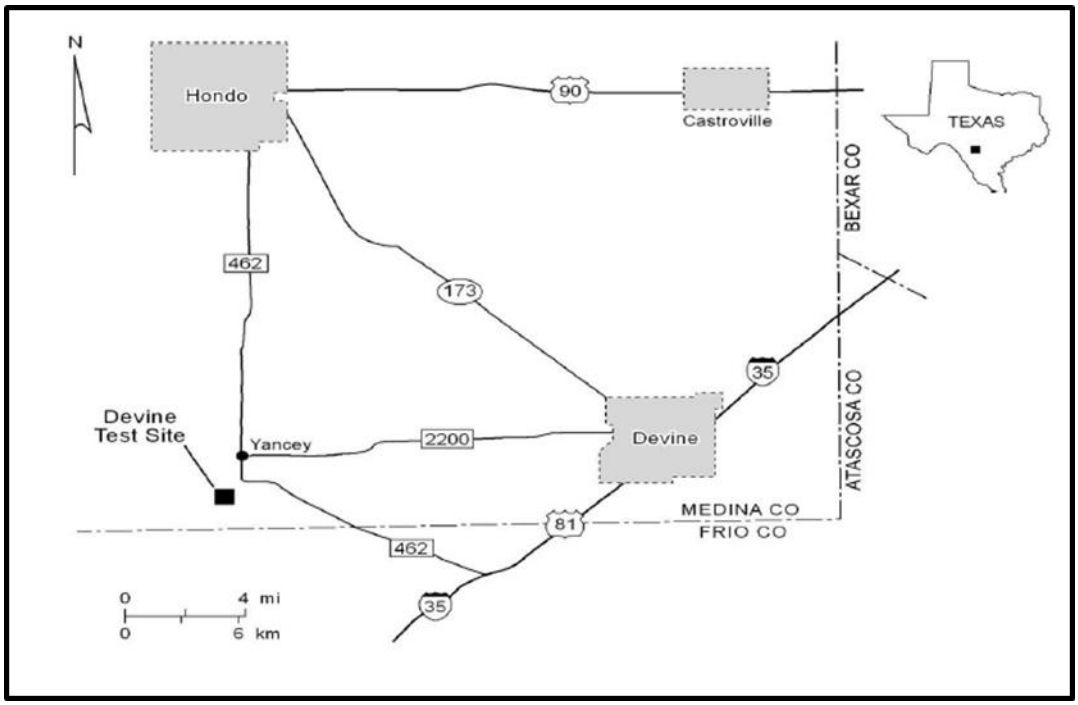

Figure 1.6: Location of Devine Test Site in Medina County, Texas.

The stratigraphy penetrated by the test wells is shown on well log curves displayed in Figure 1.8. These logs were acquired in well 4 and describe compressional velocity, shear velocity, and gamma ray measurements across in the first 3000 ft of the seismic propagation media underneath the survey area. These log readings start immediately below the base of surface casing at a depth of 532 ft, and continue to TD (true depth) at a depth of 3000 ft.

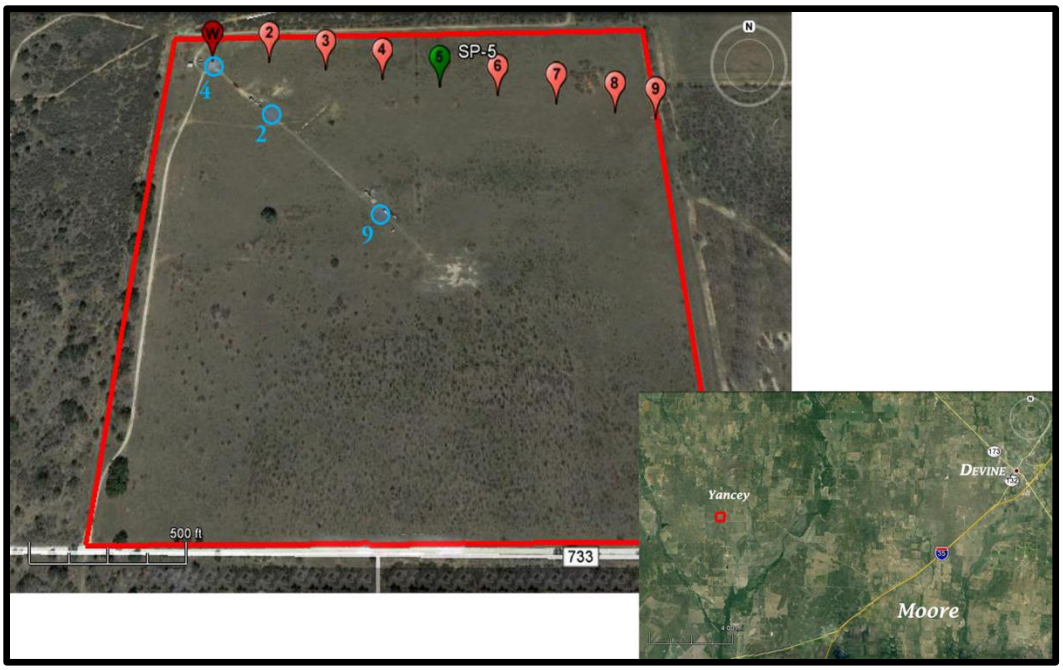

Figure 1.7: Aerial photo of test site. Receivers were deployed in test well 4.

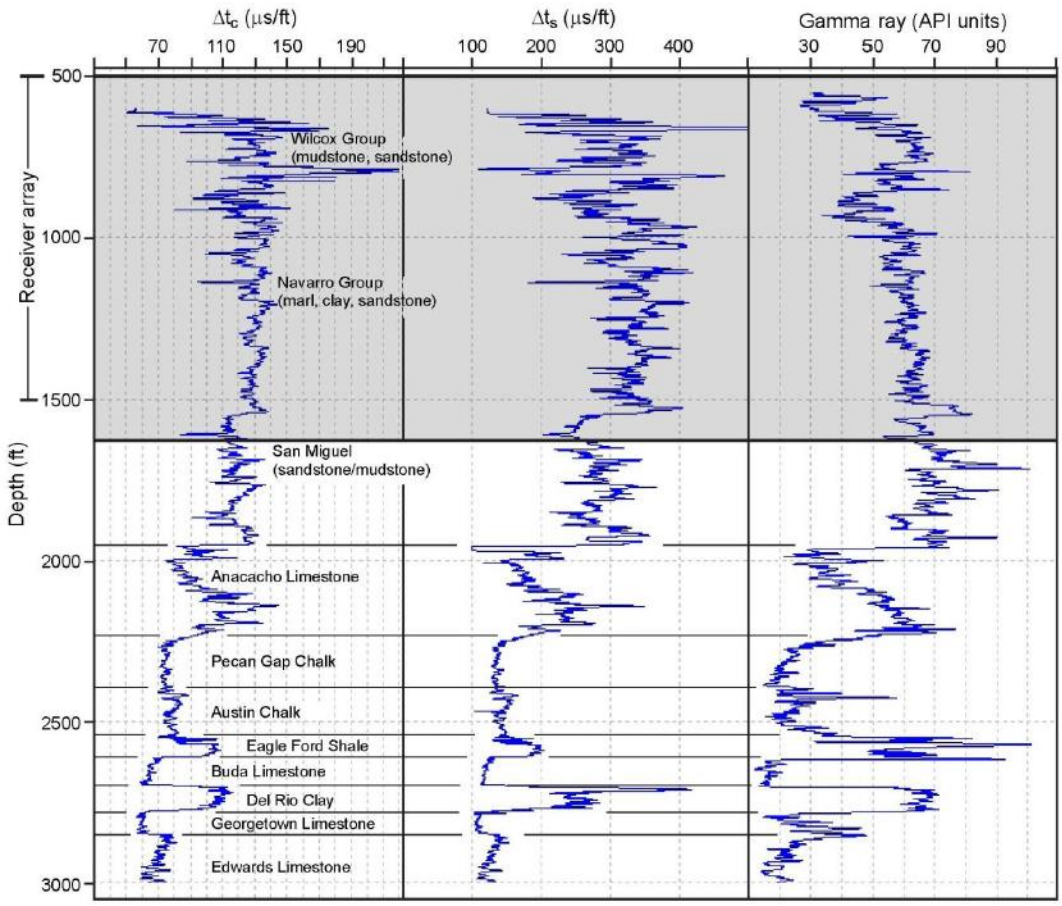

Figure 1.8: Compressional and shear wave velocity logs and gamma-ray log obtained in well 4 on the Devine Test Site.

1.5. SOURCE-RECEIVER TEST GEOMETRY

To record VSP data in well 4, a 24-station MaxiWave system supplied by Mitcham Industries was deployed. Receiver stations spanned a depth interval extending from 500 to 1632 ft. Log attributes inside the shaded area on Figure 1.8 describe the propagation medium surrounding the vertical receiver array.

The philosophy of this wave test was inspired by a study published by Robertson and Corrigan (1983). In this study, a single 3C geophone was deployed in the subsurface to analyze SH and SV radiation patterns produced by a horizontal vibrator. In our project,

this technique was expanded by deploying a vertical array of twenty-four 3C geophones, applying three kinds of sources (vertical-force, inclined force, and horizontal force), and analyzing both S-wave and P-wave radiation patterns generated by these sources.

Throughout this project the radial (inline) direction is defined as the azimuth of the straight line profile which continued through nine surface-based source points and the receiver well (Figures 1.7 and 1.9). The transverse (cross-line) direction was normal to the vertical plane of this profile. A horizontal vibrator was located at various azimuth orientations at inline source station 3 and 5 to generate data which described azimuth-dependent attributes of S-wave radiation patterns produced by a horizontal-vibrator source. Figure 1.10 displays the azimuth directions that each horizontal force was applied to the ground at these two offset stations (#3 and #5). As shown by this diagram, a horizontal vibrator source was positioned in 10^o azimuth increments by altering from a cross-line baseplate orientation (0^o azimuth of vehicle headlights on Figure 1.10) to an inline baseplate orientation (90^o azimuth of vehicle headlights).

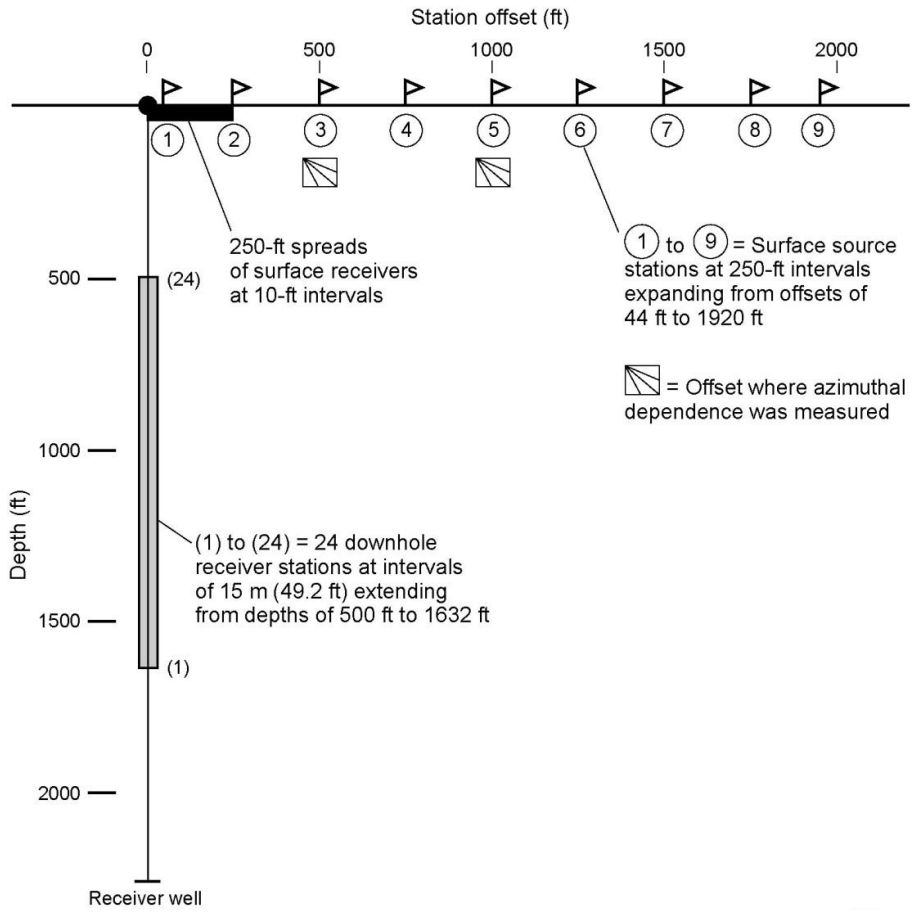

Figure 1.9: Source-receiver geometry. A 24-station vertical array of 3C geophones spaced at intervals of 15 m spanned the depth interval from 500 to 1632 ft in well 4. Source stations were offset from the well at intervals of 250 ft.

As a second type of source, inclined-impact sources were applied to the ground at each shot location. In this source test procedure, 20°, 30°, and 45° inclined source vectors were applied from opposite directions for an inline seismic line, which is parallel to the direction in which the data were acquired, and for a crossline seismic line, which is perpendicular to the acquisition direction. A diagram of this acquisition procedure is illustrated in Figure 1.11.

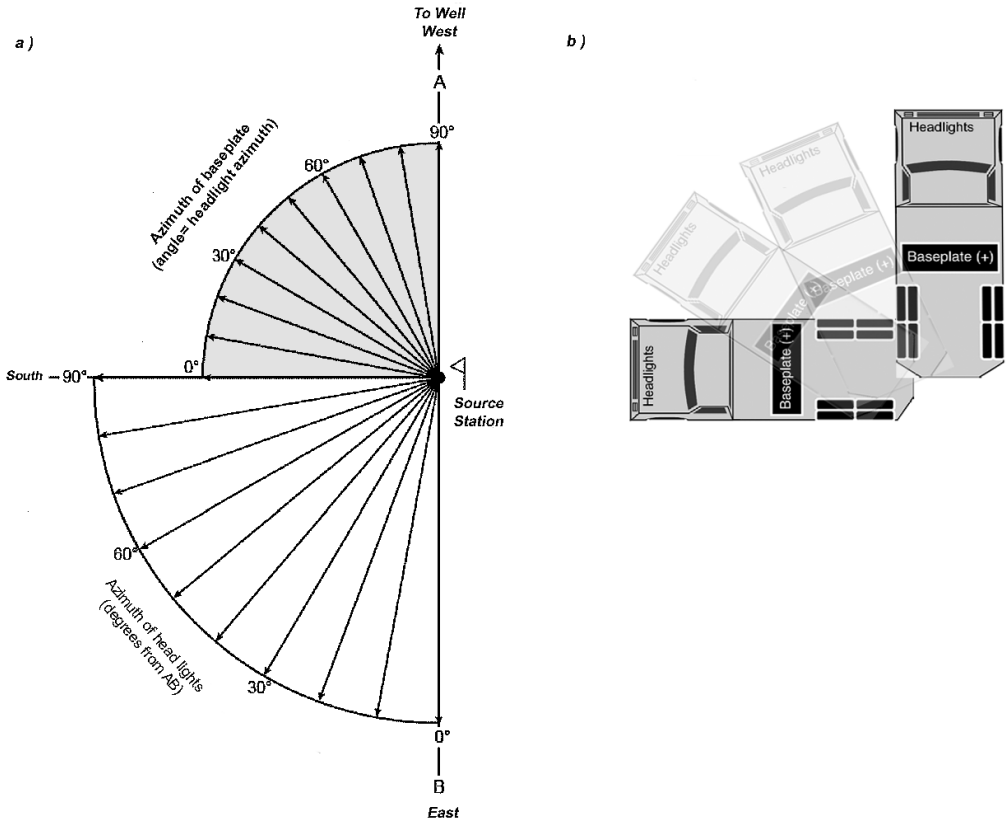

Figure 1.10: a) Map view of azimuth directions in which horizontal forces were applied at source stations 3 and 5. This figure describes the azimuth position assumed by a horizontal vibrator (bottom) and its base plate. b) Illustration of dipole source orientation.

In this project, the line which extends from the receiver well through nine shot locations is called an inline profile, and the line which is normal to the direction of data acquisition is described as a crossline profile. With these descriptions, I also assigned one of inline shot directions as 'positive', when the direction of an impulse was oriented towards the receiver well. The opposite direction was defined as 'negative'. Throughout the source test, thirteen types of seismic source orientations were recorded by the

multicomponent receiver array deployed in well-4. For both seismic lines (inline and crossline), positive 20°, 30°, 45° and negative 20°, 30°, and 45° inclined force vectors and a vertical-impact impulse were applied to the ground at each shot location.

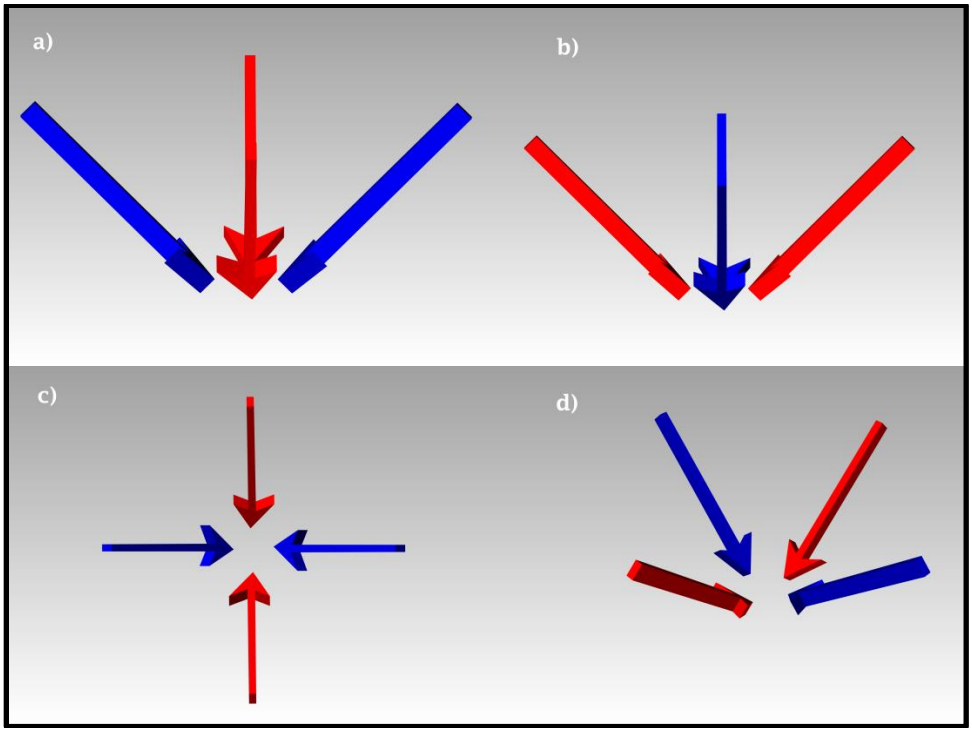

Figure 1.11: Devine test area inclined-impact procedure followed by acquisition crew during test. (a) Side view of shot directions for a single inclination degree. (b) Front view of shot directions for single inclination degree. (c) Top view of acquisition procedure. (d) A perspective view of acquisition procedure.

1.6. VERTICAL APERTURE OF TEST GEOMETRY

Recording downgoing compressional and shear wave modes that cover a wide aperture of vertical takeoff angles from surface-source stations was an important requirement of the test procedure. The maximum quantity of energy included in each wave mode that travels away from a source station can be captured for analysis if data are acquired over a large aperture. The shallowest takeoff angles involved data produced at

source station 9 (offset 1920 ft [585 m]) and recorded at downhole receiver station 24 (depth of 500 ft [152 m]). The steepest takeoff angles involve source station 2 (offset 250 ft [76 m]) and downhole receiver station 1 (depth of 1632 ft [497 m]).

By supposing that raypaths from source to downhole receiver are straight lines, a basic approximation of aperture range generated by the geometry of the source-receiver pairs is shown on Figure 1.12.

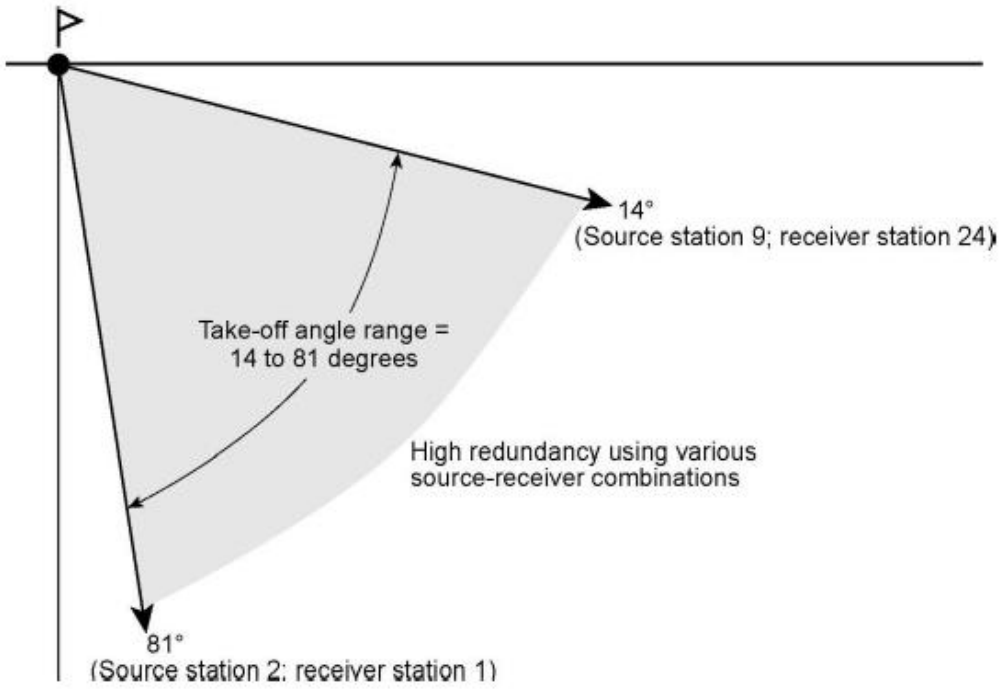

Figure 1.12: Take-off angle aperture when straight raypaths are assumed between surface sources and downhole receivers.

1.7. VERTICAL FORCE SOURCES AND DIRECT S-MODES

Vertical impacts on the earth surface or an explosion at some depth in a borehole are the most common sources of seismic energy onshore. It is commonly believed that a vertical-force source generates mainly compressional waves. However, former studies

show that a vertical-force source produce shear waves by conversion at depth and also in the immediate surrounding area of the source.

A large amount of SV shear energy can be generated by using a vertical-force source. The radiation pattern for a single force vector normal to the earth surface can be described best in spherical coordinates (r, θ, ϕ). An example of such a force vector and its coordinate system is shown on Figure 1.13. In this diagram, the radial component is assigned by subscript r, the azimuthal dependence by ϕ, and the tangential component is portrayed by θ. U_r will be described as a radial displacement which is only compressional. The tangential displacement, travelling at shear wave speed, will be portrayed as U_θ.

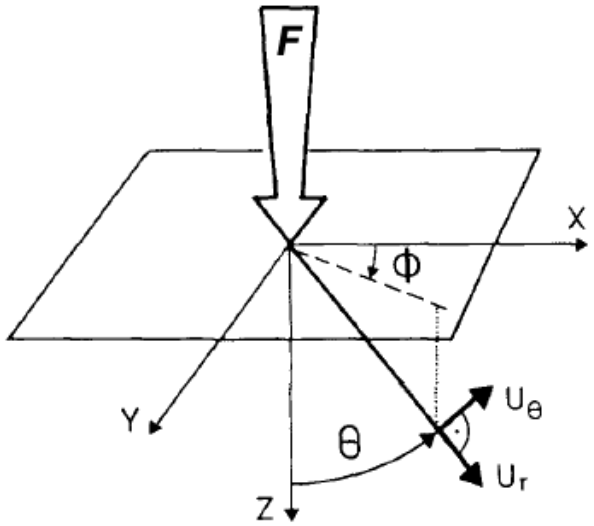

Figure 1.13: Vertical single force and coordinate system (From Fertig and Krajewski, 1989).

The radiation patterns and comparative strengths of P and SV energy which travel away from the spot where this vertical-force source is stationed is shown on Figure 1.15 for a homogeneous earth. These P and SV radiation patterns are duplicates of analyses published by Miller and Pursey (1954) and White (1983). The vertical-force source causes both P and SV wave modes to be generated at the spot where the source vector contacts the earth surface. The radial distance from the origin to the outer border of the P and SV radiation patterns defines comparative strengths of P and SV modes that propagate at any take-off angle from the source station.

Various researchers who are interested in direct-S illumination of geologic targets by using vertical sources have used this model as a starting point. Wright and Carpenter (1962) demonstrated the radiation of direct-S modes by using shot-hole explosives in order to simulate tests of buried nuclear devices. They used plaster casts of shot-hole cavities to arrive at the conclusion that explosive detonations cause asymmetric displacement. They state a small component of zero mode shear wave (when rotation is independent of azimuth) in the immediate surroundings of a source station can become large at great distance. Edelman (1981) investigated S displacement vectors by tracking raypaths inclined at arbitrary takeoff angles. By using a method which places two vibrators side by side and has them operate with opposite polarities, he showed that a strong horizontal component (ST) can be generated in addition to a radial component (SR). Fertig (1984) explained that an explosive point-source at some depth below a free surface generates direct-S modes by the conversion of P to SV at the interface between Earth and air above a shot. He also stated these waves can be identified as a “spin-off ” using standard recording equipment and a second receiver cable with inline horizontal geophones without the need of extra sources. By using the radiation diagram on Figure 1.14, Fertig and Krajewski (1989) clarified that a shot hole explosive and an air gun in a

mud-pit are also capable of generating direct-S modes, as a vertical vibrator does. Lynn and McCardle (1990) declared an air gun array in a rectangular water-pit is a VSP source that produces significant S-wave energy as well as P-wave energy. More recently, Zhou et al. (2005) demonstrated that SH and qSV modes can be recorded by using a vertical vibroseis source in a medium of vertical transverse isotropy (VTI). In 2007, Yang et al. (2007) justified the idea that explosive and controlled seismic sources (i.e. vibrators) are not only pure P-wave sources but also generate pure S-wave by presenting excellent data examples of direct-S modes produced by both vertical vibrators and shot-hole explosives.

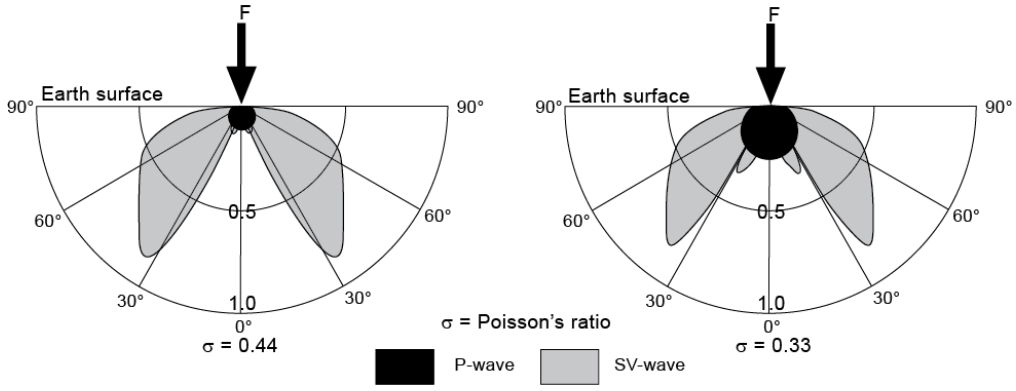

Figure 1.14: P and SV radiation patterns produced when a vertical force is applied to the surface of a homogeneous earth. Calculations are displayed for two values of the Poisson's ratio of the earth layer (From Hardage et al., 2011).

Chapter 2: Sources

Because source characteristics often limit resolution and signal-to-noise quality, a careful selection of energy source is one of the critical steps in seismic data acquisition. Penetration to the required depth, bandwidth for required resolution, signal-to-noise ratio, environment, availability, and cost are the main criteria to be considered when selecting a seismic source.

A single explosive charge was the most often used seismic source in exploration geophysics for several decades. If the goal is to study the physics and exploration application of only P-waves, a single charge, which is mostly considered impulsive point source like dynamite, is sufficient. However, as years of experimentation have shown, shear waves play a key role in hydrocarbon explorations because they contain much more information than compressional waves do. Understanding the importance of shear waves has caused multicomponent seismic technology to be developed and has led to the necessity of creating new seismic sources that produce shear waves.

Processing and interpreting multicomponent seismic data can be challenging tasks if vector motions associated with P and S seismic displacements are not taken into account. For instance, calculating the azimuth orientation of a source is not essential when acquiring land data with a vertical-displacement source (Hardage et al., 2011). However, when shear wave data are generated by a horizontal-force source, the azimuth orientation of the source baseplate and the direction of the first motion of the baseplate must be known at each shot location to avoid reversals of data polarity between source stations.

Understanding the vector displacement related to each elastic wave mode is essential when implementing a field procedure to acquire multicomponent seismic data. It

will be possible to retrieve valid rock and fluid information from the data only if source and receivers have correct and consistent vector properties.

2.1. SOURCE CATEGORIZATION

Sources that create the P and S wavefield can be classified as monopoles, dipoles, or quadrupoles (Hardage et al., 2011). Energy generated by a monopole source propagates equally in all azimuth directions. Although a monopole source is considered as only a P-wave source, an SV shear wave mode is also generated and radiates uniformly in all azimuth directions. Also, P-SV converted wave modes produced in the subsurface at P-to-SV conversion points when a vertical-displacement source is used radiates equally in all azimuths. These S-wave propagations imply that an equal radiation in all azimuth direction is a fundamental characteristic of a monopole seismic source.

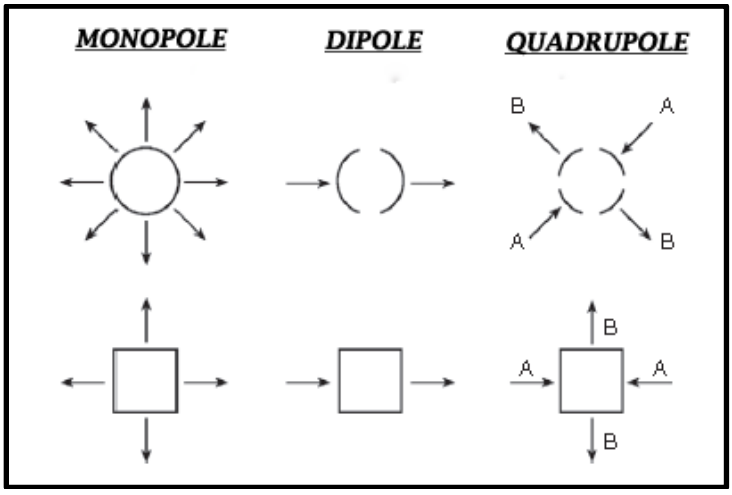

Figure 2.1: Plan views of earth-displacement vectors generated by monopole, dipole, and quadruple sources (from Hardage et al., 2011). Directions of vector displacements are indicated by arrows.

A standard shear wave source, which produces an earth-displacement oriented in a specific direction, is classified as a dipole source. When a dipole seismic source is

applied to the earth, the oriented displacement vector produced at the shot location is parallel to the earth surface. The energy radiated from a dipole seismic source is not the same in all azimuth directions and does not illuminate targets uniformly as does a vertical-force source.

As can be seen from Figure 2.1, two perpendicular pairs of force vectors oriented in specific direction are generated by a quadrupole seismic source. Each vector-force pair, labelled A and B in Figure 2.1, produces shear waves that have opposite polarity. Because this kind of source is not common in exploration geophysics, only monopole (vertical-impact, shot-hole explosive and vertical vibrator) and dipole seismic sources (inclined-impact, and horizontal vibrators) were used and compared as part of Devine Test Study to analyze shear wave modes produced by each source.

2.1.1. Shot-hole Explosives

Dynamite was the only available source until the weight-dropping technique was introduced in 1950's. Because dynamite produces more energy and a broader bandwidth than other sources, it became the traditional seismic source that was used in hydrocarbon exploration for many years. Also, because buried impulsive sources often provide an excellent signal-to-noise ratio and reflection resolution for P-wave surveys, they were consistently used as seismic sources in vertical seismic profiling studies.

Although explosives in shot holes have several advantages over other seismic sources, including easy portability to remote areas, broader bandwidth, high energy production, and ease of weathering correction, some serious drawbacks caused alternative sources to be developed. First, output energy and source signature can vary from one explosive shot location to the next station, which requires amplitude and phase corrections during processing. Also, because handling safety can be problem in some

field condition, the fate of exploration is often subject to permissions given by governments. Also, explosive land sources cost more than other sources because of the need for drilled shot holes, which is difficult and expensive in many areas. In addition to economic considerations, it is difficult to shoot several dynamite shots and maintain consistent shot wavelets in vertical seismic profiling projects.

In spite of these disadvantages, if careful attention is given to data acquisition and processing, reasonably consistent shot wavelets with high energy and broad frequency bandwidths can be obtained. In the Devine Test Study, 2-lbs (1 kg) of dynamite were placed at a depth of 20 ft (6 m) as a shot-hole explosive source.

2.1.2. Impulsive Sources

Vertical impulse forces applied to the surface of the ground are often favored over buried explosives and are viable energy sources for onshore seismic exploration because of their advantage related to absence of legal restrictions, environmental acceptability, and higher production rates. Gravity-driven weight droppers, land airguns, and other devices that use explosive gases to push a heavy baseplate vertically downward with a great force have been used as vertical-impact sources for decades. The repeatability of source signature and ease of forming source arrays are the main motivations for using impulsive sources.

However, there are some drawbacks to be considered. In surface seismic applications, multiple recordings from the same shot location are necessary to acquire seismic data with a good signal-to-noise ratio. In addition, implementing impulsive sources can require special data processing methods and large source and receiver arrays because these source types are quite band-limited compared to explosives and generate high amplitude surface waves that must be removed from data. Also, before an extensive

onshore seismic survey is started, a field test should be done to determine whether the selected impulsive source creates adequate energy with a good signal-to-noise ratio and provides an appropriate signal bandwidth at desired offset distances. The field test results should also assure that selected impulsive sources will not create severe shallow reverberations in shallow strata.

Impulsive sources have been illustrated and discussed by various scientists (Dobrin 1976; Cholet and Pauc, 1981; Telford et al. 1990; Tatham and McCormack, 1991). A vertical-impact source manufactured by United Service Alliance weighing 33,000-lb with a 1000-psi nitrogen-spring weight-acceleration system was used in Devine Test Study.

2.1.3. Inclined Impact Sources

Both compressional and shear wave body waves are produced by all onshore energy sources used in vertical seismic profilling research. If the main goal is to study the physics and exploration applications of shear waves, increasing the amount of shear wave energy is desired. To achieve this objective, surface sources that create horizontally directed impulses to the earth or vibrators that produce horizontal oscillations of the ground need be applied (Hardage, 2000). To deliver an inclined impact force to the earth, a baseplate that has cleats projecting from the bottom of the plate is used. Figure 2.2 shows how an accelerated mass impacts the baseplate at a slant angle to create vertical and horizontal earth displacements. The source of mass acceleration can be either gravity or a mixture of gravity and compressed gas depending on a manufacturer's concept.

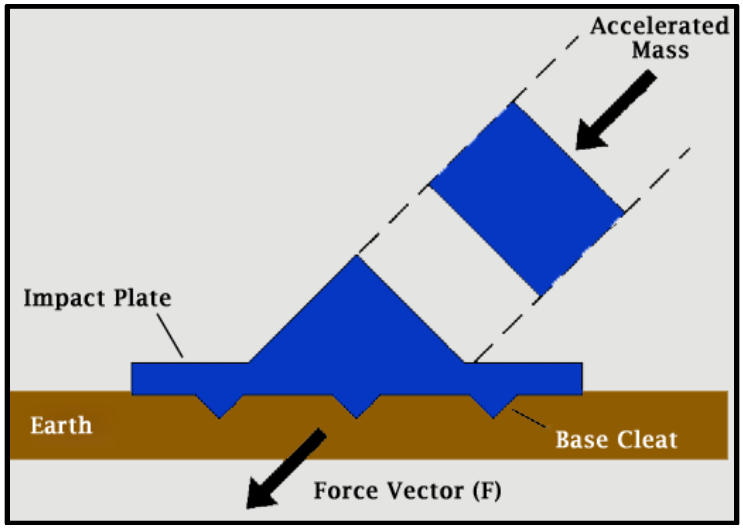

Figure 2.2: Baseplate principle associated with inclined-impact sources (modified from Hardage et al., 2011). The accelerated mass causes a hybrid force vector composed of a horizontal component and a vertical component.

Inclined-impact sources have been used to create shear wave modes for years. A tilted-impact source, called Omni Pulse, was powered by an air gun firing in a water-

filled chamber. This source was manufactured by Bolt Technology in the 1970s and 1980s and it was a distinctive adaptation of marine air gun technology to onshore source technology that produced P-wave and S-wave modes. Also in the 1980s, the ARIS (Atlantic Richfield Inclined Source) inclined-impact source, which dropped a heavy weight onto a baseplate by using a rail system, was introduced by Arco Research. An ARIS inclined impulse source applied a tilted vector force that allowed scientists to acquire a mixture of P, SR, and ST modes. In spite of its advantage of producing P, SR and ST wave modes, the ARIS source was not used widely to acquire surface seismic data because of its excessive dimensions, extreme weight, and the difficulty of moving. However, ARIS was a perfect static source to collect multicomponent VSP data at a fixed offset from a receiver well (Hardage et al., 2011).

These two unique sources are no longer used. One replacement source is VSX™ developed by Vecta Technology and manufactured by United Services Alliance in Texas (Figure 2.3). Because high-pressure nitrogen gas is used to accelerate a heavy weight, the impact generated by the source is quite strong. The heavy weight can impact a baseplate at angles varying from vertical to 45° and from any azimuth direction. This source appeals to many geophysicists because of its ability to generate useful P, SR, and ST waves at a single source position and its high-frequency source signature that can be reproduced from one shot location to another.

Figure 2.3: VSX accelerated-weight impact source provided by Vecta Technology and United Services Alliance. A vertical impact or an inclined force vector can be delivered to the Earth by this source. Note the reaction mass can be tilted to either side at an angle up to 45 degrees to produce shear waves of opposite polarities.

Vertical and horizontal displacement vectors associated with an inclined-impact source are illustrated in Figure 2.4. During data acquisition, the baseplate can be impacted by weight-driven force vectors, indicated as F (+) and F (-), inclined at any user-defined angle Θ (between 0° and 45°) from two opposing directions. If F (+) and F (-) are identical in magnitude and inclination from opposite directions, two force vectors can be added

$$F_V = F(+) + F(-) \qquad (1)$$

to create F_V, a vertical force vector which is sum of the two vertical components. Similarly, the subtraction of F (+) and F (-) creates horizontal force vector, F_H, which results from adding the two opposite-polarity horizontal components.

$$F_H = F(+) - F(-) \qquad (2)$$

While vector F_V creates radiation patterns for P and SV, vector F_H does radiation patterns for SV and SH. In data-processing, equation (1) and equation (2) are implemented by simple arithmetic addition and subtraction of data generated by inclined forces F (+) and F (-).

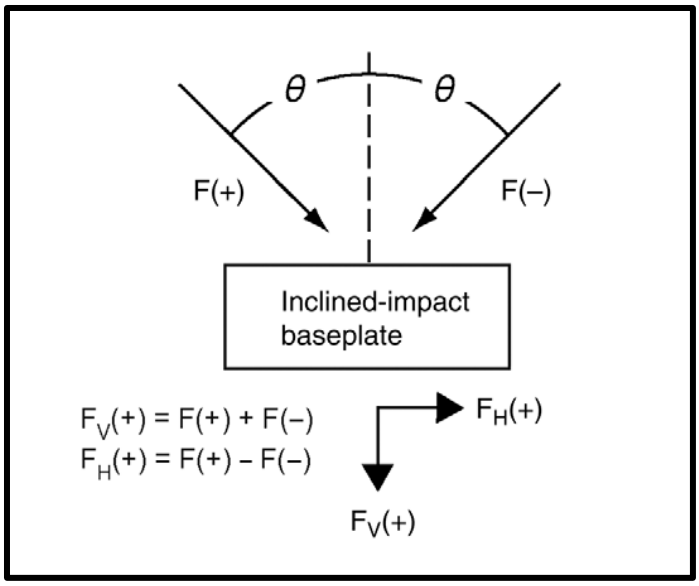

Figure 2.4: Baseplate mechanism for an inclined-impact source (From Hardage et al., 2011). Inclined sources, F (+) and F (-), impact from opposing directions. F_V (+) and F_H (+) are the directions of positive polarity P-wave displacement and S-wave displacement.

2.1.4. Vibrators

A seismic vibrator radiates energy signals into the Earth over an extended period of time and with a known frequency content. Vibrators can be divided into two groups in terms of direction of motion: vertical vibrators and horizontal vibrators.

2.1.4.1. Vertical Vibrator

After a long period of experimentation, the original vibrator source was developed by Continental Oil Company (Conoco Inc.) in 1966 and named Vibroseis™. Vibrators are a source type widely used in hydrocarbon exploration.

Vertical vibrators deliver an oscillating signal rather than an impulse signal to the earth. This signal can persist for many seconds with the input frequency changing slowly over the duration of a signal sweep.

The vibrator concept relies on the principle that if a source puts a signal containing a set of known frequencies into the earth, the received signal will be a data trace in which each earth reflection coefficient replicates that long signal. As a result, the raw traces recorded in the field are completely meaningless to the eye and a special processing method, known as the correlation process, is required to recover the reflection series. In Figure 2.5, an example of reflected signal from three different interfaces (A, B, C) is shown. The recorded trace looks incoherent and does not indicate any event arrival times before correlation because the reflection record consists of long superimposed signals from each reflection surface.

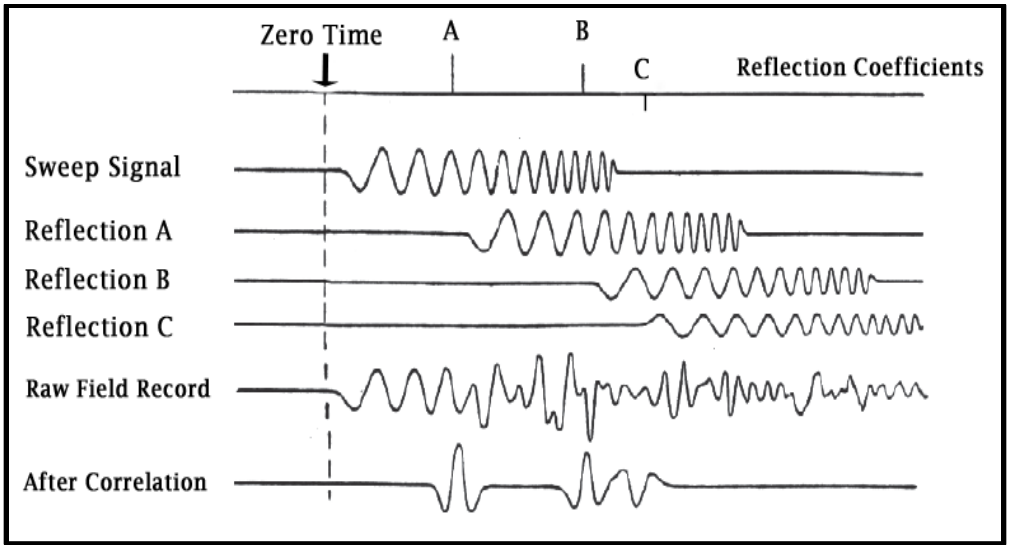

Figure 2.5: Sweep correlation of signal generated by a vibroseis source (modified from Evans, 1997).

Vibrators have become attractive seismic sources, especially in VSP studies, because of several distinctive advantages. First, it is possible to obtain an increased signal-to-noise ratio of data by using a source array consisting of several vibroseis trucks. Also, their ability to move easily allows VSP data to be generated at different shot points in an efficient manner. In areas where a high noise level is present, vibrators are ideal energy sources for VSP studies because an interpretable seismic trace can be obtained with the aid of the correlation process, and ambient noise can be cancelled by summing several sweeps within the sweep range (Hardage, 2000). Although vibrators are more expensive than surface impulsive source, their ability to control a source waveform makes them attractive as energy source for onshore VSP explorations. In the Devine Test Study, an I/O AHV IV PLS 362 with ability to deliver up to 60.000 pounds of peak force was used (Figure 2.6).

Figure 2.6: 60,000-lb vertical vibrator manufactured by Inova Geophysical Inc. In this study, this source generated a linear 8-second sweep from 8 to 96 Hz.

2.1.4.2. Horizontal Vibrators

To generate SR and ST wave modes, a horizontal force vector has to be applied to the earth by a dipole seismic source (Figure 2.1). Creating horizontal earth displacement is possible if only a source applies horizontally directed impulse to earth or oscillates horizontally. This basic condition is met by using horizontal vibrators that have a baseplate mechanism with metal cleats. A heavy pad in which its projections on bottom side extend into the ground was formerly used to transfer horizontal impact to the Earth (Figure 2.7). As it can be seen from figure, a large amount of SH energy can be generated as well as compressional wave modes with the horizontal movement of the mass that force the projections to shear the Earth.

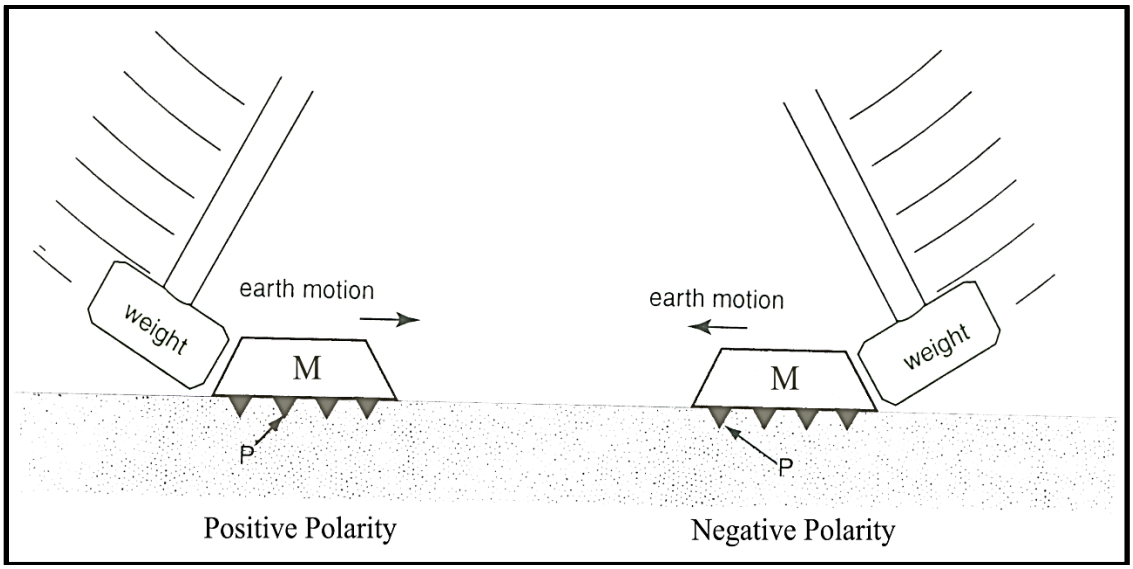

Figure 2.7: Concept of surface shear wave generator used in vertical seismic profiling (Hardage, 2000). A heavy mass, M, is coupled to the Earth with the use of projections, P, on bottom side. While projections are pressed into the ground, an impulsive source is applied. Today's technologic shear wave vibrators work based on the same principle.

Horizontal vibrators use the same principle as inclined-impact sources do (Figure 2.2). Metal cleats projecting from the bottom of baseplate are pressed into the ground by the weight of the vehicle to create a lateral coupling with the earth. The hydraulic drive-system then moves the baseplate laterally and creates a horizontal force vector as indicated in Figure 2.8.

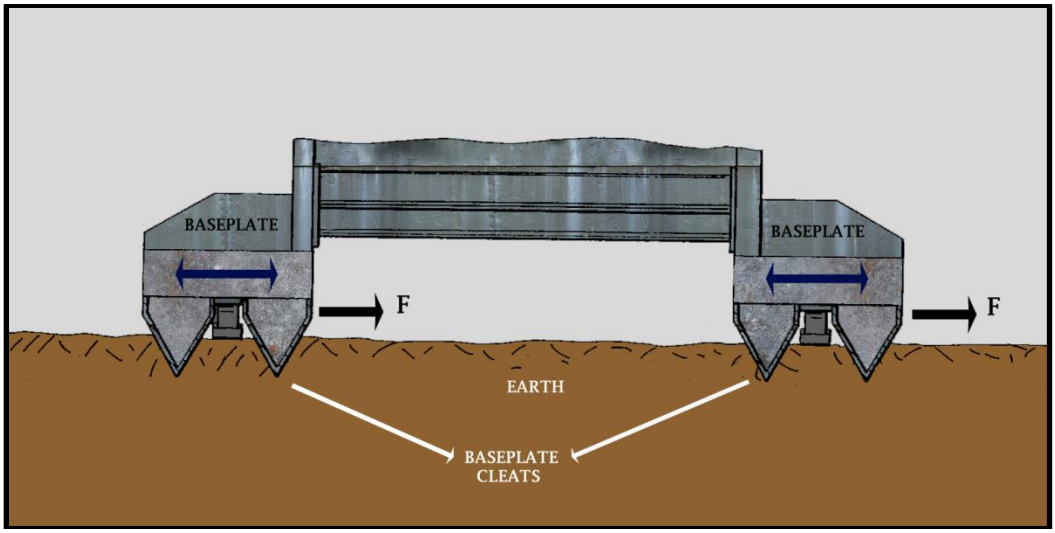

Figure 2.8: Baseplate concept associated with a horizontal vibrator. Metal cleats are pressed into the ground by the weight of track, and a horizontal force is applied to the baseplate to create horizontal force vector F.

Because earth displacement vectors oriented in a specific azimuth are created by a dipole seismic source, a consistent azimuth orientation of the source at each shot location is an important factor to be considered to avoid data-phase inconsistency between shot locations. In seismic exploration in which a dipole source is used to create a force vector, the first motion of a baseplate defines data phase. To maintain data consistency, the orientations of horizontal dipole sources must be identical at each source station throughout seismic data acquisition.

Chapter 3: Methods

This chapter discusses the methods that were applied to my data set acquired with inclined impacts and vertical impacts and will explain the mathematical procedure of geophone rotation used to segregate wave modes. One of the objectives of my thesis project was to apply a geophone rotation process at each VSP receiver station to segregate downgoing P, SR, and ST wave modes. After wave mode segregation, I present the opposite data polarity which appears in shear wave components impacting from opposite-azimuth directions at each receiver station. The main idea of processing inclined-impact data was that if shear wave components obtained from impacts that are oriented opposite to each other by 180 degrees of azimuth, are summed, then energy on shear components will cancel each other. Conversely, strong shear wave components will be obtained by subtracting data generated by two opposite inclined sources and energy on P-wave components will reduce to zero.

3.1. Wave Field Separation With Geophone Rotation

In vertical seismic profiling with a zero-offset vertical impact source, only upgoing and downgoing compressional waves are studied on Z vertical-geophone data. Because the P-wave arrives at reflectors at a normal incidence, converted waves are not generated. Thus energy recorded by a vertical Z geophone delivers full information about a P-wave field. In this case seismic data are scalar and upgoing and downgoing P-waves can be defined by their apparent velocity (Daures and Tariel, 1985). However, when a source is offset from a receiver well, the wave field becomes complicated because of the presence of converted P-SV waves which differ from P-waves in apparent velocity and direction of polarization. Because different modes of waves characterized by different polarizations appear in a seismic trace, seismic data are no longer scalar. Also, in the case

of an inclined-impact source, a complicated wavefield is an issue to be solved. For such a source, multi-component recording is required to reach a complete understanding of VSP wavefields.

Multicomponent seismic technology has come into broad use for a variety of seismic applications. However, the exploration industry experiences a challenging task to understand how receiver component orientation and their associated acquisition and processing coordinate systems are related to vector wavefields (Gaiser, 1999). The position of shots, receivers and reflection points are defined in an XYZ-type coordinate system in conventional multicomponent seismic data acquisition. When dealing with a single wavefield such as a P-wave, this conventional coordinate system would be sufficient. However, when multicomponent seismic data are needed and multicomponent sources or receivers are used, an additional user-defined coordinate system is required to specify the vector components of particle motion.

3.2. ACQUISITION COORDINATES

A rectangular polarization coordinate system is used for 2-D or 3-D seismic exploration in which multicomponent data are acquired. This means that each receiver station records three-component seismic traces which can be described as $S_X(t)$, $S_Y(t)$, and $S_Z(t)$. These components typically are named as vertical, in-line, and cross-line components, where the inline component is parallel to the direction in which receivers are deployed and cross-line is normal to the inline component direction. A right-handed coordinate system is used to describe data acquisition space as shown in Figure 3.1.

In land-based seismic exploration, the orientation of geophone components can be done carefully. For instance, to align all receivers in the same azimuth direction, some three component receivers have levelling bubbles and can be oriented horizontally by

using compasses. However, in the case of vertical seismic profiling with the receiver array in a vertical well or in marine seismic acquisition, it is not possible to control geophone orientation at each receiver station.

In vertical seismic profiling in which multicomponent data are acquired, particle displacement is measured on three orthogonal components at each receiver station in the receiver well. The Z component usually is aligned with the vertical axis, but the orientation of horizontal components is unknown because a borehole geophone may rotate around its axis on the supporting wireline cable which causes the horizontal components at each receiver station to be oriented in a different way (Hardage et al., 2011). Figure 3.2 illustrates P-wave ray paths from a source offset from a receiver well and variable geophone orientations at two receiver stations. Such inconsistent geophone orientation results in undesirable amplitude changes and phase shifts in data. To resolve this inconsistency, multi-component sensor systems must be rotated from their positions at the time of recording to a user-defined coordinate system before starting to process the data.

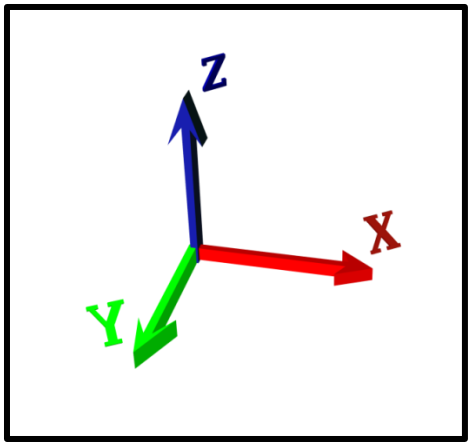

Figure 3.1: Right-handed coordinate system used in multicomponent seismic data acquisition.

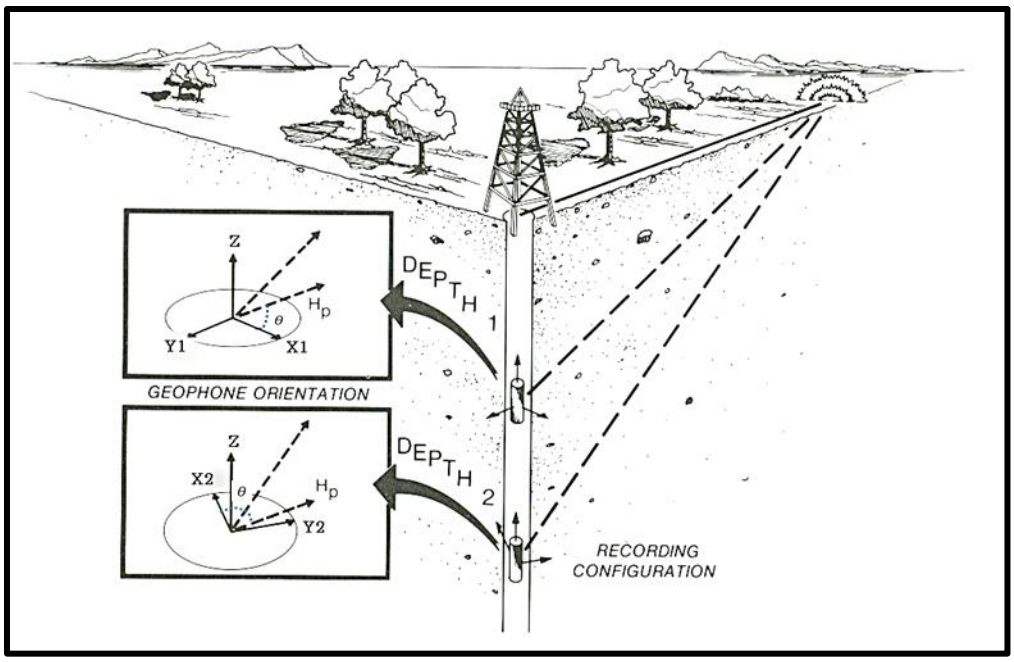

Figure 3.2: Schematic of vertical seismic profile geophone orientation problem (From DiSiena et al, 1984).

The horizontal projection of P-wave direct arrivals is in the same direction as the ray path extending from the wellhead towards the source location. Because the horizontal orientation of P raypaths is consistent from depth to depth, the ray path Hp shown in Figure 3.2 is used as fixed reference frame. Figures 3.3 and 3.4 illustrate how direct-arrival P-wave horizontal signals vary for different VSP geophone orientations at different depths. Horizontal re-orientation of geophone components causes P-wave energy divided onto components X and Y (Fig 3.3) to concentrate only on component X' (Fig 3.4).

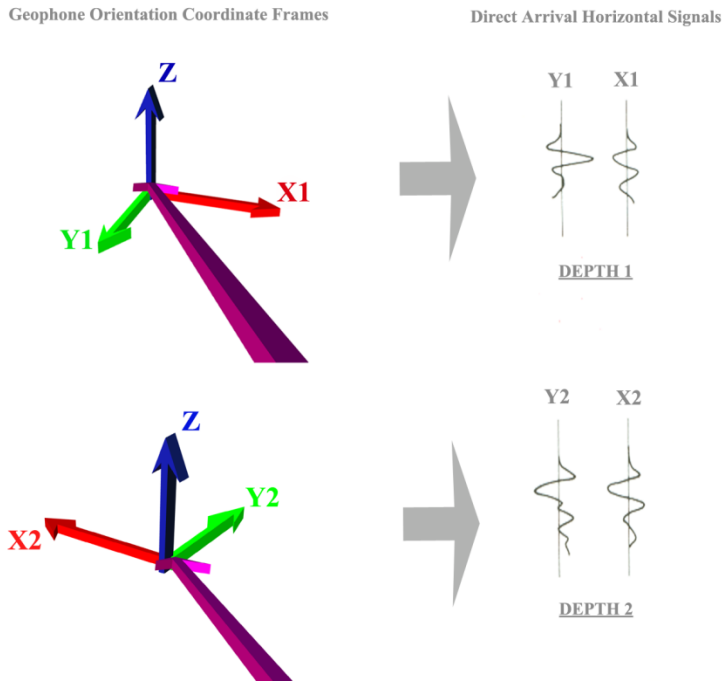

Figure 3.3: Direct P-wave arrival picks on the horizontal components of receivers X and Y deployed at different depths.

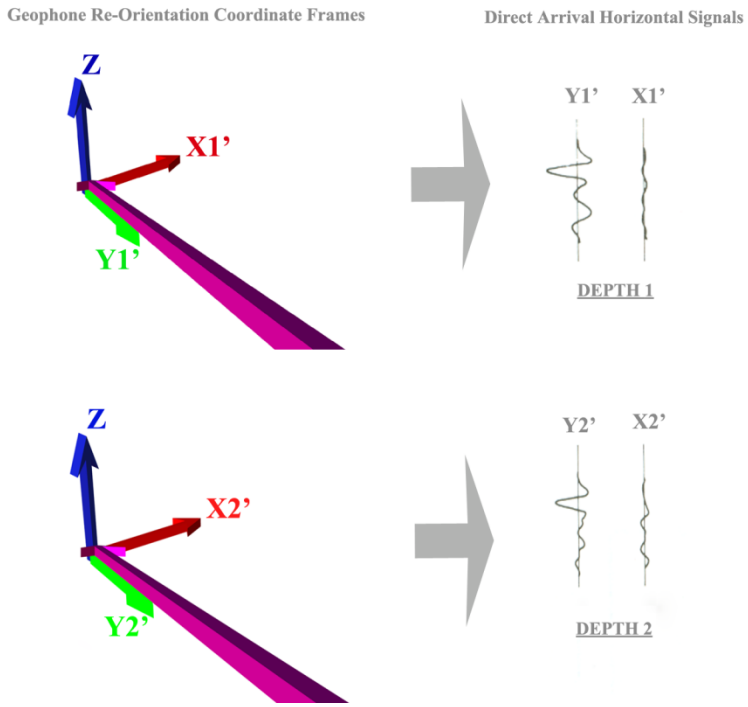

Figure 3.4: Effect of re-orientation on direct arrivals onto horizontal component X'.

This coordinate transform is performed by the following equation

$$X' = X\cos\theta + Y\sin\theta \qquad (1)$$

$$Y' = -X\sin\theta + Y\cos\theta \qquad (2)$$

where θ defines the azimuthal rotation angle between X and reference ray path H_p as illustrated on Figure 3.2. This formulation became the main principle of applying multicomponent geophone rotation.

3.3. COMPONENT ROTATION

In multicomponent seismic data, particle displacement is measured on three orthogonal components at each receiver station in a VSP well. The vertical Z component usually is aligned on the vertical axis, but the orientations of horizontal components are unknown because a borehole geophone may rotate around its axis on the supporting wireline cable to cause the horizontal components at each receiver station to be oriented in different directions (Hardage et al., 2011). To resolve this inconsistency, multi-component sensor systems must be rotated from their positions at the time of recording to a user-defined coordinate system before starting to process data. This coordinate transformation is accomplished through projection of the data onto new coordinate axes.

The rotation of multicomponent seismic data detected by orthogonal sensors in receiver well can be performed by using a rotation matrix R

$$W = RU \qquad (3)$$

where U is the raw data and W is rotated data. Multicomponent seismic data typically are acquired in a coordinate system consisting of vertical component Z and two horizontal components Y and X as illustrated on Figure 3.1. If ϕ is defined as the angle between the axis of the X geophone and vertical plane that passes through the source station and the receiver station, the operation,

$$\begin{bmatrix} Z \\ R \\ T \end{bmatrix} = \begin{bmatrix} 1 & 0 & 0 \\ 0 & \cos\phi & \sin\phi \\ 0 & -\sin\phi & \cos\phi \end{bmatrix} \begin{bmatrix} Z \\ X \\ Y \end{bmatrix} \qquad (4)$$

rotates the seismic data horizontally from the field-acquisition coordinate system (X, Y, Z) into a new system (Z, R, T) in which R and T define radial and transverse components as the Z component remains constant. This matrix operation enables us to transform horizontal projection data from inline / crossline data coordinates to radial / transverse coordinates.

A coordinate rotation in three-dimensional space can be decomposed into two separate 2- dimensional rotations. In the case of three-component seismology, a rotation in the horizontal plane (SR-ST) is followed by a rotation in the plane defined by the vertical component and the rotated SR component. In most cases, this second rotation around the T- axis by an incident angle θ is needed because a P-wave arrives at each VSP receiver station at a different inclination angle. Equation 5 defines the matrix operation which allows us to rotate the data around the transverse component by leaving transverse component stable and concentrating energy on the radial component and vertical components.

$$\begin{bmatrix} P \\ SR \\ ST \end{bmatrix} = \begin{bmatrix} \cos\theta & -\sin\theta & 0 \\ \sin\theta & \cos\theta & 0 \\ 0 & 0 & 1 \end{bmatrix} \begin{bmatrix} Z \\ R \\ T \end{bmatrix} \qquad (5)$$

These two rotations (Eqs. 4 and 5) can be combined into a single rotation matrix described by the matrix operation in the Equation 6.

$$\begin{bmatrix} P \\ SR \\ ST \end{bmatrix} = \begin{bmatrix} \cos\phi & \cos\theta\sin\phi & \sin\phi\sin\theta \\ -\sin\phi & \cos\theta\cos\phi & \sin\theta\cos\phi \\ 0 & -\sin\theta & \cos\theta \end{bmatrix} \begin{bmatrix} Z \\ X \\ Y \end{bmatrix} \qquad (6)$$

By using matrix operation (6), rotated data traces have compressional wave energy concentrated on sensor P, vertical shear energy on sensor SR and horizontal shear energy on sensor ST. A projection of rotations is represented on Figure 3.5. In Figure 3.5, (B) shows a rotation of X and Y axes by an angle ϕ. Note that the direction of the vertical component is unaffected by this rotation. The new coordinate axes R and T after rotation are shown in (C) and (D). The second rotation, performed in the plane defined by the vertical axis and R, is illustrated in (E). In this case the angle θ is measured from the vertical axis in the direction of R. Note that this second rotation leaves the direction of the rotated T component unchanged. The last position of components after rotation is illustrated in (F).

3.4. AZIMUTH AND INCLINATION

Estimating the orientation of geophones is one of the functions of multicomponent analysis and data processing tools. This process is done through knowing the source and receiver locations, using the rotation angle, and by assuming that

the P-wave first break energy arrives in the vertical plane containing the source and receiver.

In multicomponent seismic data, receiver component orientation is defined in terms of azimuth and inclination. Azimuth can be expressed as the number of degrees east of north in which a component points. The azimuth of a component heading towards east is 90°, south is 180°, and west is 270°. North is considered to have a azimuth of 0°.

In Cartesian coordinates, acquisition geometry can be used to calculate the theoretical azimuth which is the angle from receiver to the source by the following equation (Maercklin, 2010)

$$\phi = \arctan\left(\frac{Y_S - Y_R}{X_S - X_R}\right) \qquad (7)$$

with receiver coordinates (X_R, Y_R) and source coordinates (X_S, Y_S). In spherical coordinates, the same equation can be written as

$$\phi = \left(\frac{\sin(X_S - X_R)\cos(Y_S)}{\cos(Y_R)\sin(Y_S) - \sin(Y_R)\cos(Y_S)\cos(X_S - X_R)}\right) \qquad (8)$$

where the longitude and latitude of a receiver are represented as (X_R, Y_R) and those for a source are represented as (X_S, Y_S).

Inclination is the number of degrees that a component is inclined from a vertical axis. Generally the value of inclination is described from 0° to 180° with 0° being vertically upward, 90° being horizontal and 180° being vertically downward. It is clear that not only does acquisition geometry play a key role in computing inclination angle, θ,

but also seismic velocity structure around the receiver affects the computation. Figure 3.6 shows a random component orientation with an azimuth of 45° and inclination of 20°.

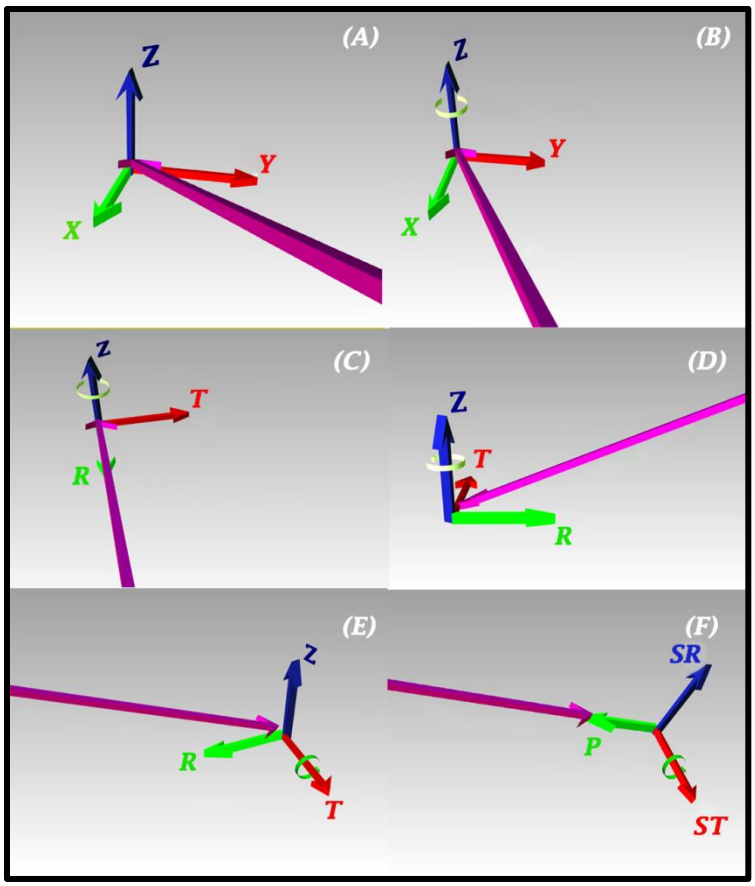

Figure 3.5: A projection of sensor rotations. Pink arrows indicate P-wave ray paths in each section. (A) Component orientation of a 3C geophone before rotation. (B) The first rotation around Z axis. (C) View of geophone components after first rotation. (D) A second view of components that shows a rotation around the X axis. (E) The second rotation in the vertical plane. (F) Final view of geophone components after rotations are done.

When a compressional wave mode activates a geophone, a positive first motion is detected in the direction that the P displacement points. However, in crosswell seismic

applications in which a source is located below a receiver, the first motion is detected in the negative direction.

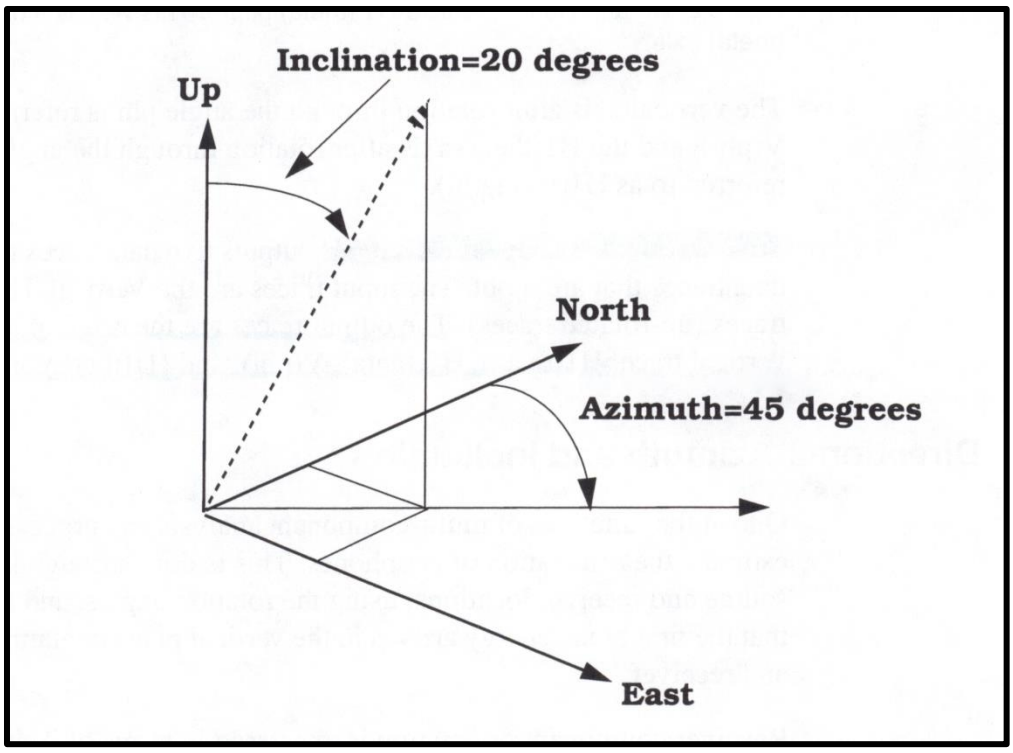

Figure 3.6: A random component orientation that has an inclination of 20° and an azimuth of 45°.

Figure 3.7 shows how each data component behaves in terms of the azimuth approach of a P ray. The data exhibited in Figure 3.7 were recorded at receiver station 5 (at the depth of 746-ft) when a 20° inclined-impact source was applied in the inline plane. The data were mathematically rotated in the horizontal plane by 1° from 0° to 360°. Points A and B (Fig. 3.7b) define the azimuth approach angle where P-wave energy is almost zero on the radial geophone. Similarly, point C on the transverse geophone describes the angle where P-wave energy is almost zero, while point D defines the point where P-wave energy on the transverse component reaches a maximum. The differences

between point A and B must be 180° for an isotropic, homogenous medium. For the same reason, the differences between point C and D must be 90° assuming S-waves modes produced by a horizontal vector source propagate along the same ray path as the P-wave mode. Because data were rotated only in the horizontal plane, the response of the vertical geophone remains constant for all azimuth rotations.

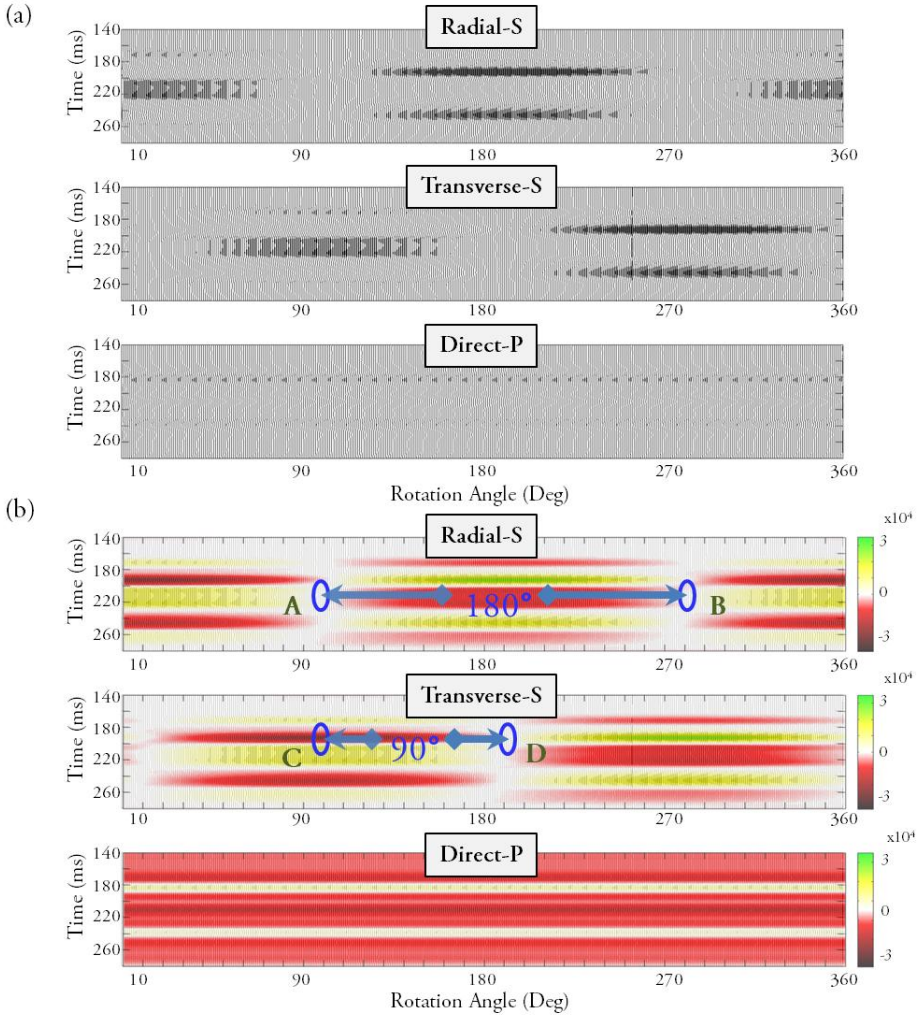

Figure 3.7: (a) Behavior of the geophone components at receiver station 5 in terms of azimuth rotation of sensors. (b) Energy distribution on the components at receiver station 5 in term of azimuth rotation of sensors.

3.5. AMPLITUDE PARAMETERS

In most multicomponent processes, the direction of particle motion is identified by the peak vector amplitude of a wavelet. The vector amplitude (magnitude) of the data in any given data window can be represented as the square root of the sum of squared amplitudes of data of all the data existing in that window. The peak vector amplitude R_i in Equation 9 defines the largest vector amplitude of all the vector samples in the analysis window.

$$R_i = \sqrt{X_i^{\,2} + Y_i^{\,2} + Z_i^{\,2}} \qquad (9)$$

The energy of the wavefield at each time sample is proportional to $R_i^{\,2}$. By averaging the energy in a moving time window of N samples (Eq. 10), a smoother energy trace can be obtained (Maercklin, 2010).

$$R_q^{\,2} = \frac{1}{N}\sum_{i=1}^{N}\left(X_i^{\,2} + Y_i^{\,2} + Z_i^{\,2}\right) \qquad (10)$$

The square root R_q is the RMS amplitude.

Chapter 4: Analysis of VSP Data

The objective of this section is to display how VSP data were analyzed and to compare data quality of different types of seismic sources in terms of the shear wave energy they create. Multicomponent seismic data generated by inclined impact, vertical impact, shot hole explosive, vertical vibrator, and horizontal vibrator were processed using EGL tools written in MATLAB. Each step of data processing will be explained.

4.1. PROCEDURES BEFORE ROTATION PROCESS

4.1.1. File Conversion

Most seismic data are acquired in SEG-Y format, one of several standards developed by the Society of Exploration Geophysicists (SEG) for storing geophysical data. The SEG-Y format was originally developed in 1970s and has achieved widespread usage within the geophysical industry. The format has evolved over the years to meet industry requirements for data analysis and processing. A SEG-Y file provides crucial information in traces and headers information which defines the geometry used to acquire the data. A seismic volume may be composed of one or more input SEG-Y files. In EGL tools, the SDF format, an acronym for Seismic Data Format, is used for seismic data processing. Therefore, the first data-processing step is to convert data from field acquisition format, SEG-Y, to SDF format.

4.1.2. Geometry Definition

Because the geometry of data acquisition plays a key role in data processing, processing software usually requires that the data be described in terms of the field geometry used during the data acquisition. To process data, the data should be in either CMP (Common Mid-Point) or CSG (Common Shot-Gather) order. Therefore, the geometry of the field layout, including source and receiver coordinates, group interval,

and station numbers must be defined in order to sort seismic data into CMP or CSG order. Throughout this step, source elevations and receiver depths are also defined in the database. In Table 1, all the shot locations used in the Devine Test Site Study acquisition geometry are displayed.

	Point	Latitude	Longitude	Northing	Easting	Elevation
Well 4	1	29 06 30.04670N	99 08 42.11317W	10564277.57	1594119.83	677.67
250'	2	29 06 29.66177N	99 08 39.32811W	10564238.4	1594366.74	675.26
500'	3	29 06 29.27683N	99 08 36.54305W	10564199.23	1594613.65	673.55
750'	4	29 06 28.89186N	99 08 33.75789W	10564160.06	1594860.57	669.4
1000'	5	29 06 28.50698N	99 08 30.97284W	10564120.9	1595107.48	665.88
1250'	6	29 06 28.12199N	99 08 28.18780W	10564081.73	1595354.39	662.26
1500'	7	29 06 27.73698N	99 08 25.40276W	10564042.56	1595601.3	660.72
1750'	8	29 06 27.35195N	99 08 22.61762W	10564003.39	1595848.22	657.22
1920'	9	29 08 27.09008N	99 08 20.72379W	10563976.75	1596016.12	654.6

Table 4.1: Locations of source positioning in Devine Test study. Latitudes and longitudes are in NAD83. Northing and easting are in UTM zone 14. Elevations are in NAWD88. Latitudes and longitudes are in degrees.

To obtain dependable multicomponent VSP seismic data, the source and receiver geometry used to record the walkaway VSP data must be defined for the seismic processing tool kit. The seismic acquisition geometry used in the Devine Test study is displayed in Figure 4.1.

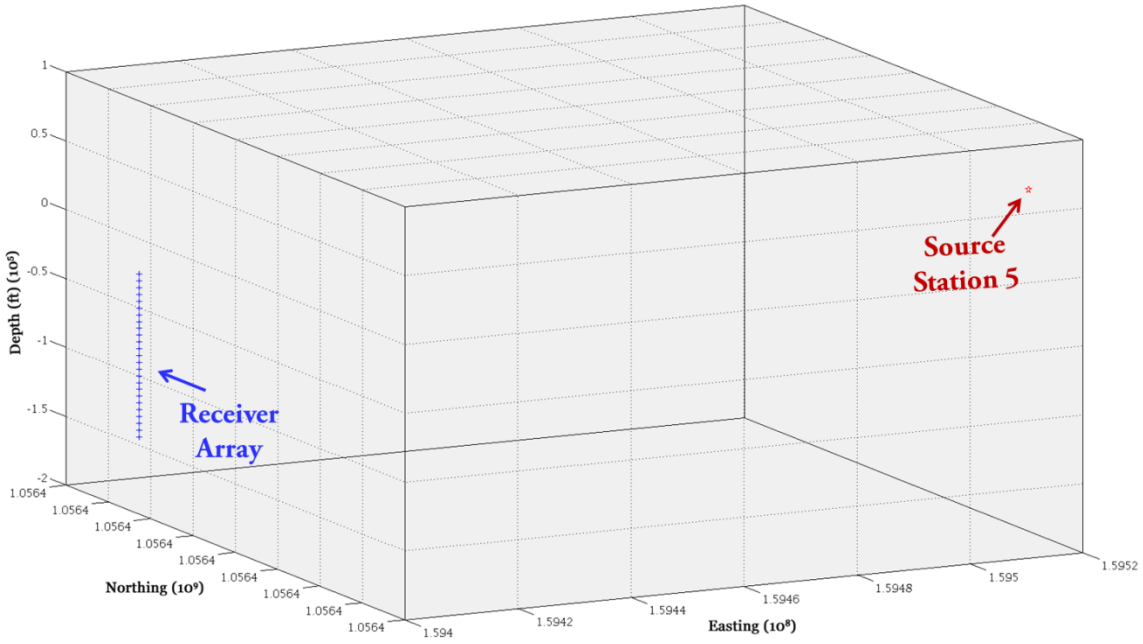

Figure 4.1: Presentation of acquisition geometry in MATLAB. Red star refers shot location 5 offset from 1000 ft from the receiver well. Blue line represents multicomponent receiver array with a geophone spacing of 49.2 ft.

4.2. EXAMINING MULTICOMPONENT VSP DATA

As discussed in Figure 1.5, receivers must be mathematically oriented to obtain data acquired as if those receivers were deployed in a consistent azimuth and inclination orientation. This geophone rotation process involves a 2-step rotation; one rotation in the horizontal plane and a second rotation in the vertical plane. In step 1, the two horizontal geophones X and Y at each receiver station were mathematically rotated until the P-wave first-arrival energy on the radial component reached a maximum and the P-wave energy on the transverse component approached zero. In step 2, vertical and reoriented radial geophones were vertically rotated at each receiver station until the P-wave first-arrival energy on the vertical geophone became a minimum. This 2-step rotation principle is displayed in Figure 4.2.

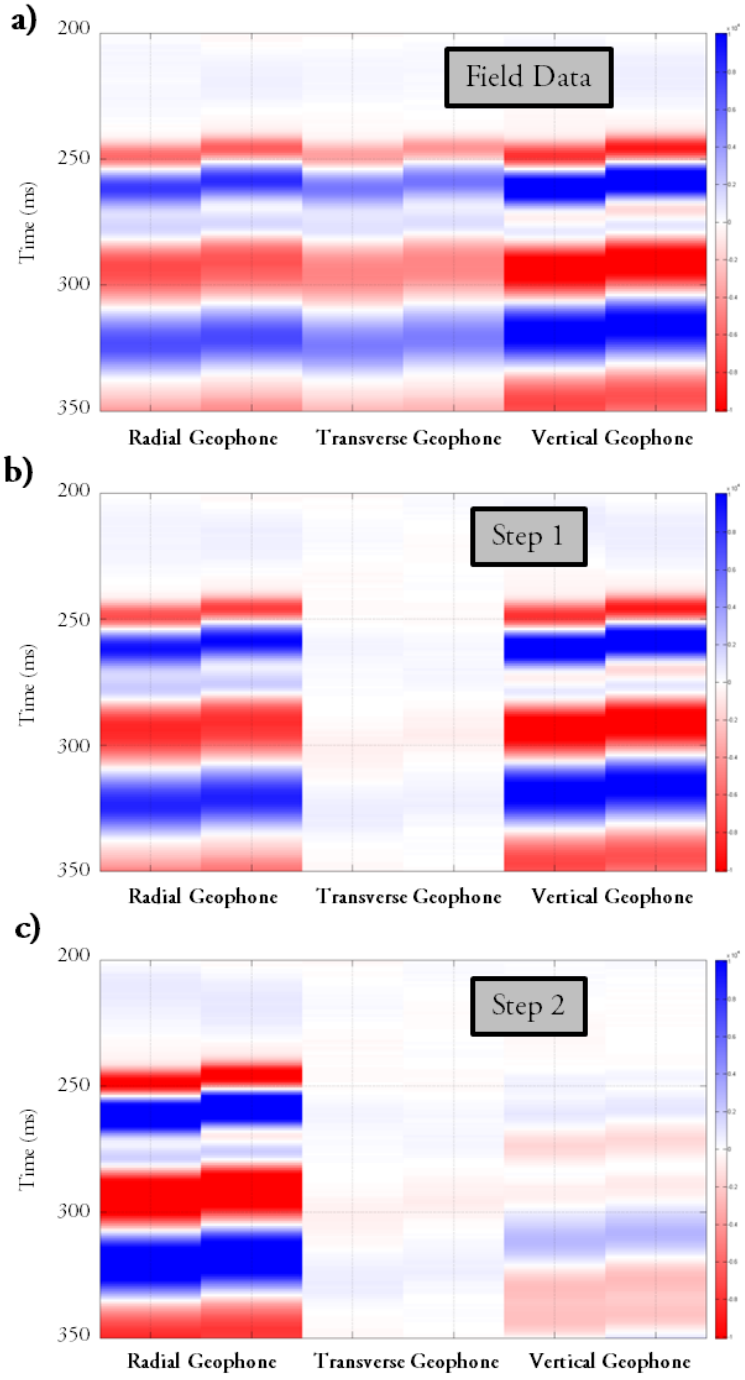

Figure 4.2: An example of rotation process for receiver station 22. a) Raw unprocessed data acquired in arbitrary azimuth and inclination orientation. b) After a 122° rotation in the horizontal plane. Note there is no alteration on the vertical geophone. c) After an additional 32° rotation in the vertical plane.

After reorientation of each of the 24 geophones deployed in the VSP receiver well, the common assumptions used for separation of P and S wavefields in VSP data were verified.

Each direct wavefield used for creating direct-S radiation patterns contains some contamination from other companion wave modes. Because the positions of receiver stations and source stations are the same for all seismic sources, it can be assumed the amount of contamination for the re-oriented data is the same for all sources tested. Thus it is reasonable to assume P and SV arrival azimuths and inclination angles for any source-receiver pair tested are almost the same, especially for homogenous non-layered media. Therefore, I believe the radiation patters presented in my project are valuable and informative for future studies.

The receiver orientation procedure applied to vertical impact, shot-hole explosive, vertical vibrator, inclined-impact, and horizontal vibrator sources located at shot location 5 are illustrated on Figures 4.3 through 4.19. Because the signal quality is not satisfactory for receivers 6 and 23, those receivers were eliminated from processing. Data windows spanning 40-ms from the onset of the P-wave direct arrivals on each receiver station were used to determine geophone azimuth and inclination angles applied in the rotation steps (top row of Figures 4.3 through 4.19).

Because different amounts of seismic energy are produced by each seismic source, a different gain was used to illustrate data generated by each source. A constant gain was used for inclined-impact, shot-hole explosive and vertical-impact sources, but a different gain was needed to display data generated by horizontal and vertical vibrators because the shear wave energy produced by these vibrator sources was much stronger than shear modes produced by other sources.

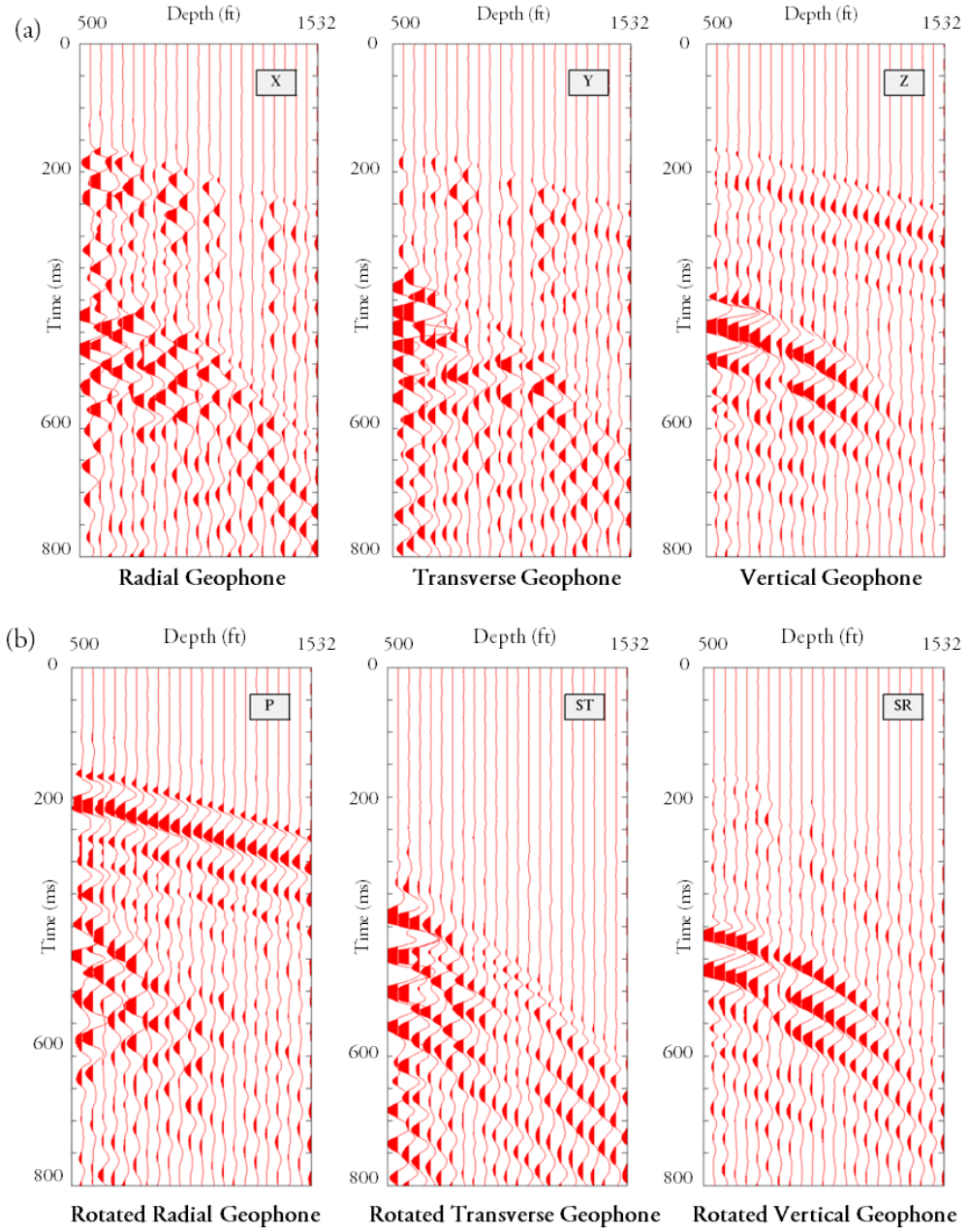

Figure 4.3: (a) Illustration of X, Y, Z data acquired with the multicomponent vertical sensor array when a negative 20° inclined impact was applied in the inline plane, at shot location 5, which was offset 1000 ft (305 m) from the array. (b) Data rotated to P, SR, and ST data space from initial acquisition coordinates.

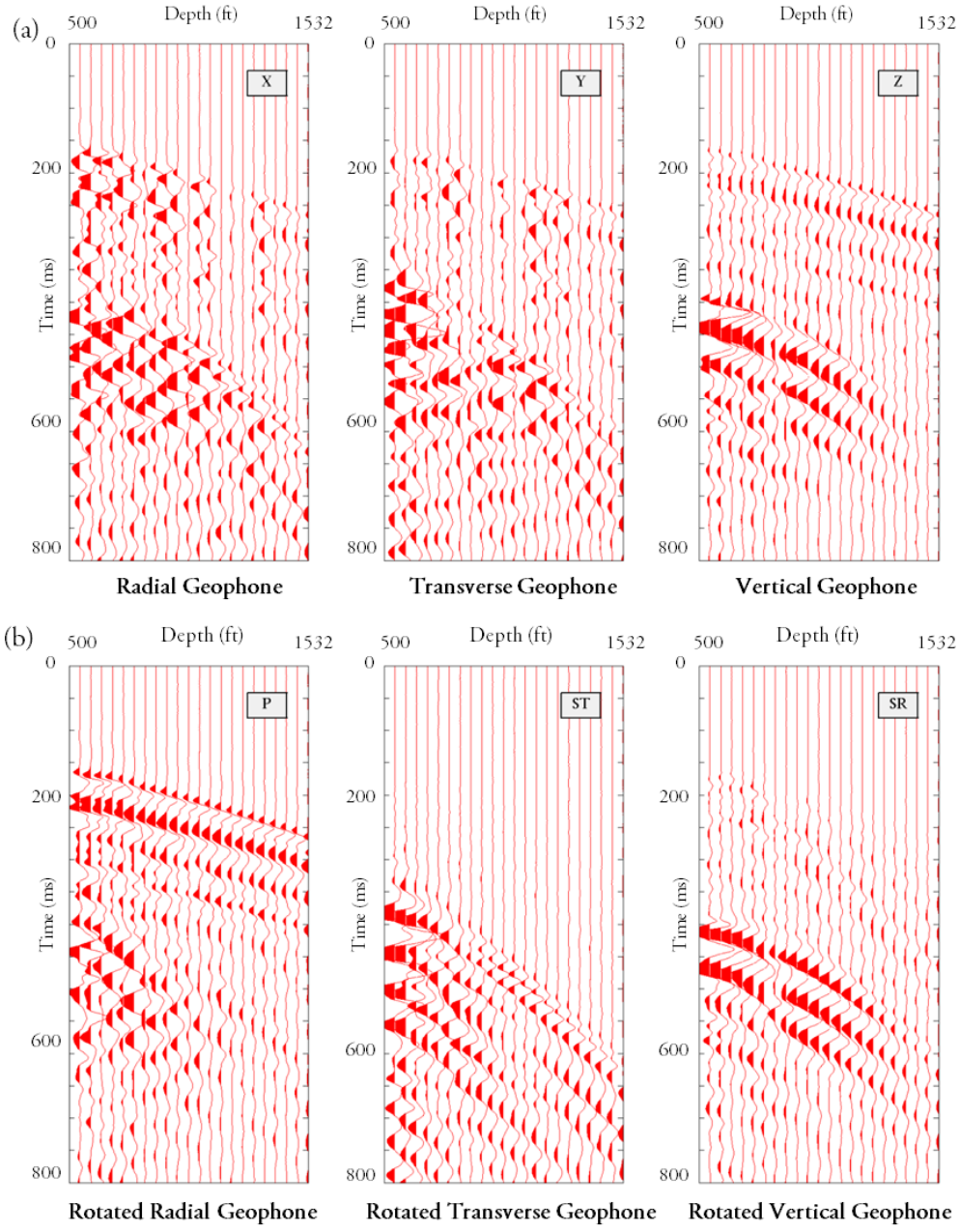

Figure 4.4: (a) Illustration of X, Y, Z data acquired with the multicomponent vertical sensor array when a negative 30° inclined impact was applied in the inline plane, at shot location 5, which was offset 1000 ft (305 m) from the array. (b) Data rotated to P, SR, and ST data space from initial acquisition coordinates.

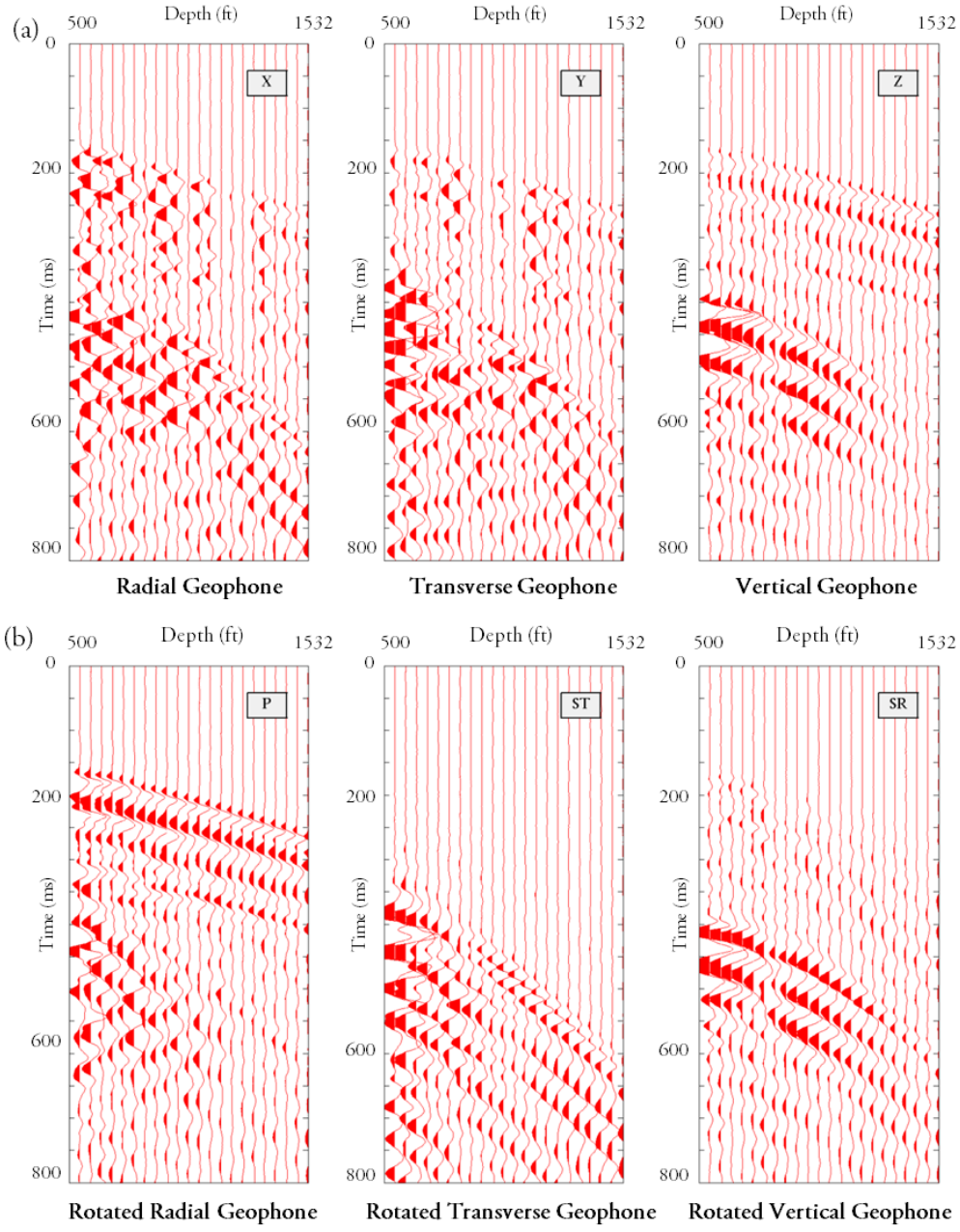

Figure 4.5: (a) Illustration of X, Y, Z data acquired with the multicomponent vertical sensor array when a negative 45° inclined impact was applied in the inline plane, at shot location 5, which was offset 1000 ft (305 m) from the array. (b) Data rotated to P, SR, and ST data space from initial acquisition coordinates.

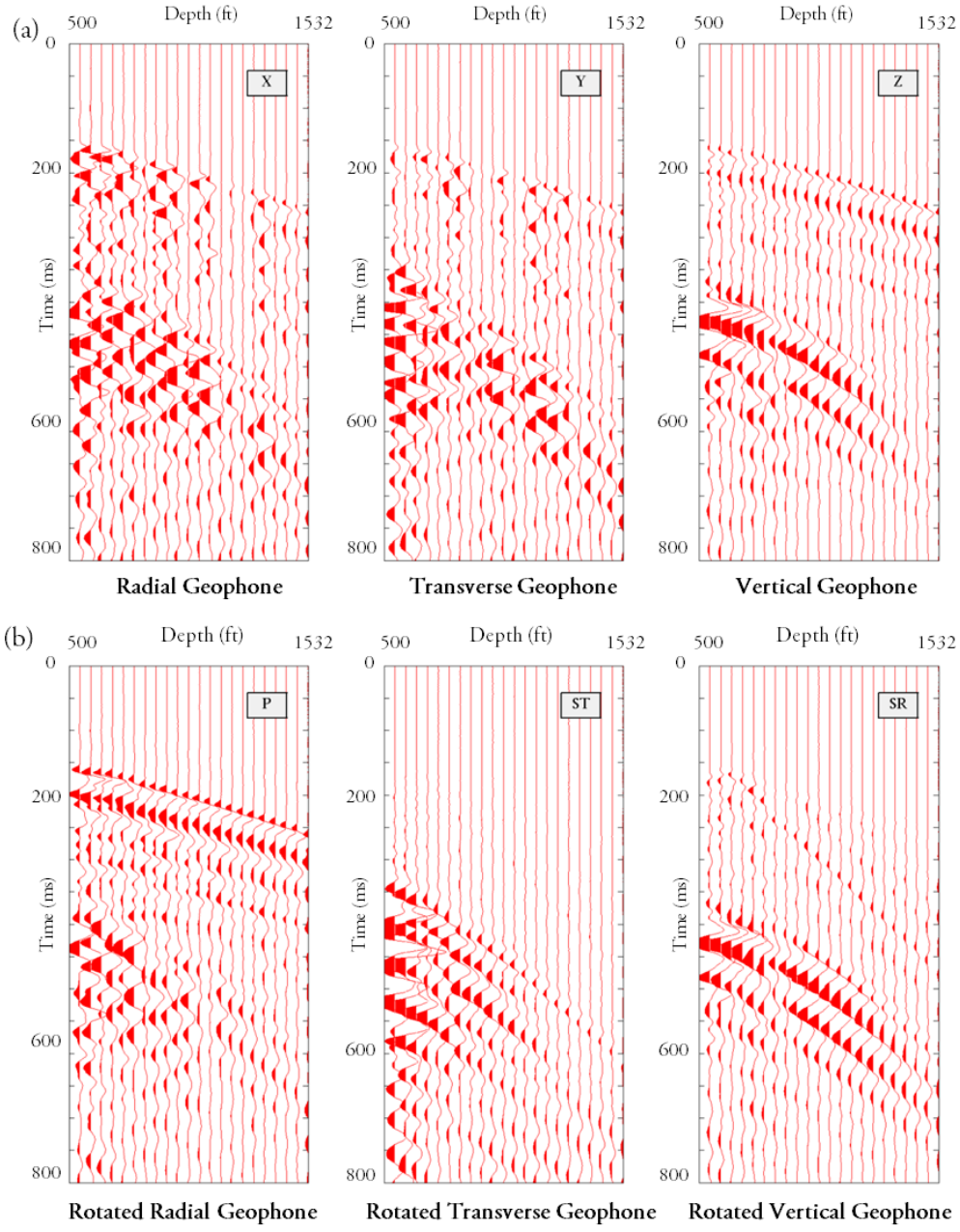

Figure 4.6: (a) Illustration of X, Y, Z data acquired with the multicomponent vertical sensor array when a positive 20° inclined impact was applied in the inline plane, at shot location 5, which was offset 1000 ft (305 m) from the array. (b) Data rotated to P, SR, and ST data space from initial acquisition coordinates.

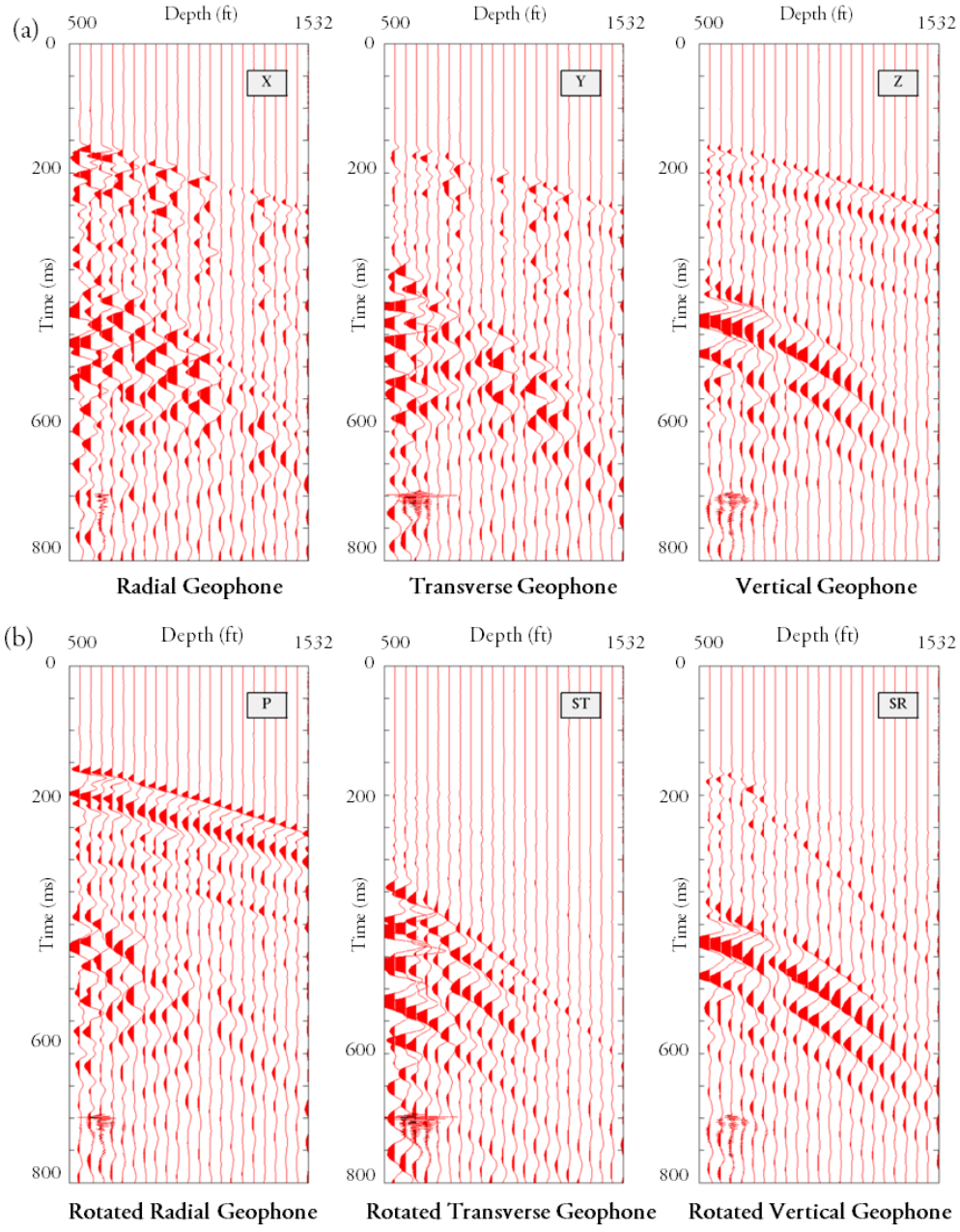

Figure 4.7: (a) Illustration of X, Y, Z data acquired with the multicomponent vertical sensor array when a positive 30° inclined impact was applied in the inline plane, at shot location 5, which was offset 1000 ft (305 m) from the array. (b) Data rotated to P, SR, and ST data space from initial acquisition coordinates.

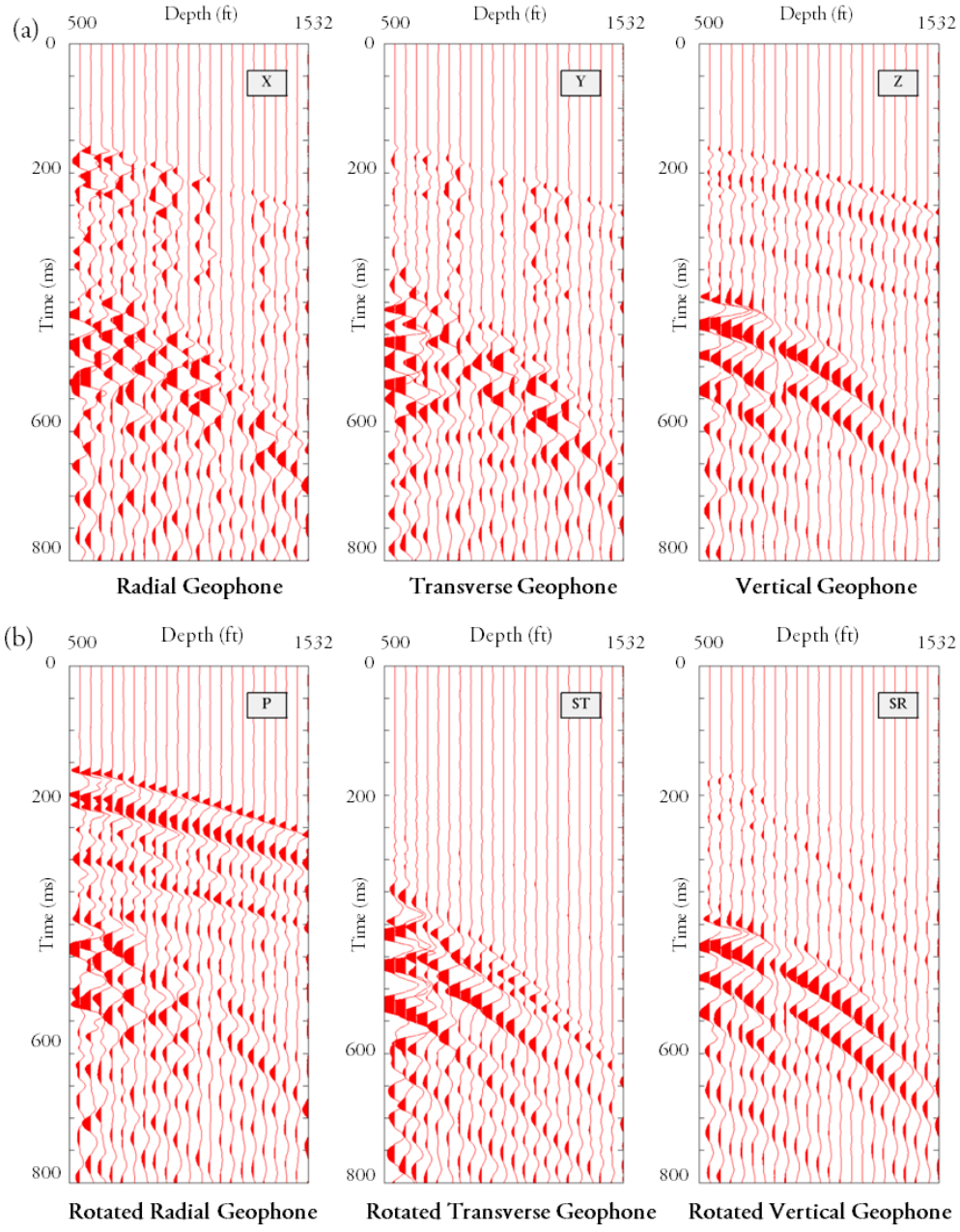

Figure 4.8: (a) Illustration of X, Y, Z data acquired with the multicomponent vertical sensor array when a positive 45° inclined impact was applied in the inline plane, at shot location 5, which was offset 1000 ft (305 m) from the array. (b) Data rotated to P, SR, and ST data space from initial acquisition coordinates.

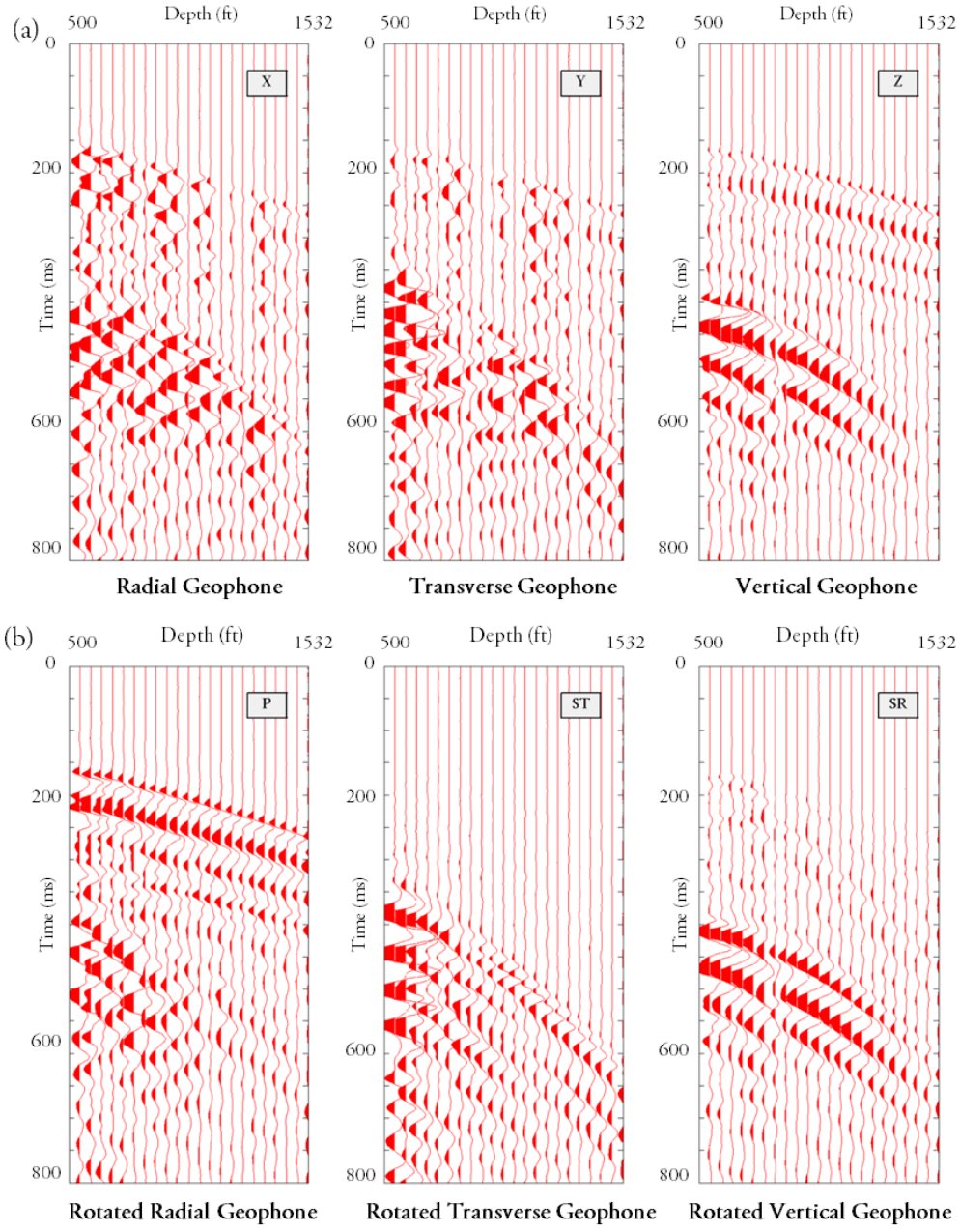

Figure 4.9: (a) Illustration of X, Y, Z data acquired with the multicomponent vertical sensor array when a negative 20° inclined impact was applied in the crossline plane, at shot location 5, which was offset 1000 ft (305 m) from the array. (b) Data rotated to P, SR, and ST data space from initial acquisition coordinates.

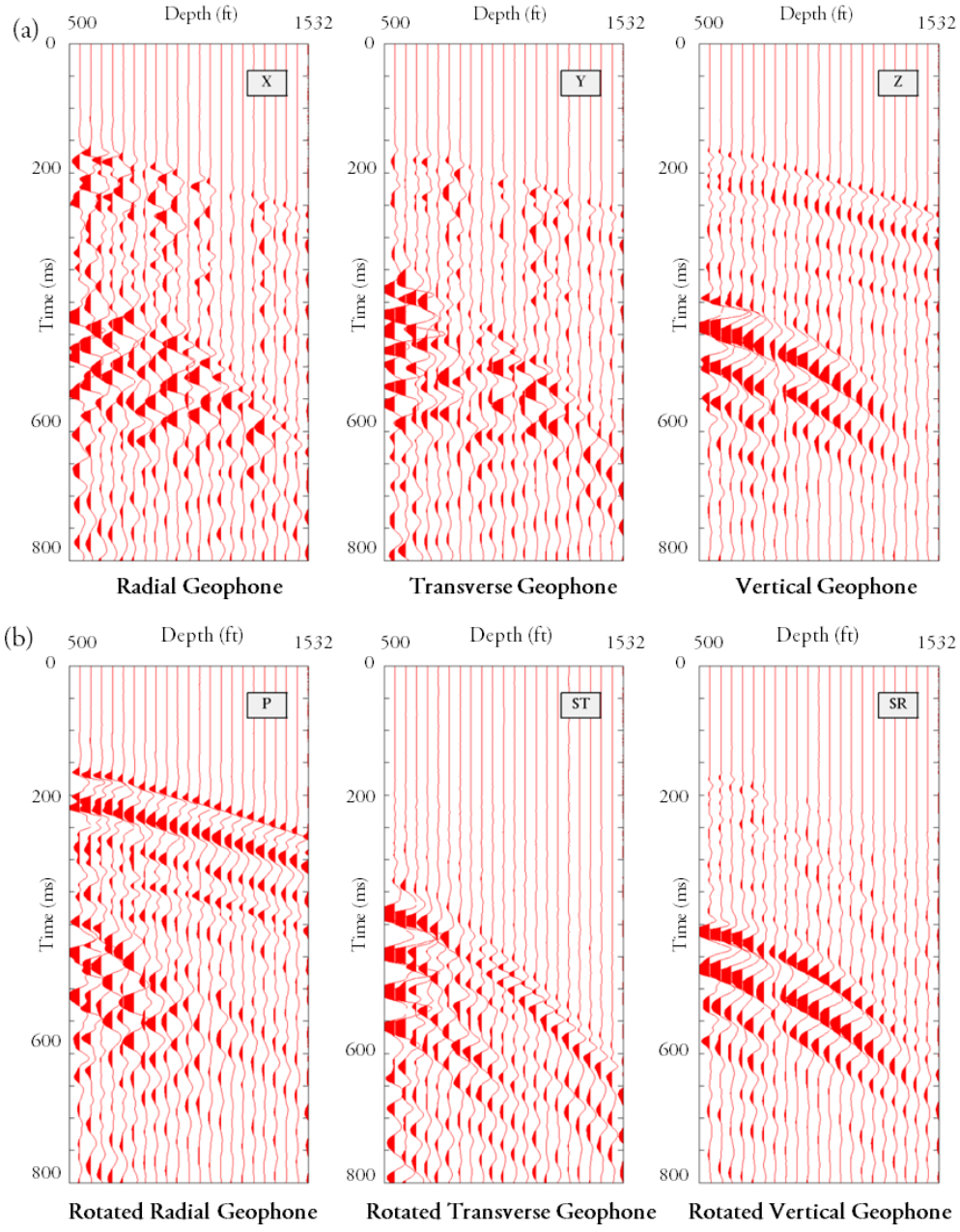

Figure 4.10: (a) Illustration of X, Y, Z data acquired with the multicomponent vertical sensor array when a negative 30° inclined impact was applied in the crossline plane, at shot location 5, which was offset 1000 ft (305 m) from the array. (b) Data rotated to P, SR, and ST data space from initial acquisition coordinates.

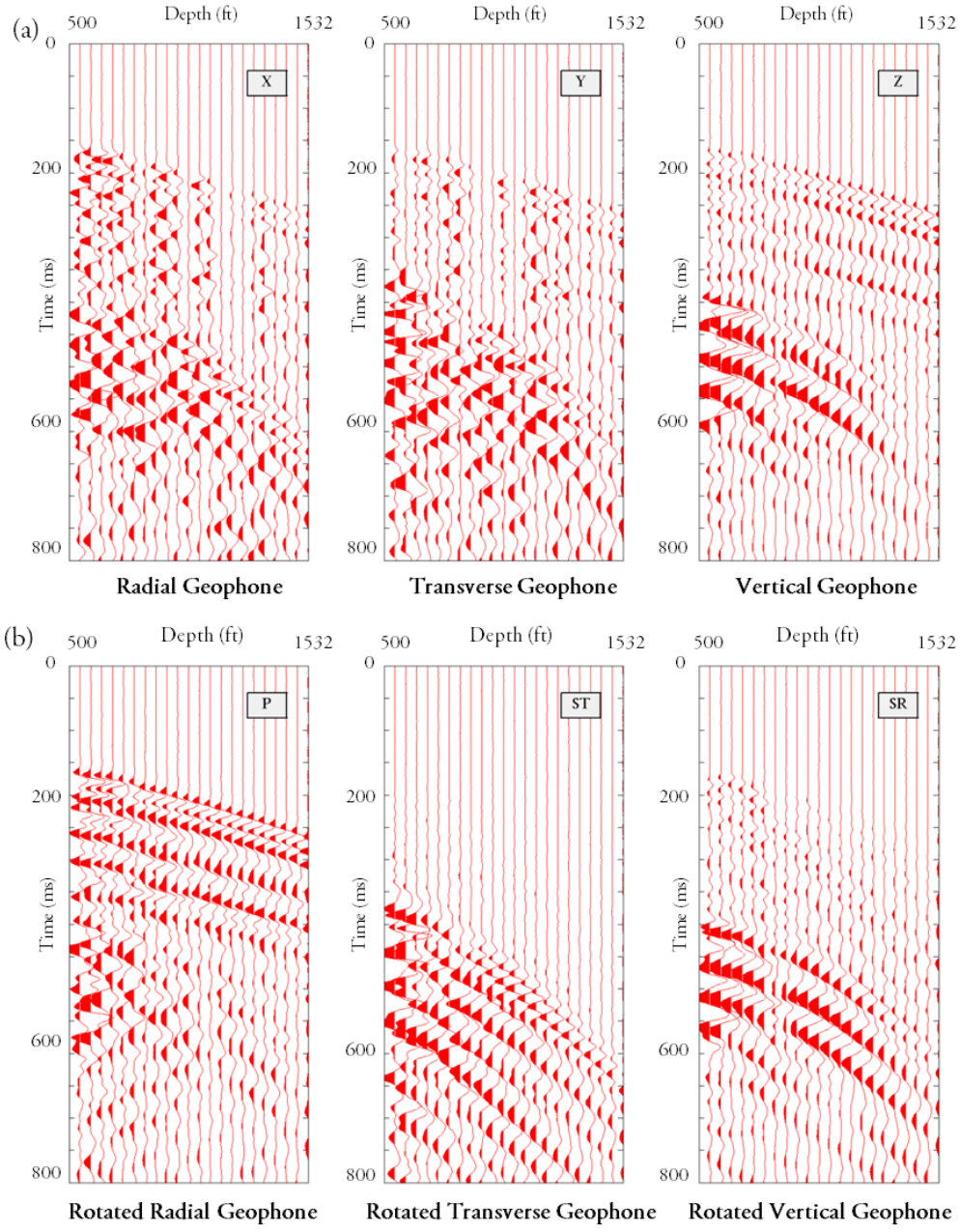

Figure 4.11: (a) Illustration of X, Y, Z data acquired with the multicomponent vertical sensor array when a negative 45° inclined impact was applied in the crossline plane, at shot location 5, which was offset 1000 ft (305 m) from the array. (b) Data rotated to P, SR, and ST data space from initial acquisition coordinates.

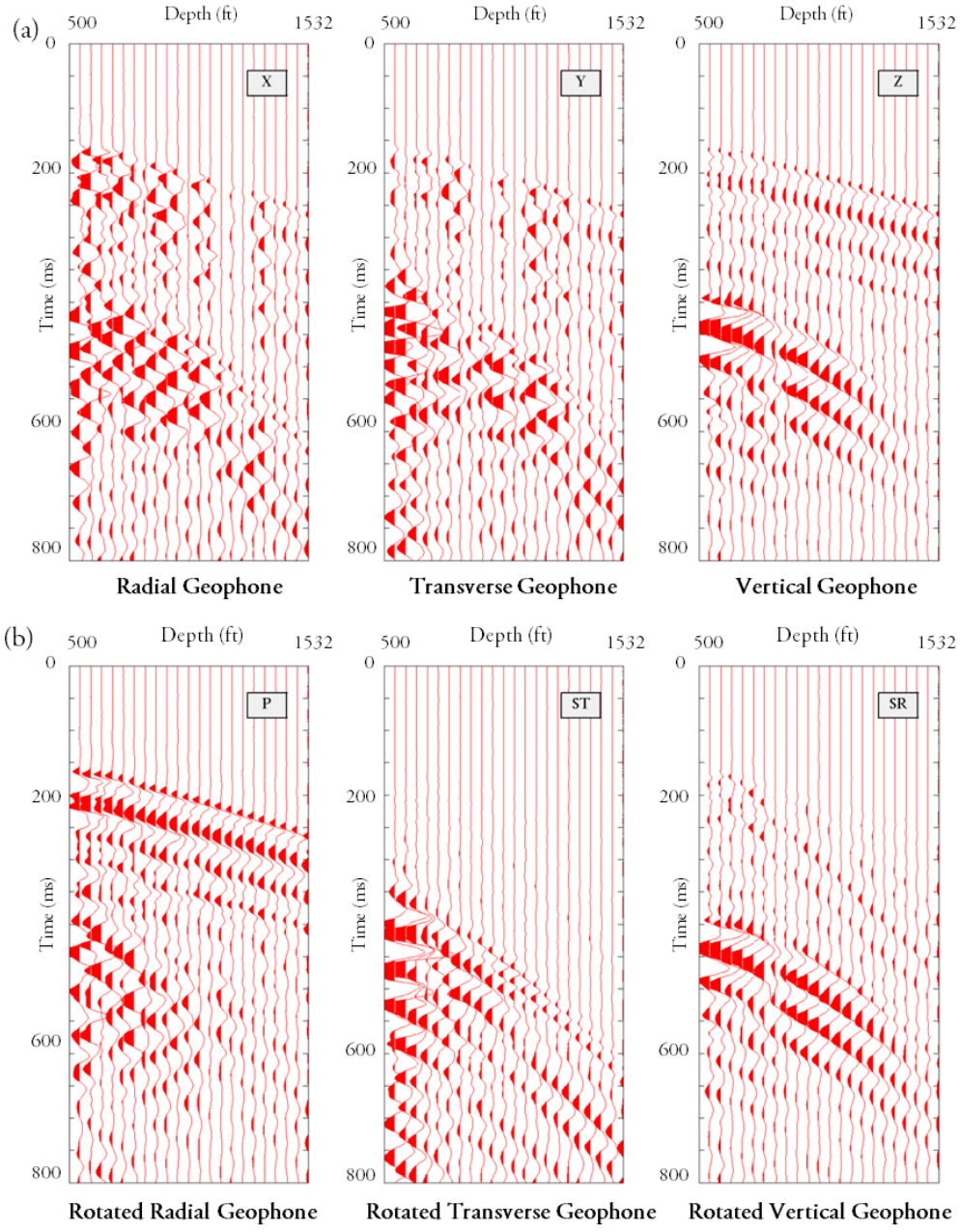

Figure 4.12: (a) Illustration of X, Y, Z data acquired with the multicomponent vertical sensor array when a positive 20° inclined impact was applied in the crossline plane, at shot location 5, which was offset 1000 ft (305 m) from the array. (b) Data rotated to P, SR, and ST data space from initial acquisition coordinates.

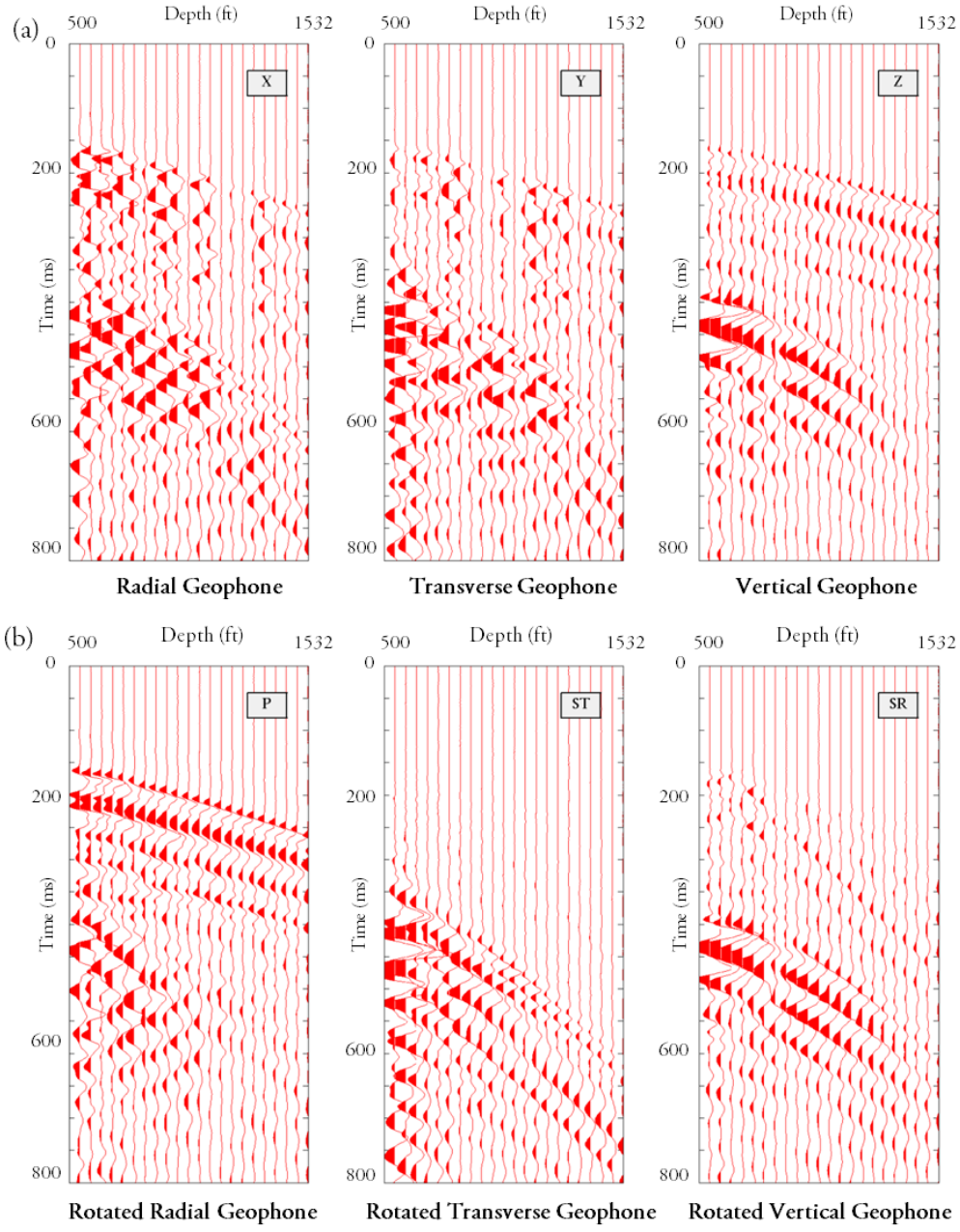

Figure 4.13: (a) Illustration of X, Y, Z data acquired with the multicomponent vertical sensor array when a positive 30° inclined impact was applied in the crossline plane, at shot location 5, which was offset 1000 ft (305 m) from the array. (b) Data rotated to P, SR, and ST data space from initial acquisition coordinates.

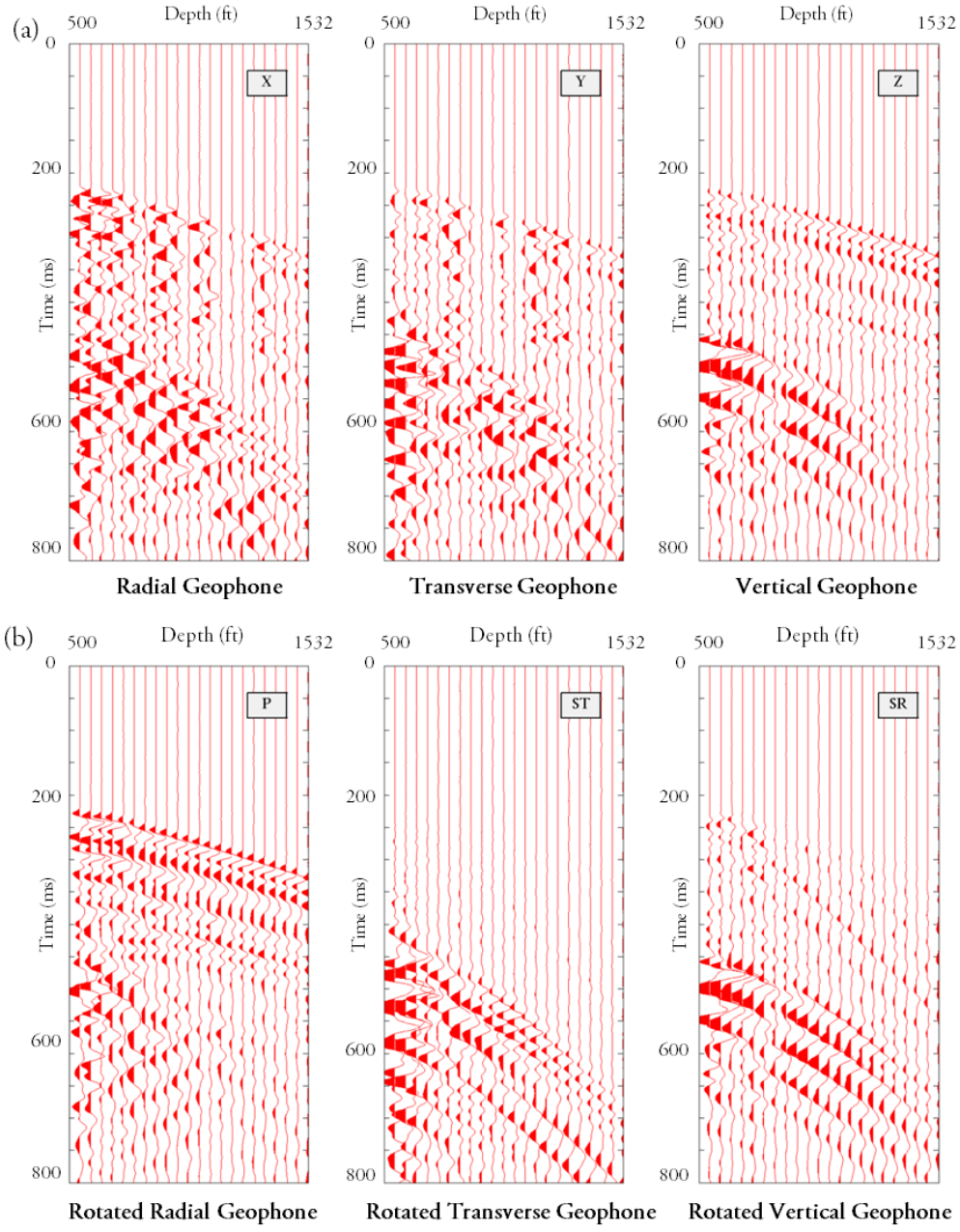

Figure 4.14: (a) Illustration of X, Y, Z data acquired with the multicomponent vertical sensor array when a positive 45° inclined impact was applied in the crossline plane, at shot location 5, which was offset 1000 ft (305 m) from the array. (b) Data rotated to P, SR, and ST data space from initial acquisition coordinates.

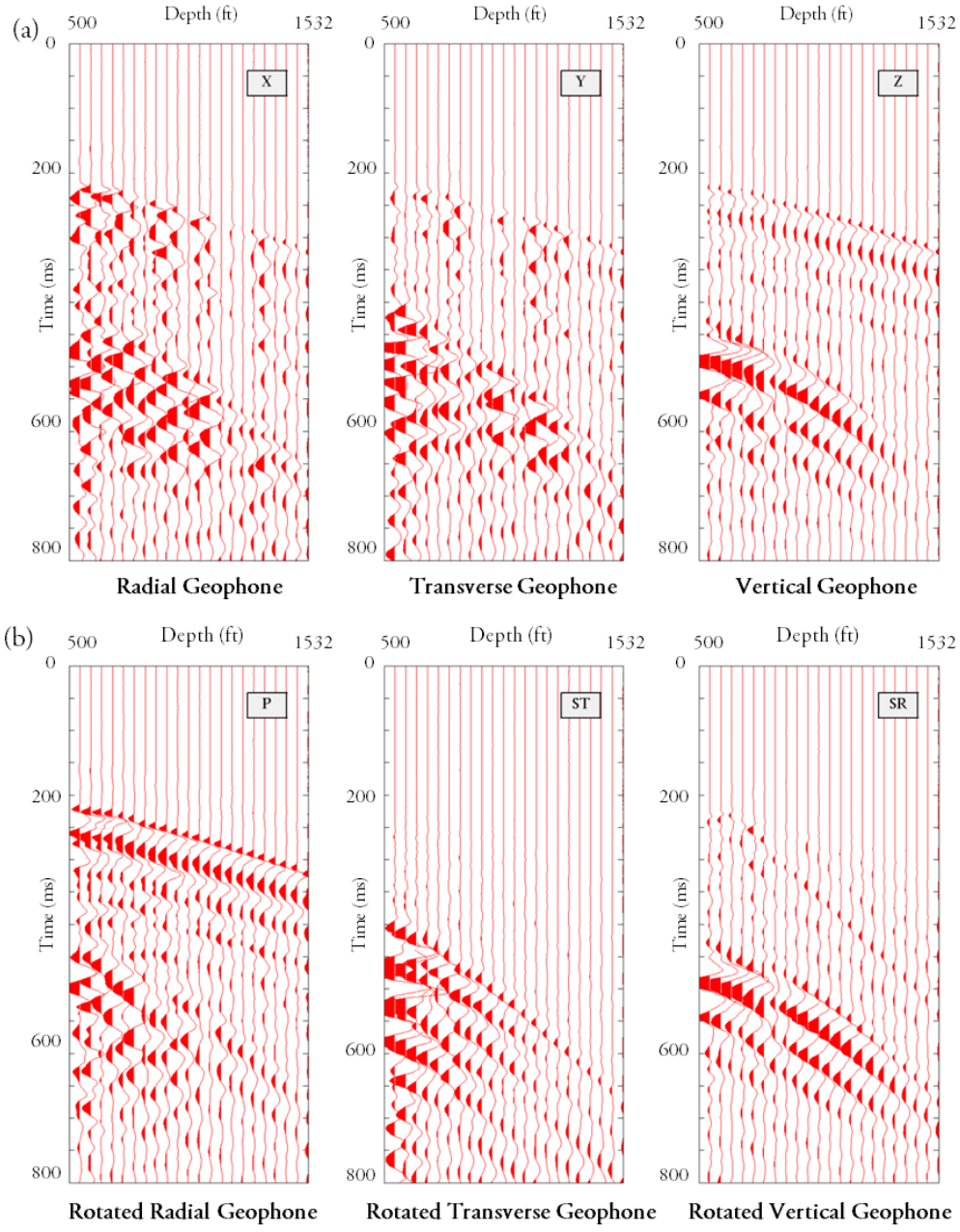

Figure 4.15: (a) Illustration of X, Y, Z data acquired with the multicomponent vertical sensor array when a vertical impact was applied at shot location 5, which was offset 1000 ft (305 m) from the array. (b) Data rotated to P, SR, and ST data space from initial acquisition coordinates.

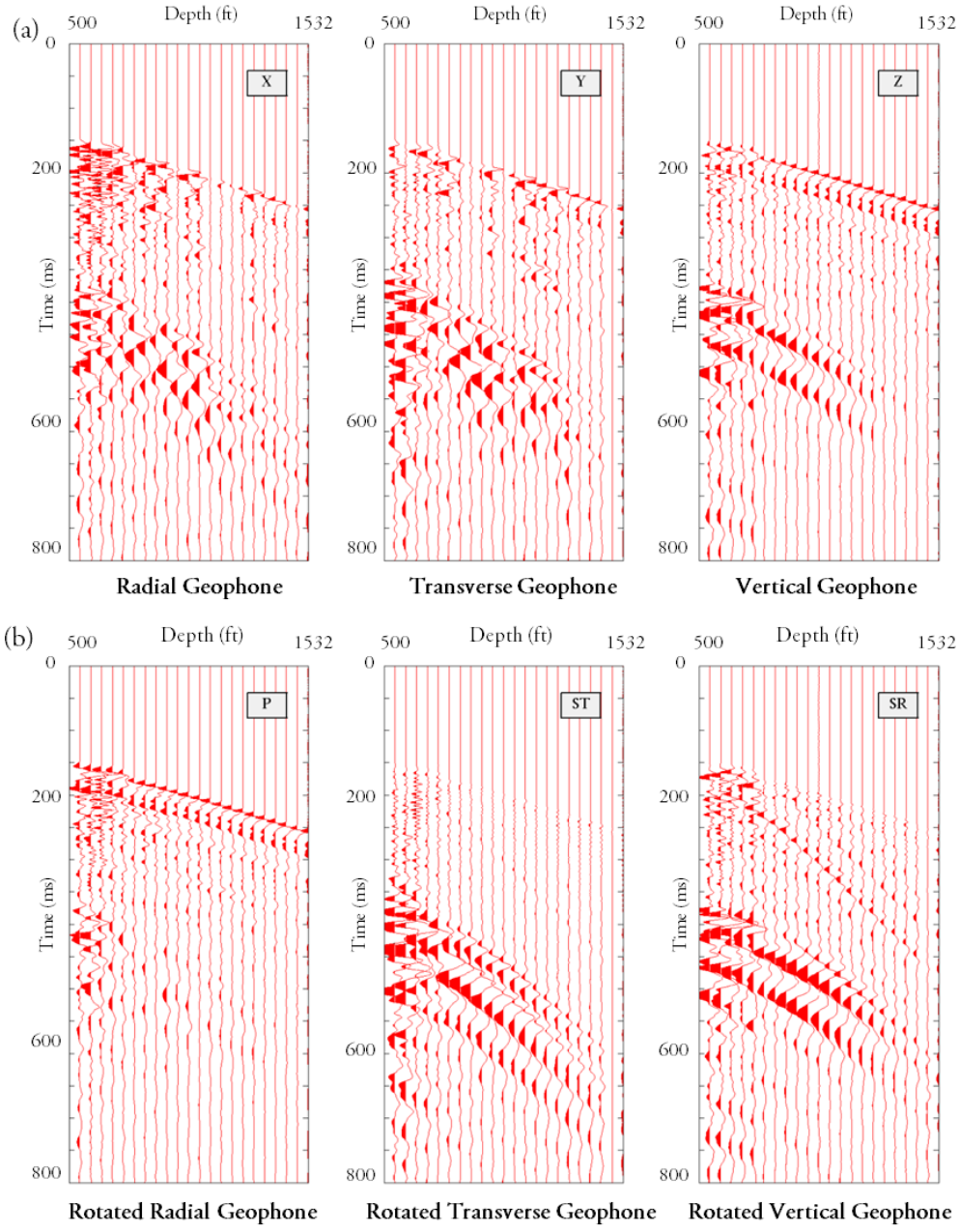

Figure 4.16: (a) Illustration of X, Y, Z data acquired with the multicomponent vertical sensor array when a shot-hole explosive was fired at shot location 5, which was offset 1000 ft (305 m) from the array. (b) Data rotated to P, SR, and ST data space from initial acquisition coordinates.

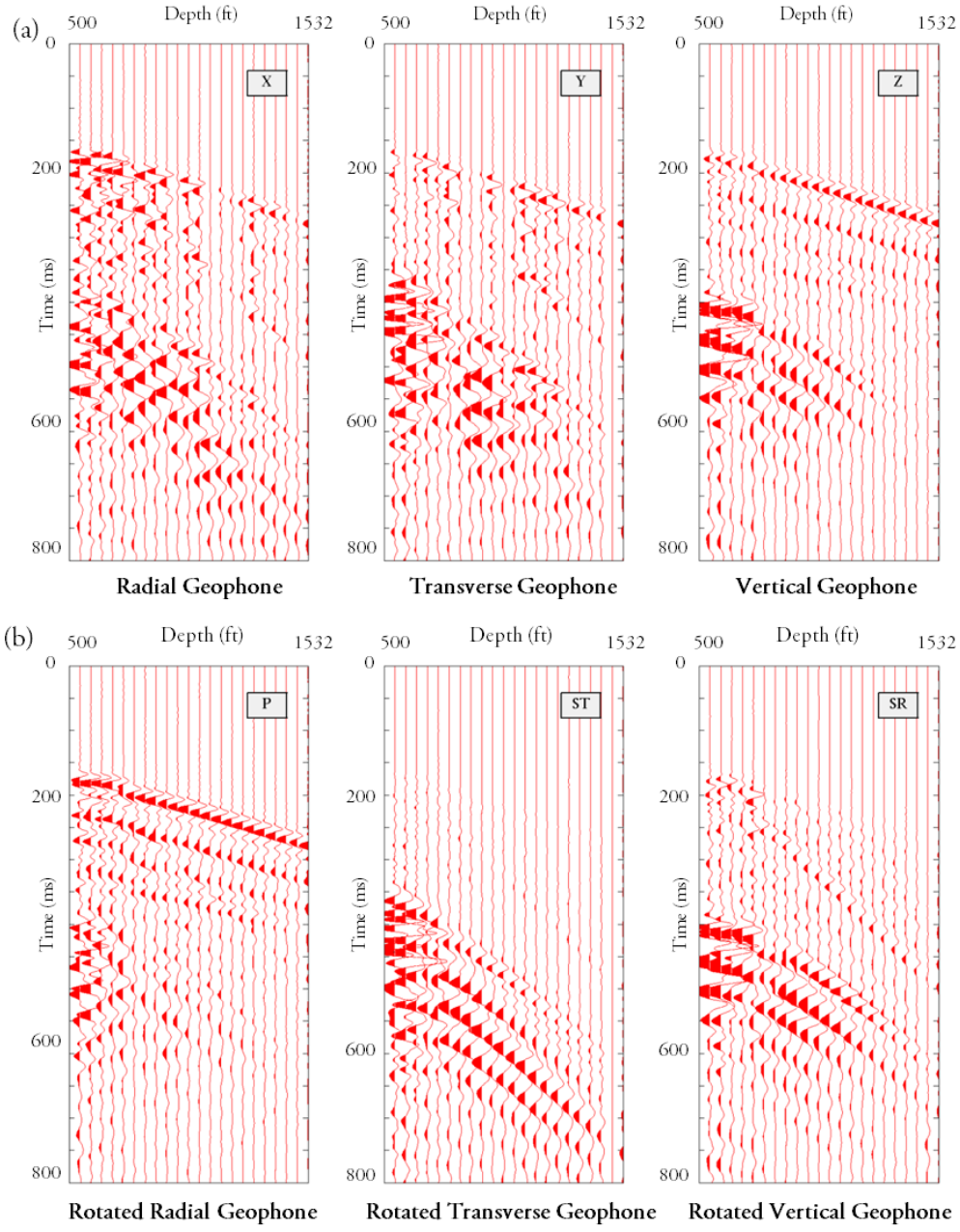

Figure 4.17: (a) Illustration of X, Y, Z data acquired with the multicomponent vertical sensor array when a vertical vibrator was applied at shot location 5, which was offset 1000 ft (305 m) from the array. (b) Data rotated to P, SR, and ST data space from initial acquisition coordinates.

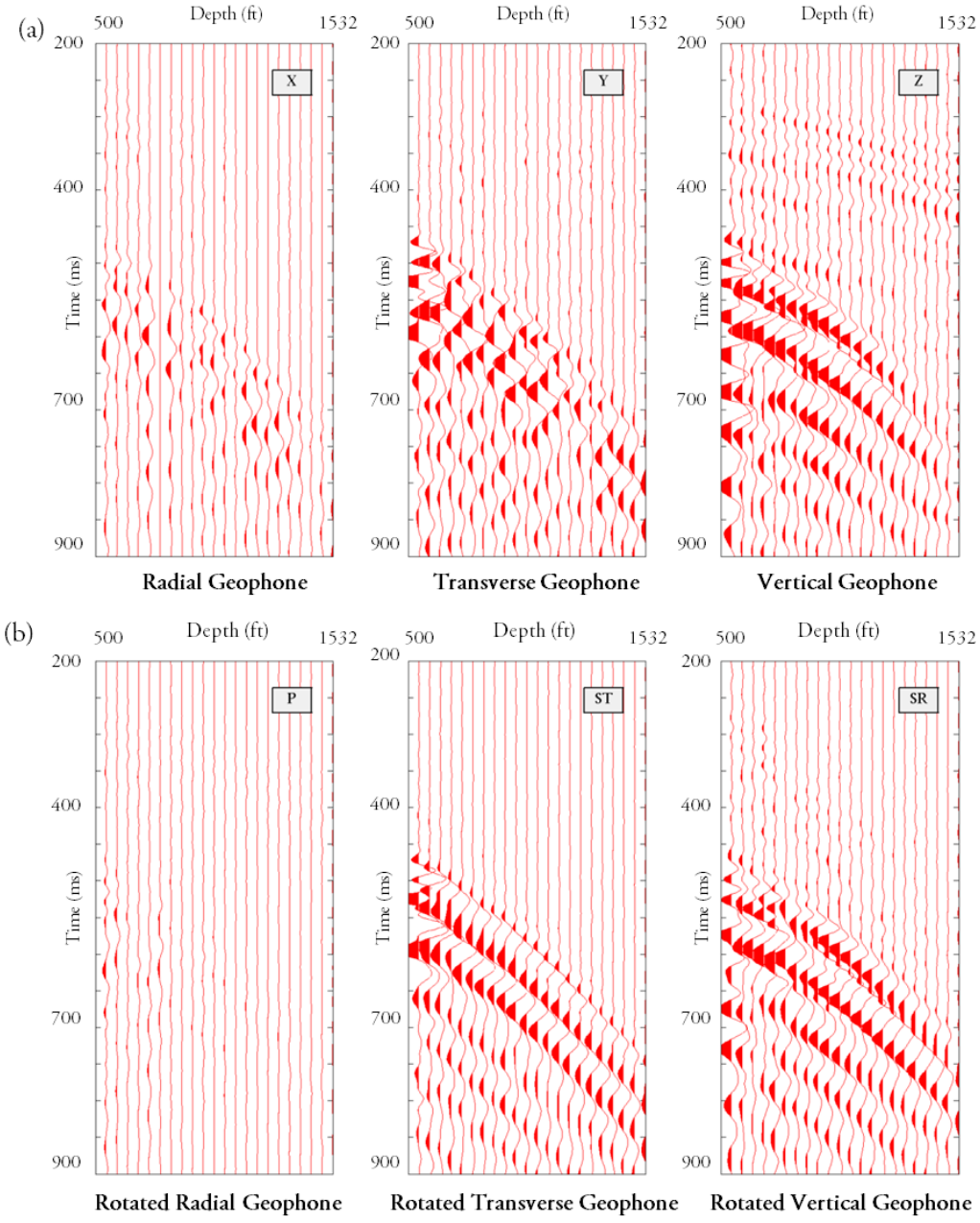

Figure 4.18: (a) Illustration of X, Y, Z data acquired with the multicomponent vertical sensor array when a horizontal vibrator was applied in the inline plane, at shot location 5, which was offset 1000 ft (305 m) from the array. (b) Data rotated to P, SR, and ST data space from initial acquisition coordinates.

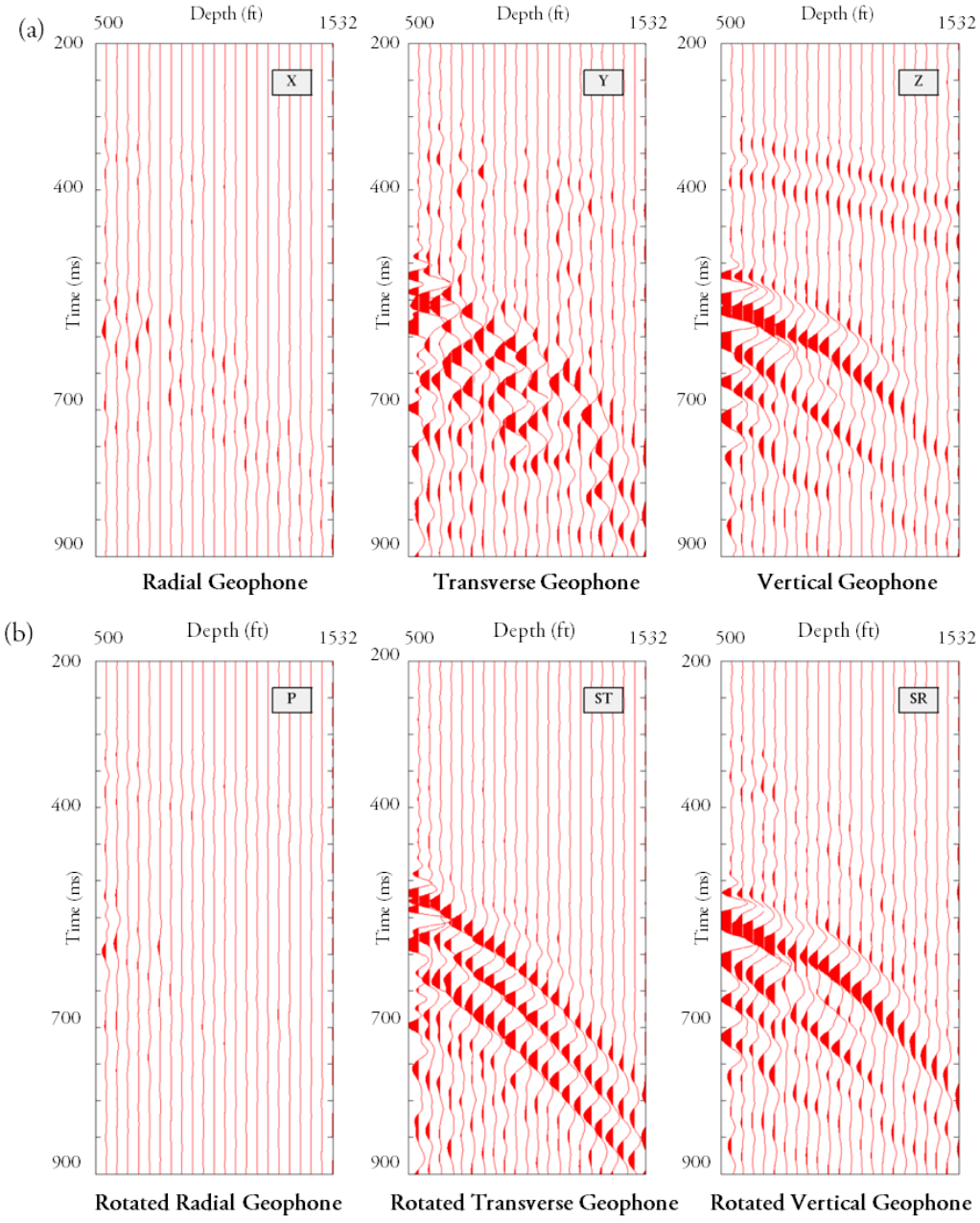

Figure 4.19: (a) Illustration of X, Y, Z data acquired with the multicomponent vertical sensor array when a horizontal vibrator was applied in the crossline plane, at shot location 5, which was offset 1000 ft (305 m) from the array. (b) Data rotated to P, SR, and ST data space from initial acquisition coordinates.

4.2.1. Comparison of Inclined-Impact Sources Applied from Opposing Directions

Because inclined impact vector sources create both vertical and horizontal displacements in the earth, two inclined-impact vectors applied from opposing directions should create opposite-polarity S-wave wavefields. To display this reversed-polarity phenomenon, the next step was to apply static time shifts to optimize the phase alignments of direct-S modes produced by positive-direction and negative-direction impacts. An example of the static corrections applied at receiver station 10 for data generated by positive 30° and negative 30° inclined-impact sources is illustrated in Figure 4.20. Figure 4.20a displays transverse-S data after direct-S modes on the transverse geophone are aligned for impacts applied from negative and positive direction. The amount of static time delay that existed in the raw transverse-S data before and after a static time shift can be seen from Figure 4.20b. Similarly, a static time shift applied to direct-S modes recorded by the radial geophone is displayed in Figures 4.20c and 20d. To maintain consistency between components, the same time shift was applied to both radial-S and transverse-S data. However, when there were different inclined-impact angles, a different static time shift was applied for each source. The results of applying appropriate time shifts to all geophones are illustrated on Figures 4.21 through 4.23. The static corrections displayed in Figures 4.21 through 4.23 were applied for all inclination angles (20°, 30°, and 45°) and for shots applied in both planes (inline and crossline).

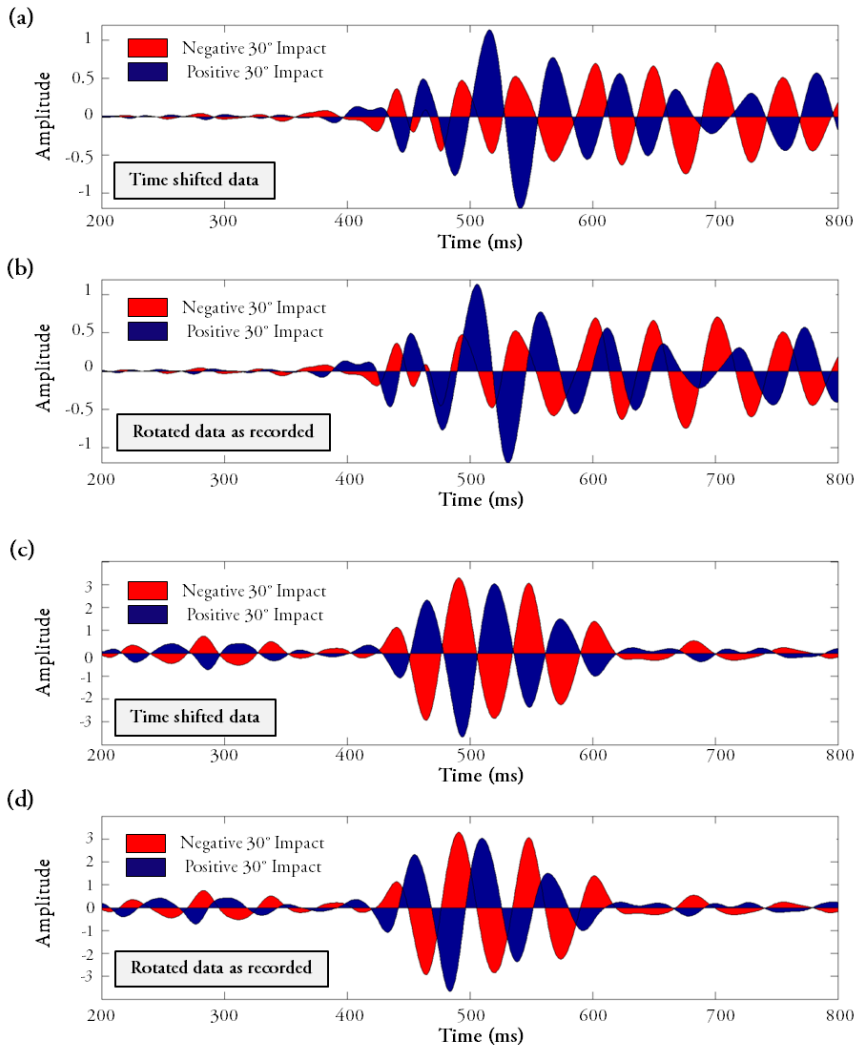

Figure 4.20: Applying static time shifts for receiver station 10 when the impacts were inclined -30° and +30° in the inline plane. (a) Phase-aligned direct-S mode on the transverse geophone. (b) Rotated transverse-S data before static time shift. (c) Phase-aligned direct-S mode on the radial geophone. (b) Rotated radial-S data before static time shift.

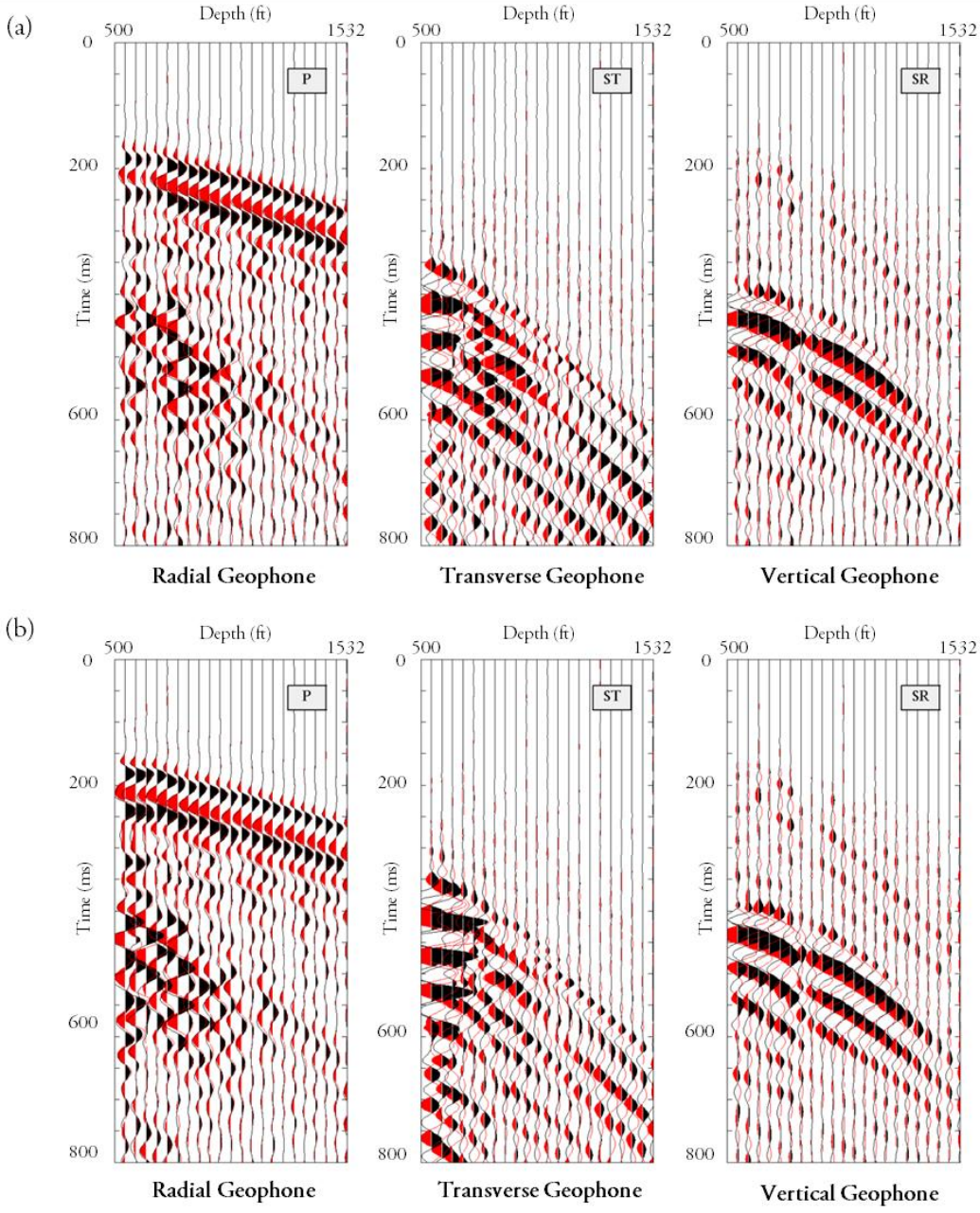

Figure 4.21: The data generated by positive (+20°) and negative (-20°) inclined-impact sources after time-shift alignment at all receiver stations. Red traces were produced by a positive 20° inclined impact. Black traces were generated by a negative 20° inclined impact. (a) Data recorded in the inline plane. (b) Data recorded in the crossline plane.

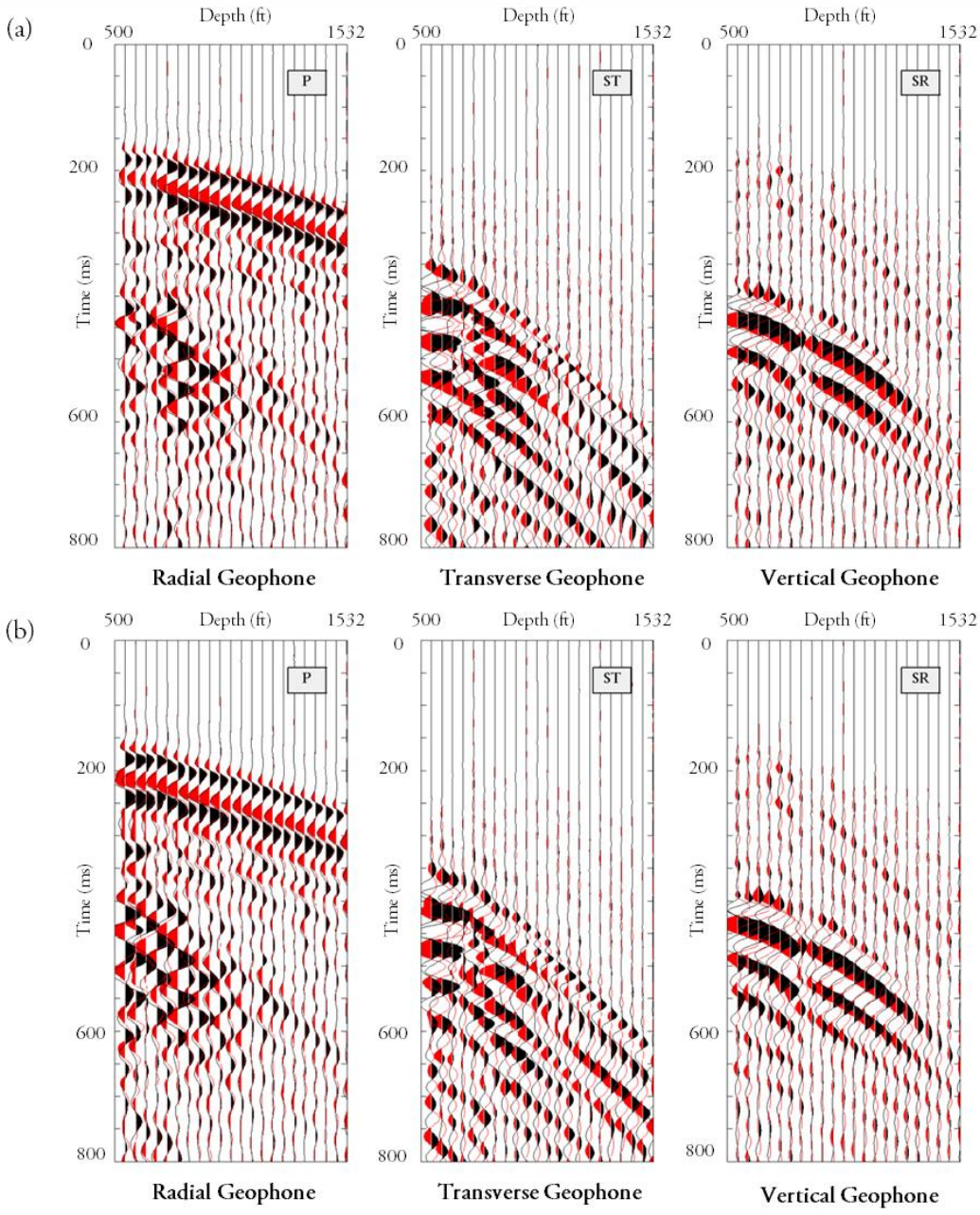

Figure 4.22: The data generated by positive (+30°) and negative (-30°) inclined-impact source after time-shift alignment at all receiver stations. Red traces were produced by a positive 30° inclined impact. Black traces were generated by a negative 30° inclined impact. (a) Data recorded in the inline plane. (b) Data recorded in the crossline plane.

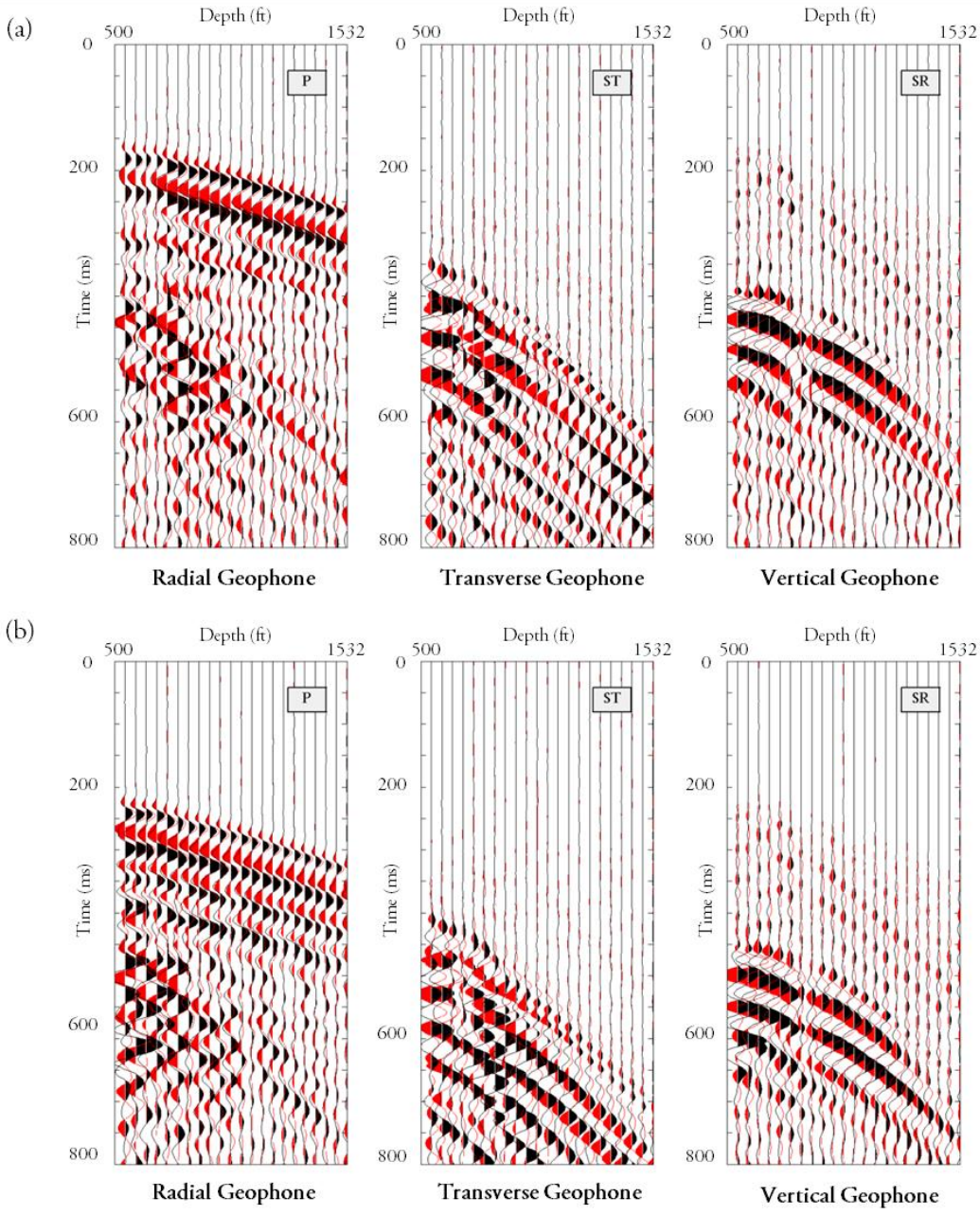

Figure 4.23: The data generated by positive (+45°) and negative (-45°) inclined-impact source after time-shift alignment at all receiver stations. Red traces were produced by a positive 45° inclined impact. Black traces were generated by a negative 45° inclined impact. (a) Data recorded in the inline plane. (b) Data recorded in the crossline plane.

After data generated by two opposite-azimuth inclined sources are phase aligned, it is possible to isolate direct-S and direct-P modes via simple subtraction and addition processes. As discussed and illustrated in Figure 4.2, adding data generated by positive and negative inclined-impact sources strengthens their common direct-P mode but cancels their opposite polarity direct-S modes. Similarly, subtracting data produced by positive and negative inclined impacts reinforces their opposite-polarity direct-S modes and eliminates their equal-polarity direct-P modes. Therefore, this simple addition provides isolated direct-P modes, and isolated direct-S modes are obtained by simple subtraction.

The displays in Figure 4.24 through 4.29 show applications of these simple addition and subtraction process to the data displayed in Figures 4.21 through 4.23. Isolated direct-P modes for various inclination angles are obtained by adding two wavefields generated by opposing impact directions (Figures 4.24a, 4.25a, 4.26a, 4.27a, 4.28a, 4.29a). Similarly, the subtraction of the same wavefields produces the isolated direct-S modes illustrated in Figures 4.24b, 4.25b, 4.26b, 4.27b, 4.28b, 4.29b. The direct-S modes obtained from subtraction of data applied from opposing directions are now comparable with the data produced by a vertical-impact source.

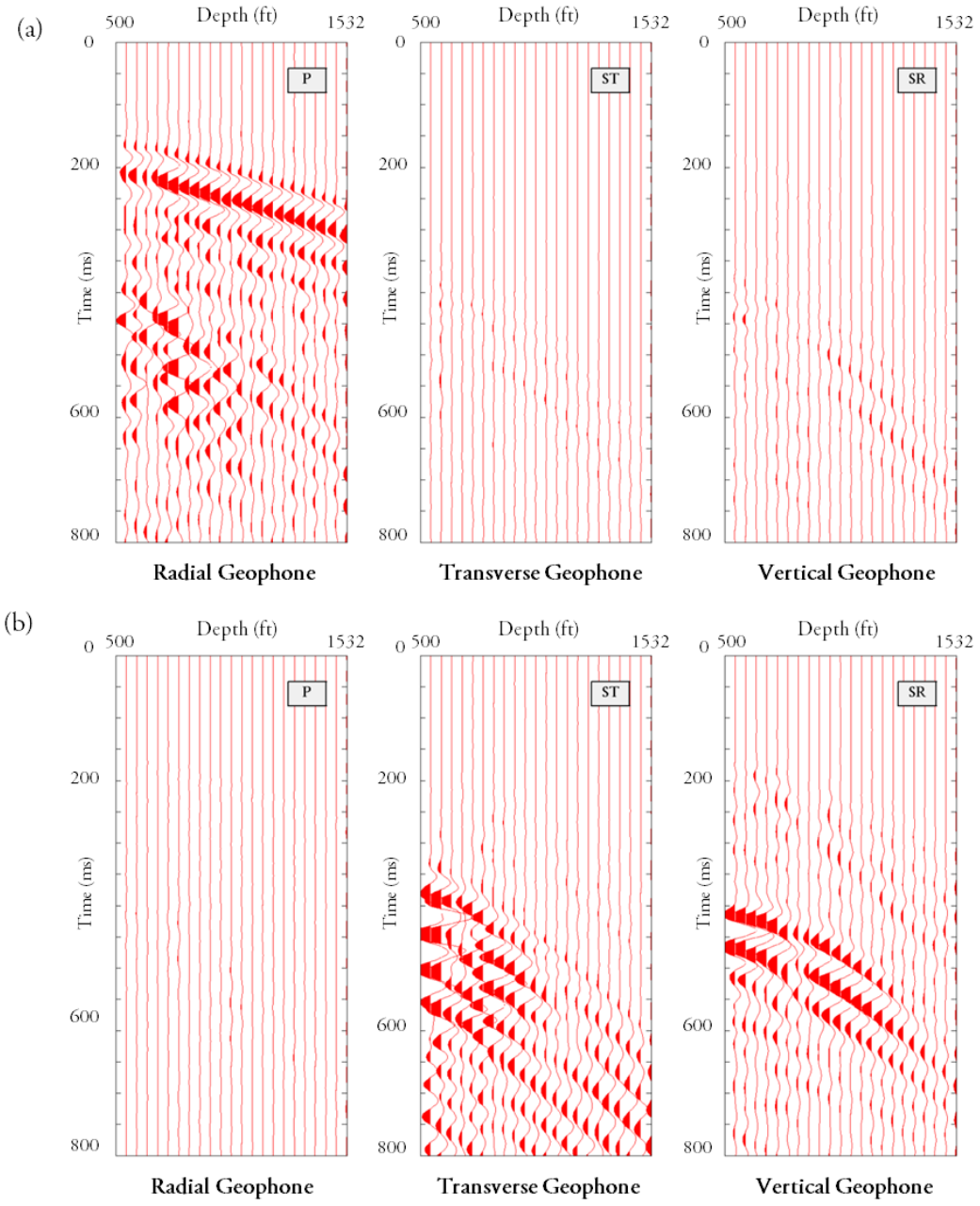

Figure 4.24: (a) Addition of the positive and negative 20° inline inclined-impact wavefields displayed in Figure 4.21. Addition process yields isolated direct-P mode and provides effective cancellation of the direct-S modes. (b) Subtraction of the positive and negative 20° inline inclined-impact wavefield illustrated in Figure 4.21. Re-enforced direct-S modes are obtained with an effective cancellation of the direct-P mode.

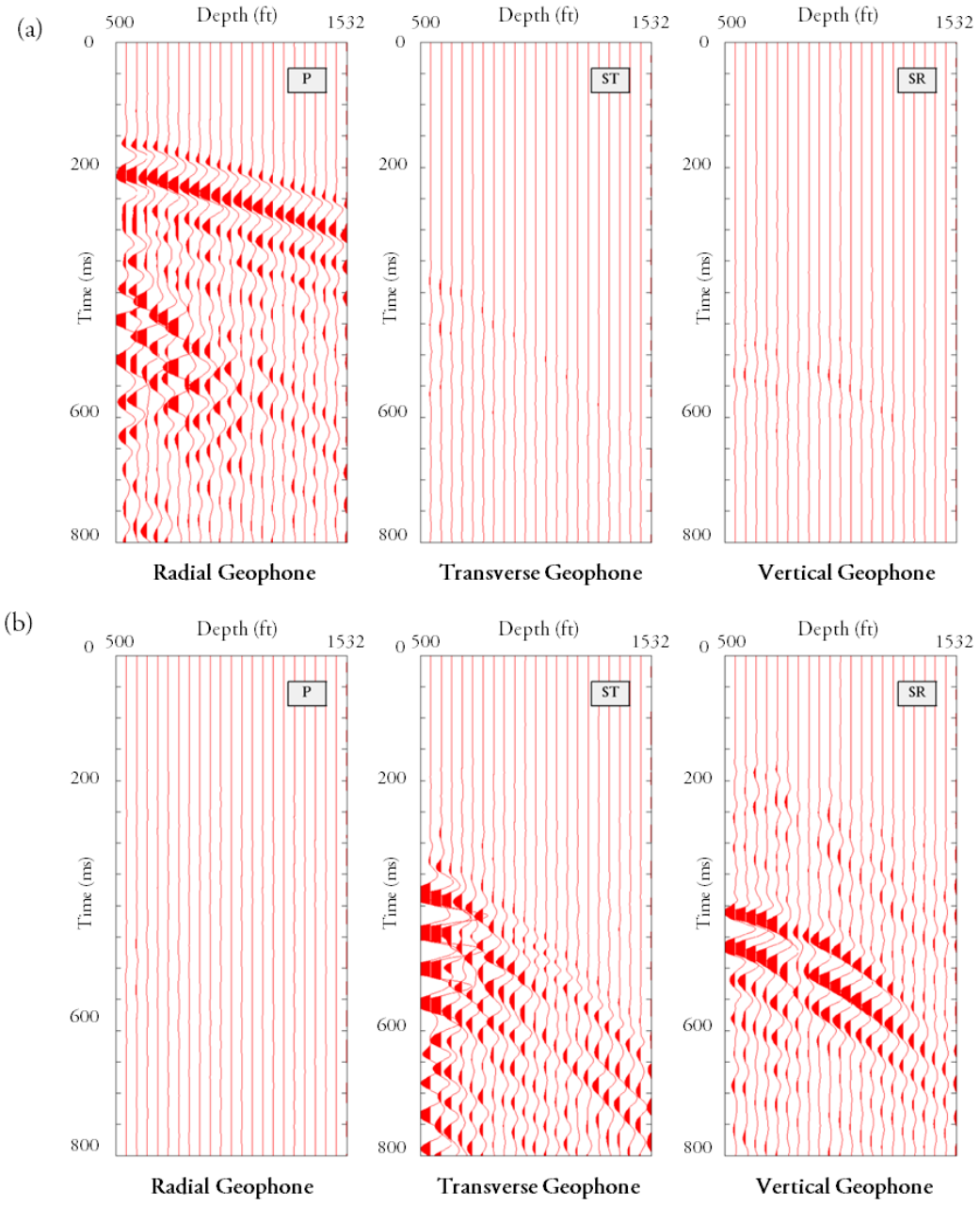

Figure 4.25: (a) Addition of the positive and negative 20° crossline inclined-impact wavefields displayed in Figure 4.21. Addition process yields isolated direct-P mode and provides effective cancellation of the direct-S modes. (b) Subtraction of the positive and negative 20° crossline inclined-impact wavefield illustrated in Figure 4.21. Re-enforced direct-S modes are obtained with an effective cancellation of the direct-P mode.

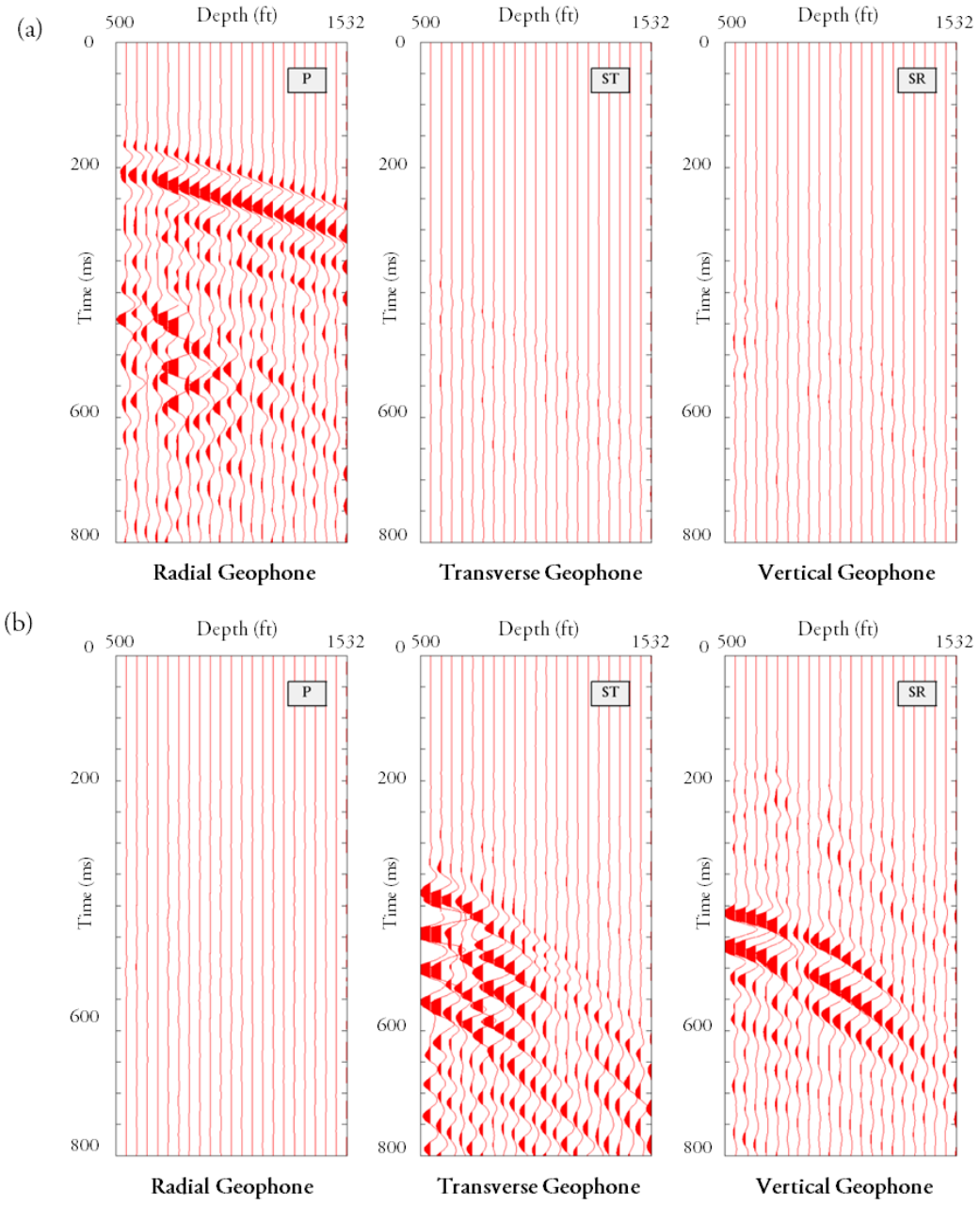

Figure 4.26: (a) Addition of the positive and negative 30° inline inclined-impact wavefields displayed in Figure 4.22. Addition process yields isolated direct-P mode and provides effective cancellation of the direct-S modes. (b) Subtraction of the positive and negative 30° inline inclined-impact wavefield illustrated in Figure 4.22. Re-enforced direct-S modes are obtained with an effective cancellation of the direct-P mode.

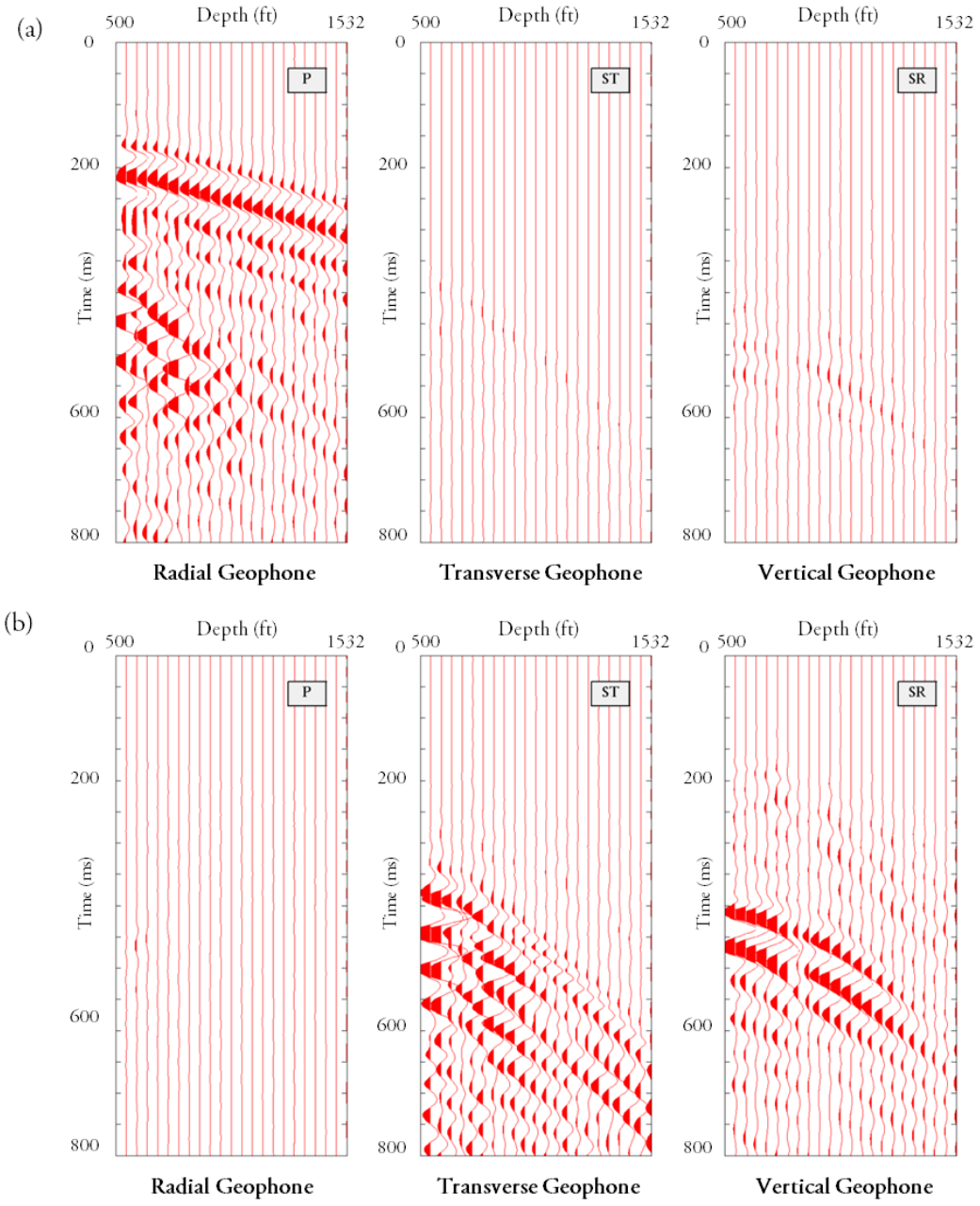

Figure 4.27: (a) Addition of the positive and negative 30° crossline inclined-impact wavefields displayed in Figure 4.22. Addition process yields isolated direct-P mode and provides effective cancellation of the direct-S modes. (b) Subtraction of the positive and negative 30° crossline inclined-impact wavefield illustrated in Figure 4.22. Re-enforced direct-S modes are obtained with an effective cancellation of the direct-P mode.

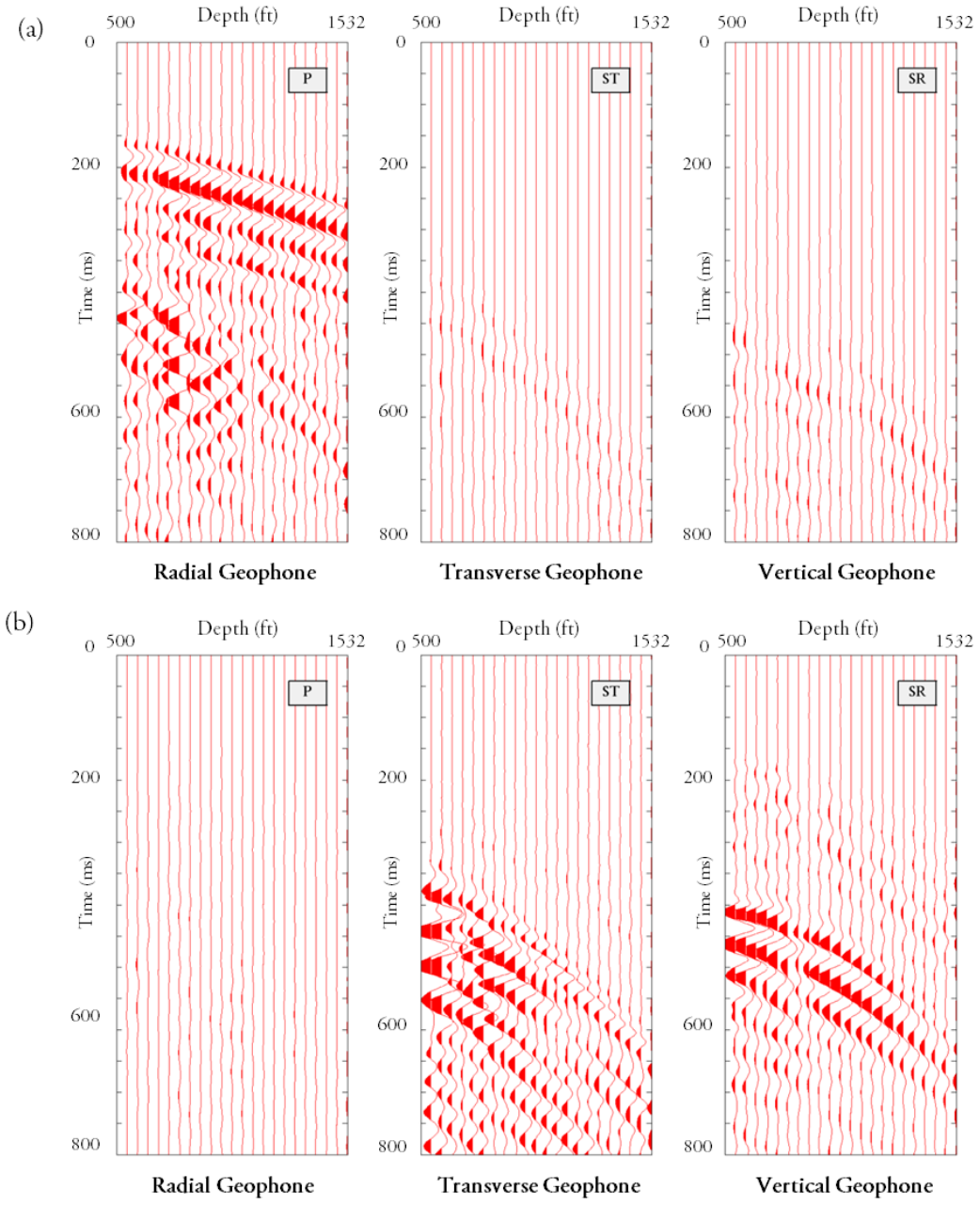

Figure 4.28: (a) Addition of the positive and negative 45° inline inclined-impact wavefields displayed in Figure 4.23. Addition process yields isolated direct-P mode and provides effective cancellation of the direct-S modes. (b) Subtraction of the positive and negative 45° inline inclined-impact wavefield illustrated in Figure 4.23. Re-enforced direct-S modes are obtained with an effective cancellation of the direct-P mode.

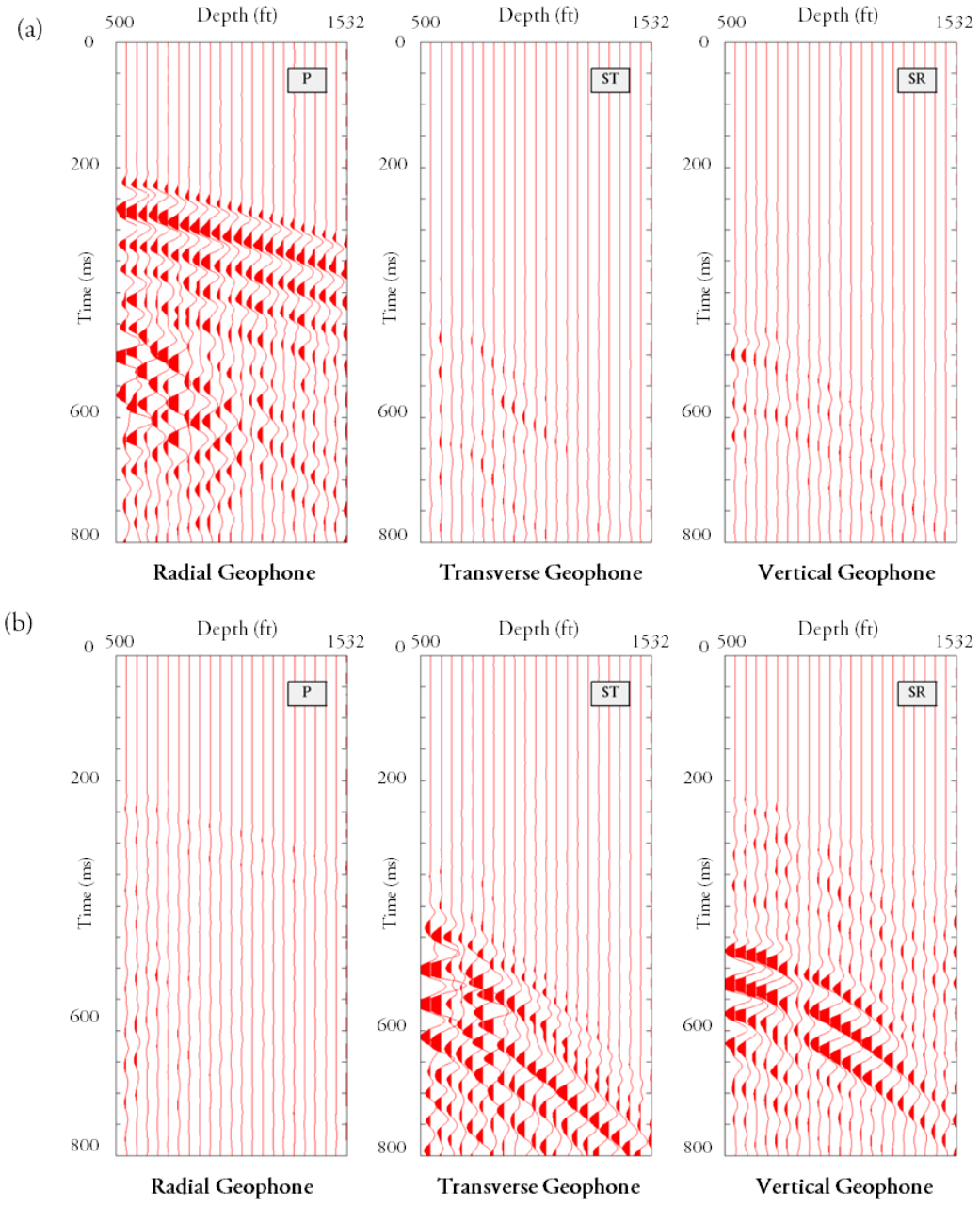

Figure 4.29: (a) Addition of the positive and negative 45° crossline inclined-impact wavefields displayed in Figure 4.23. Addition process yields isolated direct-P mode and provides effective cancellation of the direct-S modes. (b) Subtraction of the positive and negative 45° crossline inclined-impact wavefield illustrated in Figure 4.23. Re-enforced direct-S modes are obtained with an effective cancellation of the direct-P mode.

4.2.2. Comparison of Direct-S modes Produced by Impact Vector Sources

One purpose of my thesis is to compare direct-S modes produced by a vertical impact, an inclined-impact and a shot-hole explosive in order to determine similarities and differences among these sources. These comparisons may test the hypothesis that a vertical-force source and its companion horizontal-force sources generate equivalent direct-S modes. The data recorded when the VSX source (Figure 2.3) applied a vertical impact to the earth at source station 5 and when a shot-hole explosive was fired at the same source station are displayed in Figures 4.15 and 4.16. The raw vertical impact and shot-hole explosive data were processed with the same strategy as the inclined-impact data were. After geophone rotation processes were done for shot-explosive and vertical-impact data, direct-S wavefields produced by vertical impact and 30° inclined-impact sources were compared by plotting two S-wave wavefields as overlays (Figure 4.30) to understand similarities and differences between the wavefields. When a bulk time shift is applied to optimize phase alignment of the inclined-impact data, we observed that the two sets of direct-S traces are essentially identical but have opposite polarity. The close correlation between the superimposed wavefields in Figure 4.30 supports the principle that a vertical-force source and horizontal-force source create the same direct-S wavefield. To display phase shifts and reversed polarities of direct-S wavefields and to compare energy strengths of direct-S modes in equal time windows, a bulk normal move out (NMO) correction is applied (Figures 4.31 through 4.36).

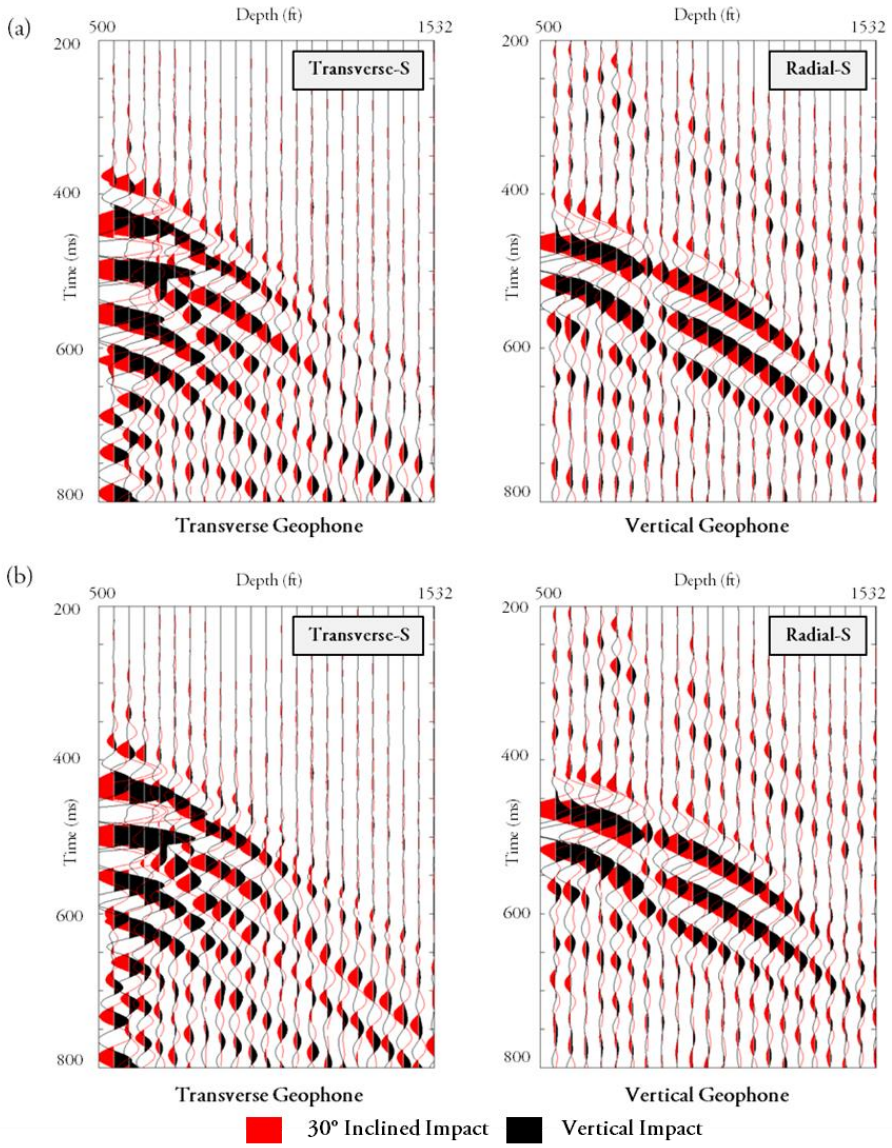

Figure 4.30: Direct-S modes generated by a vertical impact (black) and by inclined impact (red). The incident angle of inclined-impact source was 30° in (a) the inline plane and (b) in the crossline plane. A bulk time shift was applied to vertical-impact data to minimize phase differences.

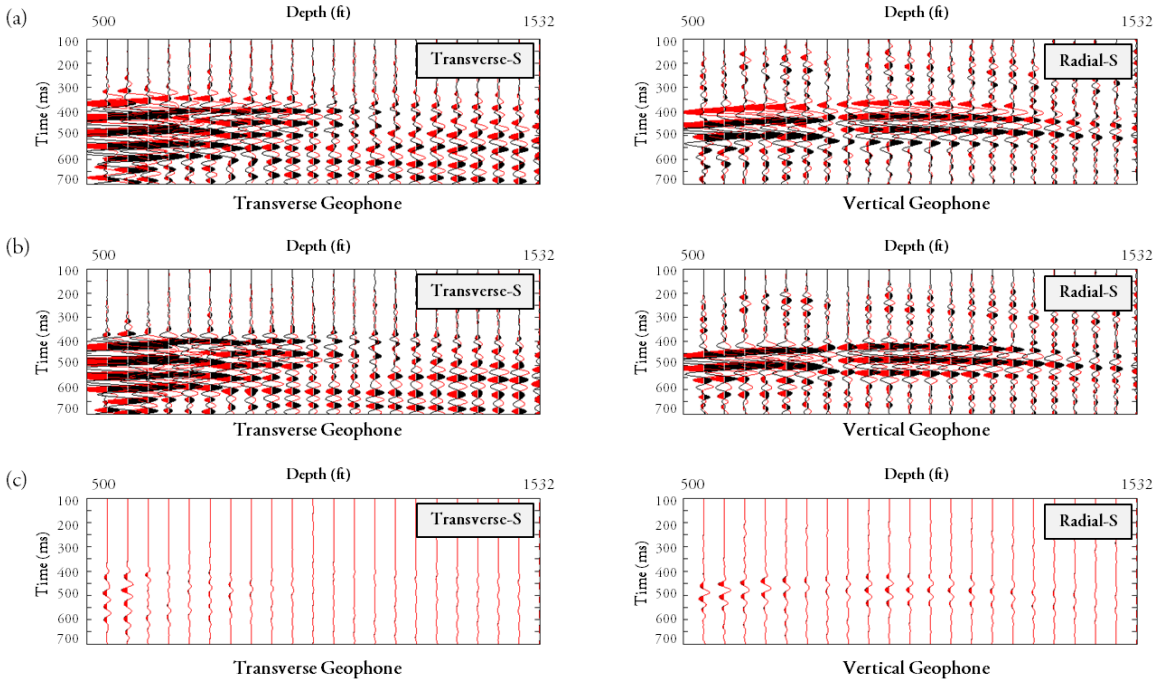

Figure 4.31: Comparison of shear wave components for vertical-impact data and data obtained by subtracting 20° inclined impacts applied from opposite directions in the inline plane. Vertical-impact data after geophone rotation are displayed as black wiggle traces. Red wiggle traces represent the subtraction of opposite-azimuth inclined-impact data. (a) Raw data. (b) Time-shifted data. (c) Differences between red and black traces.

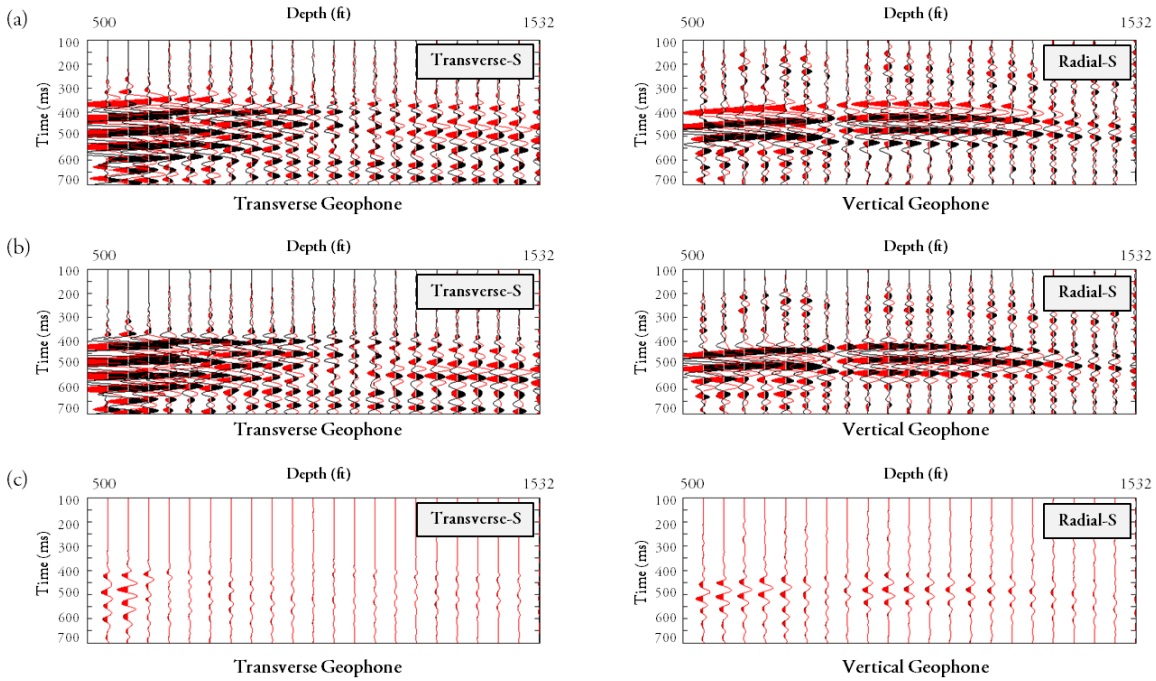

Figure 4.32: Comparison of shear wave components for vertical-impact data and data obtained by subtracting 20° inclined impacts applied from opposite directions in the crossline plane. Vertical-impact data after geophone rotation are displayed as black wiggle traces. Red wiggle traces represent the subtraction of opposite-azimuth inclined-impact data. (a) Raw data. (b) Time-shifted data. (c) Differences between red and black traces.

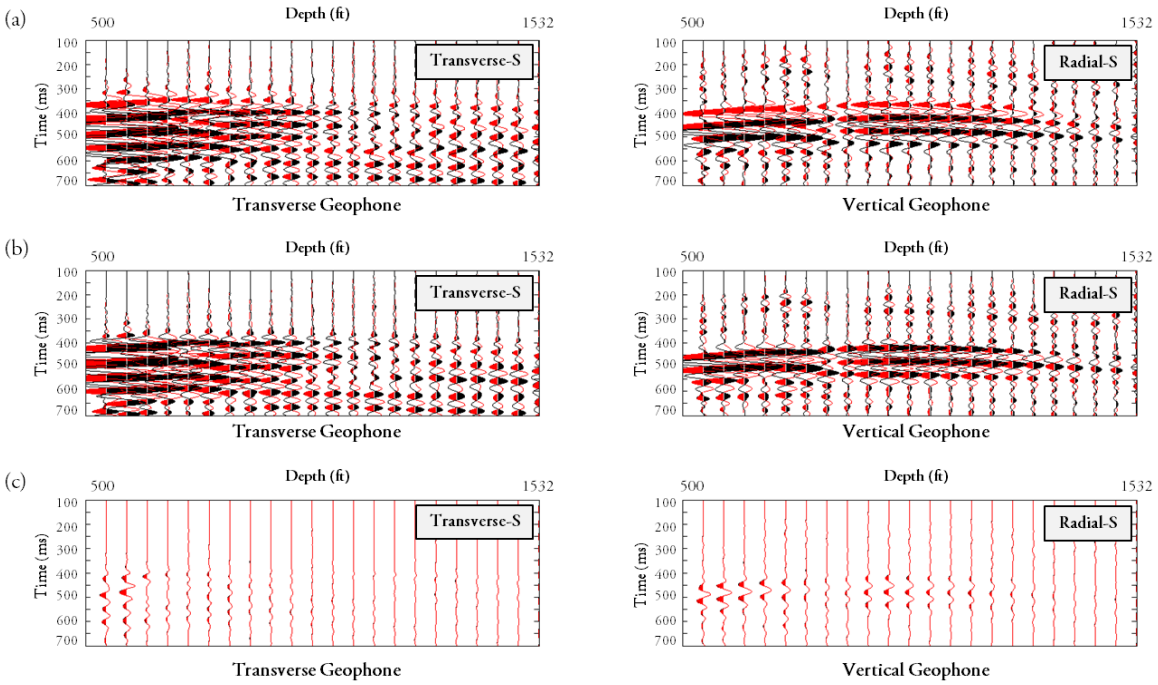

Figure 4.33: Comparison of shear wave components for vertical-impact data and data obtained by subtracting 30° inclined impacts applied from opposite directions in the inline plane. Vertical-impact data after geophone rotation are displayed as black wiggle traces. Red wiggle traces represent the subtraction of opposite-azimuth inclined-impact data. (a) Raw data. (b) Time-shifted data. (c) Differences between red and black traces.

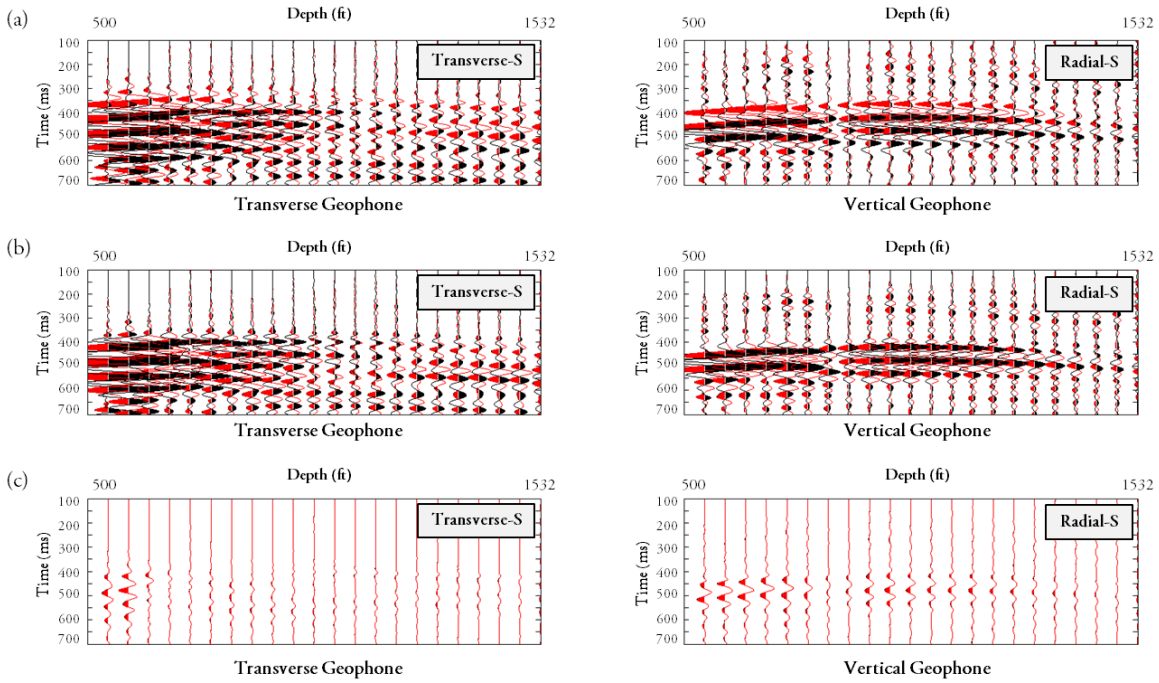

Figure 4.34: Comparison of shear wave components for vertical-impact data and data obtained by subtracting 30° inclined impacts applied from opposite directions in the crossline plane. Vertical-impact data after geophone rotation are displayed as black wiggle traces. Red wiggle traces represent the subtraction of opposite-azimuth inclined-impact data. (a) Raw data. (b) Time-shifted data. (c) Differences between red and black traces.

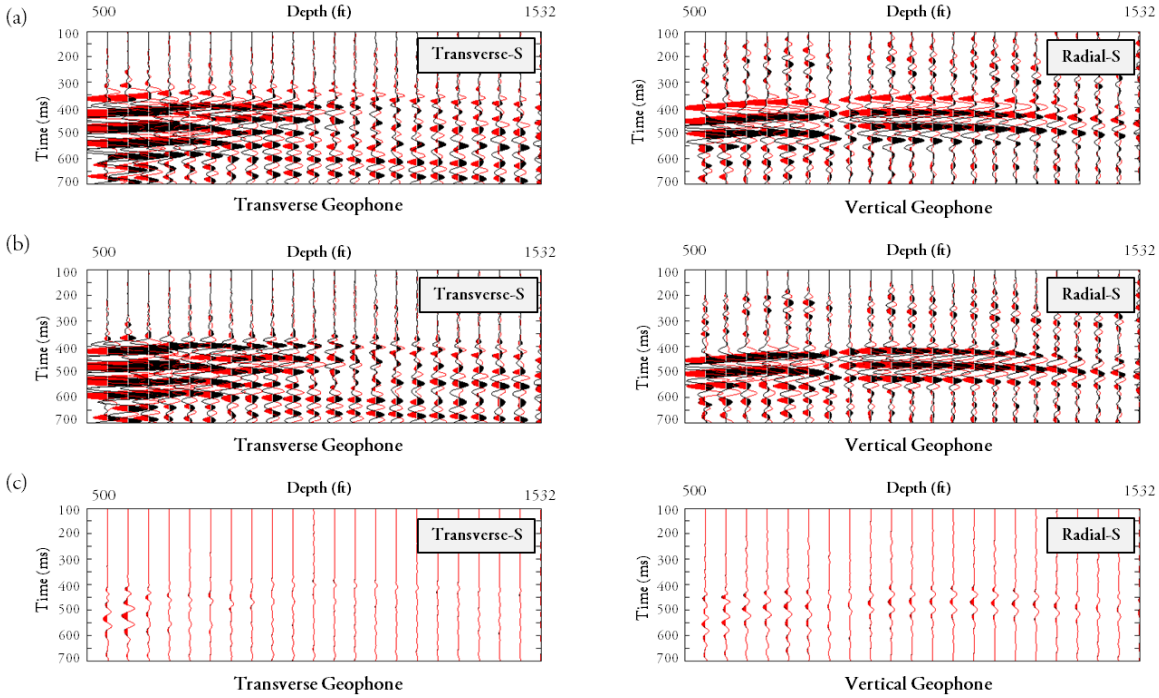

Figure 4.35: Comparison of shear wave components for vertical-impact data and data obtained by subtracting 45° inclined impacts applied from opposite directions in the inline plane. Vertical-impact data after geophone rotation are displayed as black wiggle traces. Red wiggle traces represent the subtraction of opposite-azimuth inclined-impact data. (a) Raw data. (b) Time-shifted data. (c) Differences between red and black traces.

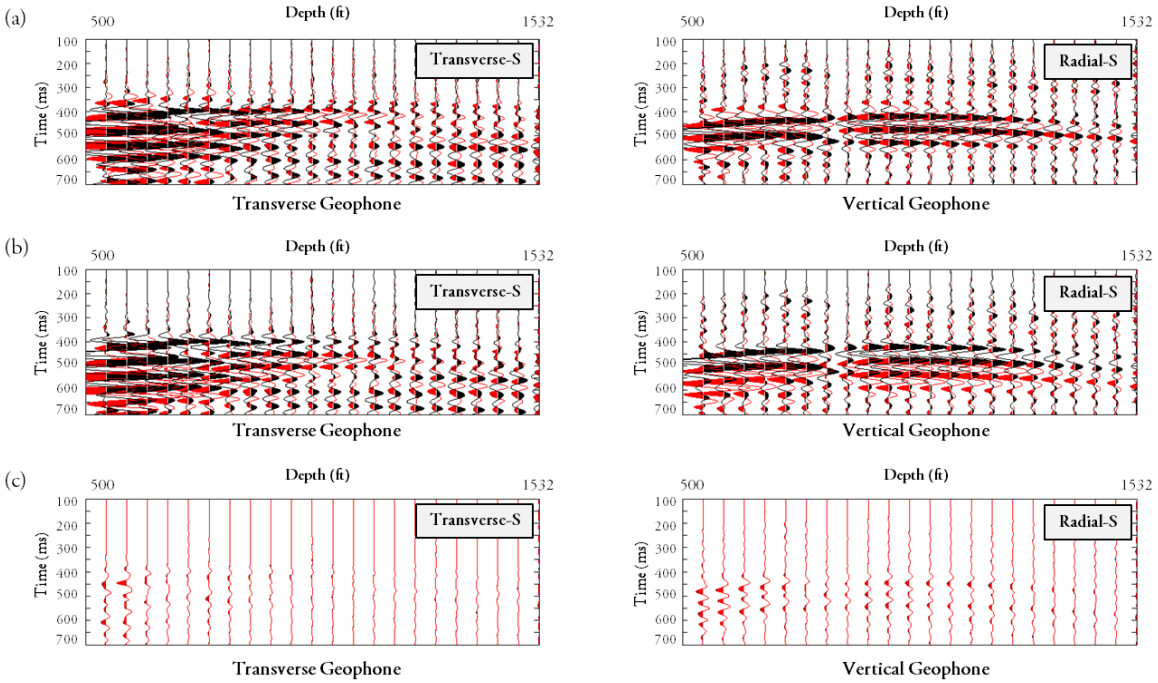

Figure 4.36: Comparison of shear wave components for vertical-impact data and data obtained by subtracting 45° inclined impacts applied from opposite directions in the crossline plane. Vertical-impact data after geophone rotation are displayed as black wiggle traces. Red wiggle traces represent the subtraction of opposite-azimuth inclined-impact data. (a) Raw data. (b) Time-shifted data. (c) Differences between red and black traces.

The time difference between data generated by two different impacts must be resolved (Figures 4.31a, 4.32a, 4.33a, 4.34a, 4.35a, and 4.36a). After a time shift to align first arrivals, wiggle traces for both data sets seem to have almost same shear response wave with opposite polarity (Figures 4.31b, 4.32b, 4.33b, 4.34b, 4.35b, and 4.36b). By adding the red and black wiggle traces, energy on each panel cancels each other (Figures 4.31c, 4.32c, 4.33c, 4.34c, 4.35c, and 4.36c).

In addition to the same direct-S wavefields, it is important to compare the energy level of direct-S modes produced by a vertical impact, shot-hole explosive and inclined

impacts. RMS amplitudes of direct-S first arrivals produced by these sources are analyzed and compared in Figures 4.37 and 4.38. Wavelet amplitudes were analyzed and calculated in 90-ms windows starting at the first-break time of each first arrival. For each wave mode, wiggles captured by the same window represent the downgoing illuminating wavefield.

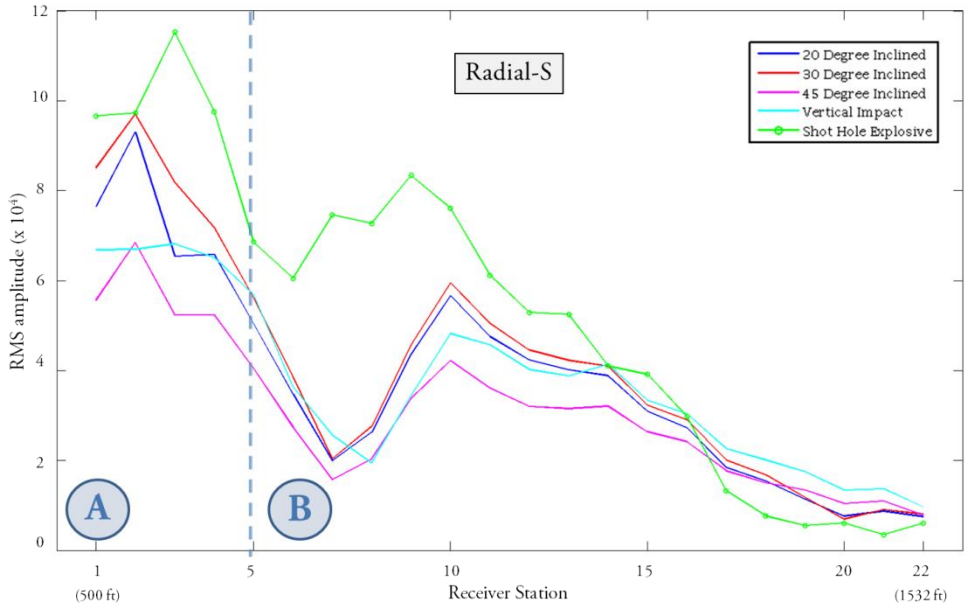

Figure 4.37: Comparison of the amplitude strengths of radial-S direct modes generated by a vertical impact, a range of inclined impacts, and a shot-hole explosive. The explosive source was a 1-kg (2.2-lb) charge placed at a depth of 6 m (20-ft). A= domain of shallow reverberations. B= domain of representative body waves.

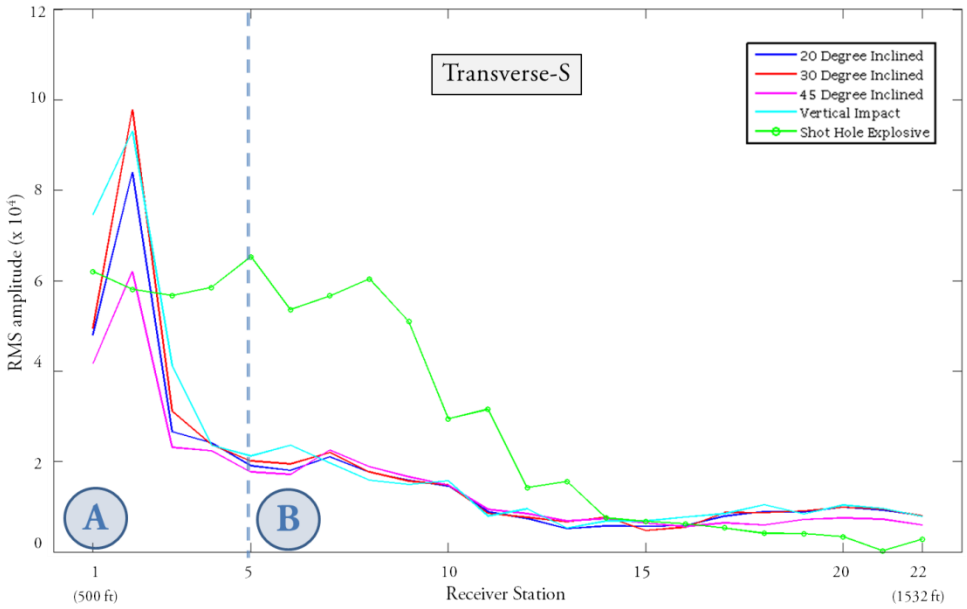

Figure 4.38: Comparison of the amplitude strengths of transverse-S direct modes generated by a vertical impact, a range of inclined impacts, and a shot-hole explosive. The explosive source was a 1-kg (2.2-lb) charge placed at a depth of 6 m (20-ft). A= domain of shallow reverberations. B= domain of representative body waves.

To compare energy contents in a fair way, the amplitudes of the data generated by the vertical impact are multiplied by 2 because the amplitudes of inclined-impact sources contain energy generated by two opposing impacts. Because of the large offset distance of the same (1000 ft) large amplitude reverberating refractions are captured by the shallowest receivers displayed in domain A (Figures 4.37 and 4.38). The data recorded at stations deeper than receiver station 5 (depth = 697 ft) displayed in domain B (Figures 4.37 and 4.38) are more representative of the amplitudes of shear body waves that illuminate deeper targets. Figures 4.37 and 4.38 show that a vertical impact, an inclined impact, and a 1-kg shot-hole explosive at a depth of 6 m produce almost the same amount of direct-S illumination energy. These figures also reveal an interesting point that shear rate of decay of wave energy embedded in transverse-S and radial-S modes produced by

an inclined-impact or a vertical impact source is less than that of the rate of decay of shear wave energy produced by a shot-hole explosive.

Another objective of this project is to compare the frequency spectra of S-wave data produced by inclined-impact, vertical-impact, and shot-hole explosive sources. Frequency attributes of the wave modes produced by the sources are displayed as Figures 4.39 through 4.48. These displays illustrate the data windows spanning the downgoing illumination wavelets where frequency spectra were analyzed. The data highlighted in the analysis window have negligible non-mode noise and are almost pure S-wave-mode signal. Therefore, a reasonable indication of the signal-frequency content for each downgoing S-wave illumination wavefield is indicated by each calculated frequency spectrum. Amplitudes that are more than 10 dB below the peak of an amplitude spectrum are considered to be too small to make a significant contribution and are ignored. The frequency spectrum extending above each 10 dB defines the effective signal frequency contents of each wave mode.

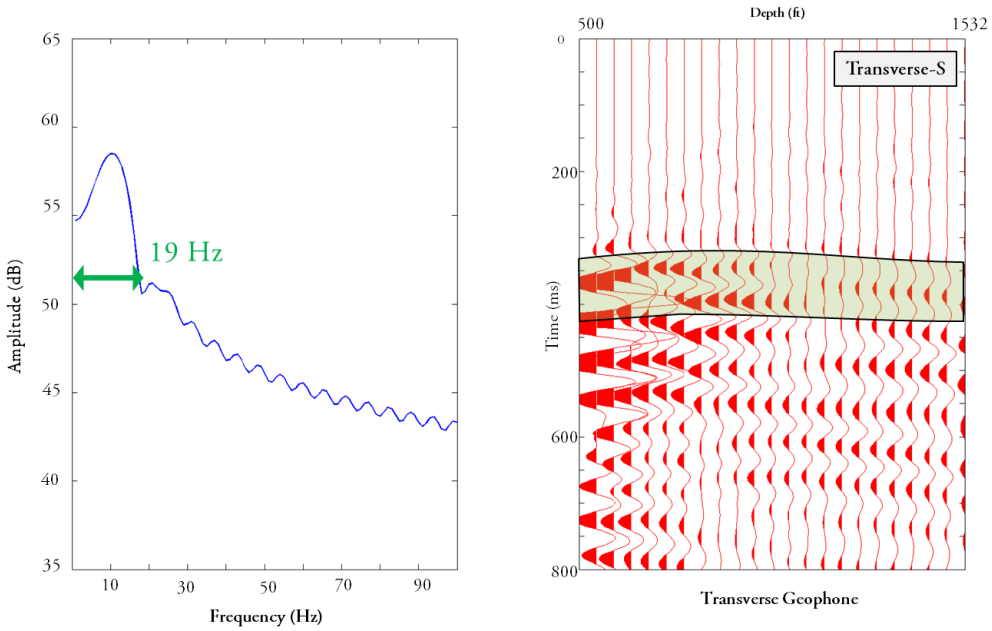

Figure 4.39: Frequency analysis of transverse-S modes produced by a 20° inclined-impact source applied in the inline direction. Amplitudes of the frequency spectra define relative strengths of the transverse direct-S mode propagating away from source station 5.

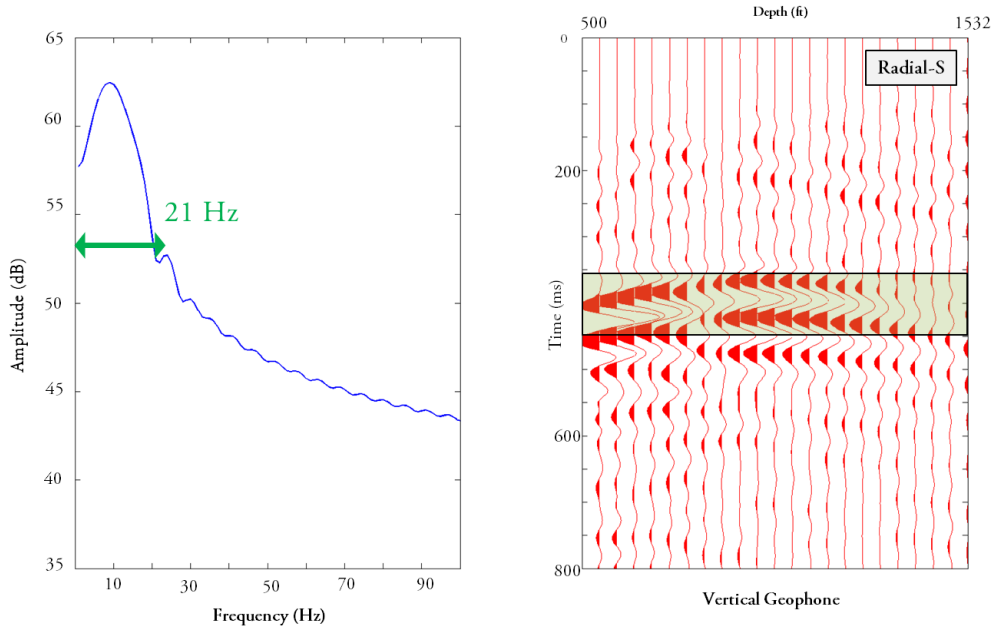

Figure 4.40: Frequency analysis of radial-S modes produced by a 20° inclined-impact source applied in the inline direction. Amplitudes of the frequency spectra define relative strengths of the radial direct-S mode propagating away from source station 5.

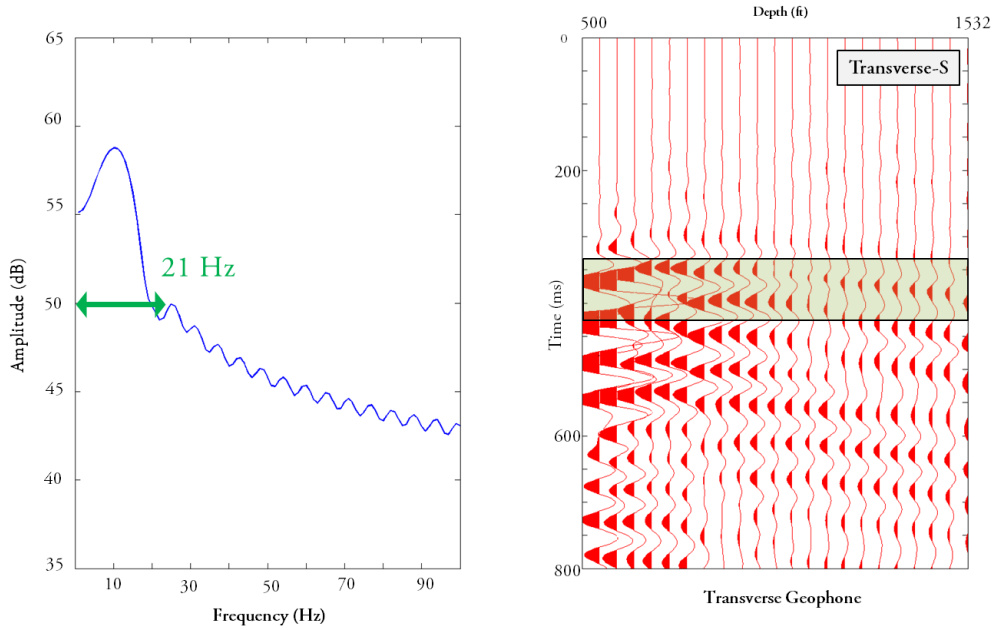

Figure 4.41: Frequency analysis of transverse-S modes produced by a 30° inclined-impact source applied in the inline direction. Amplitudes of the frequency spectra define relative strengths of the transverse direct-S mode propagating away from source station 5.

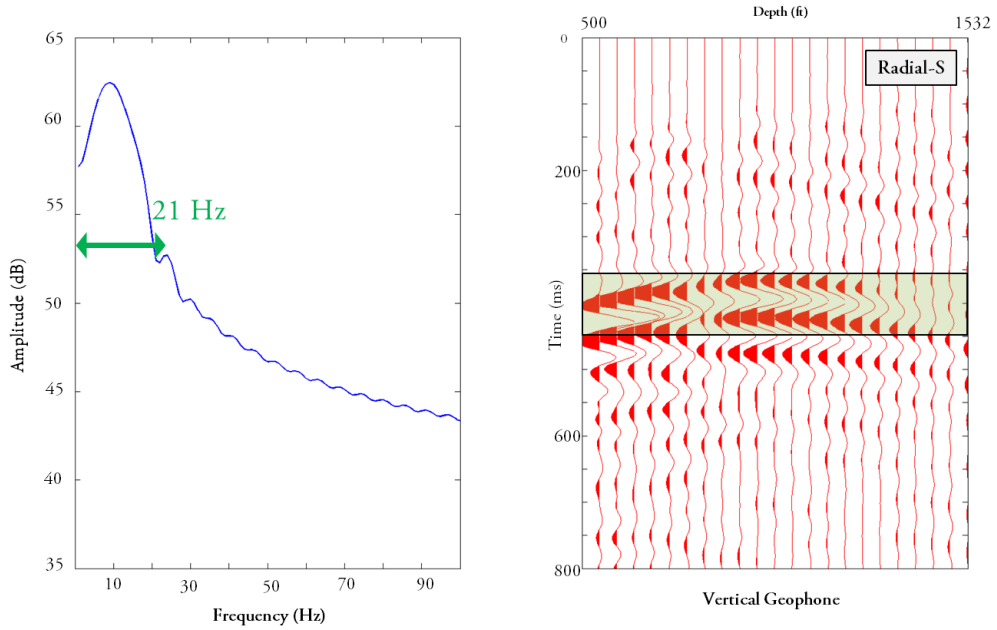

Figure 4.42: Frequency analysis of radial-S modes produced by a 30° inclined-impact source applied in the inline direction. Amplitudes of the frequency spectra define relative strengths of the radial direct-S mode propagating away from source station 5.

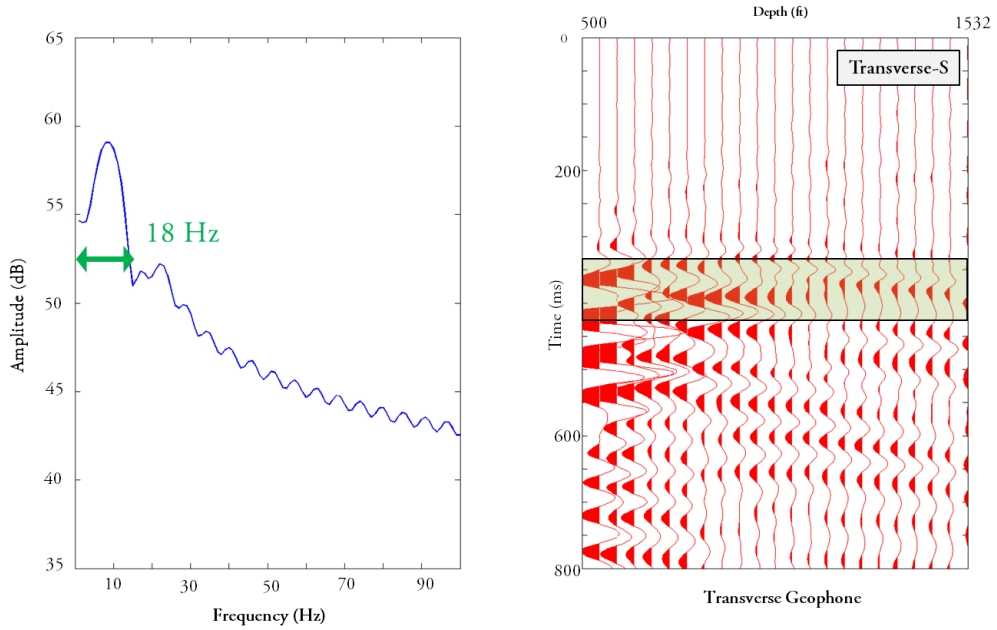

Figure 4.43: Frequency analysis of transverse-S modes produced by a 45° inclined-impact source applied in the inline direction. Amplitudes of the frequency spectra define relative strengths of the transverse direct-S mode propagating away from source station 5.

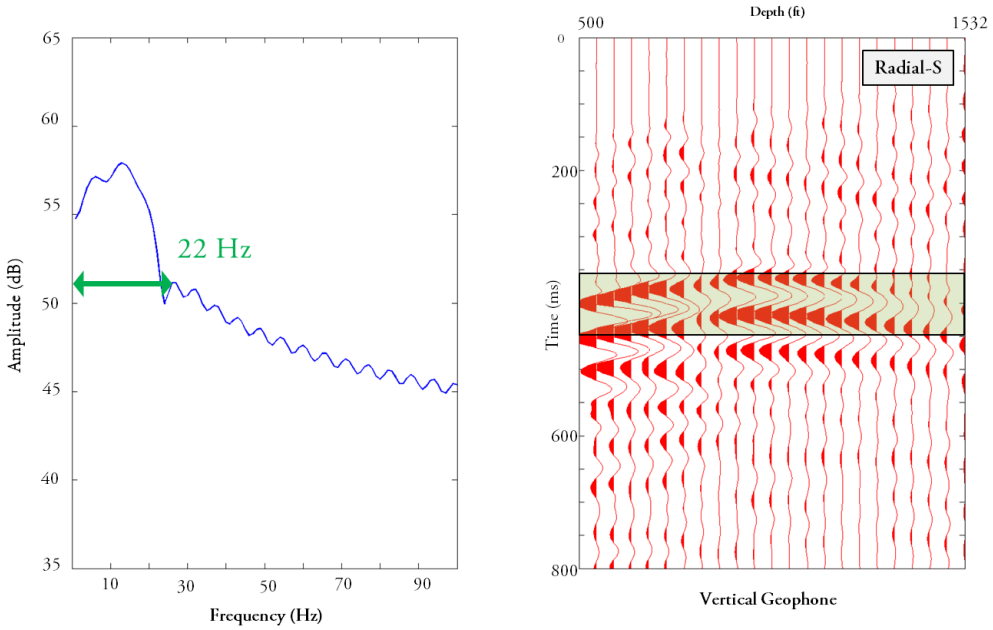

Figure 4.44: Frequency analysis of radial-S modes produced by a 45° inclined-impact source applied in the inline direction. Amplitudes of the frequency spectra define relative strengths of the radial direct-S mode propagating away from source station 5.

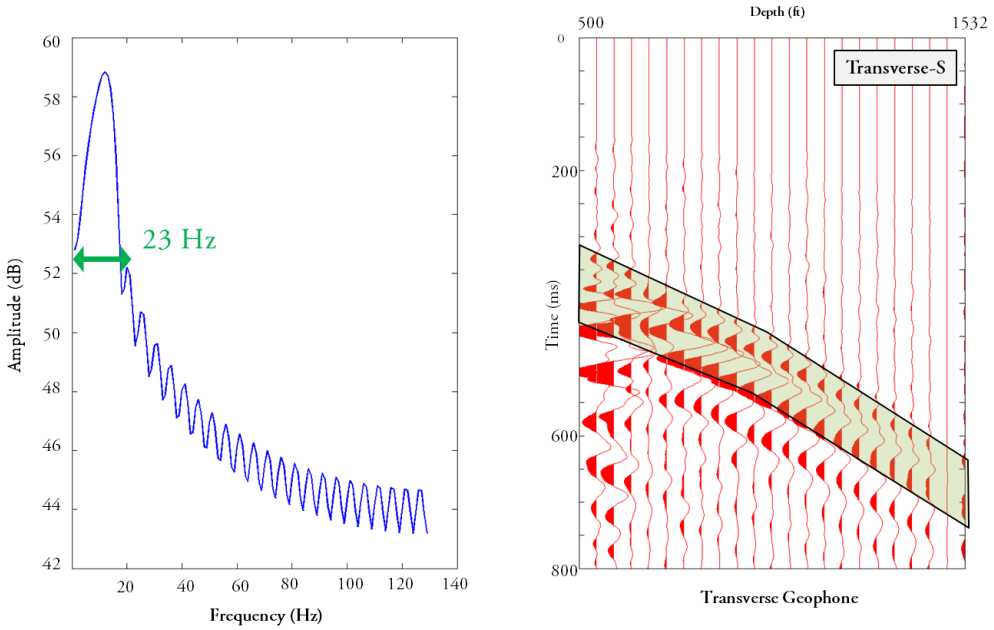

Figure 4.45: Frequency analysis of transverse-S modes produced by a shot-hole explosive buried at a depth of 6 m (20 ft). Amplitudes of the frequency spectra define relative strengths of the transverse direct-S mode propagating away from source station 5.

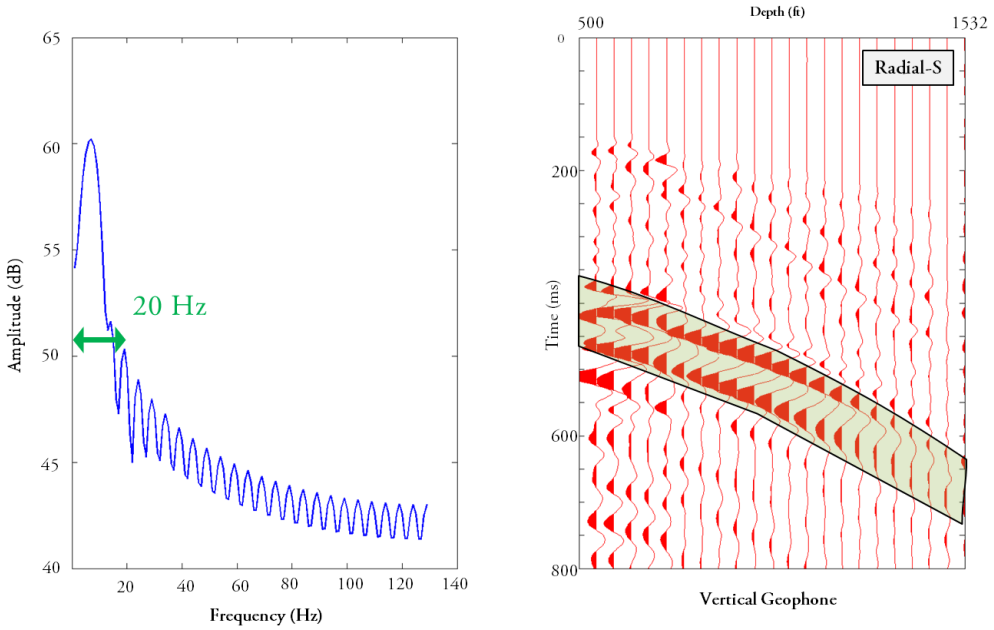

Figure 4.46: Frequency analysis of radial-S modes produced by a shot-hole explosive buried at a depth of 6 m (20 ft). Amplitudes of the frequency spectra define relative strengths of the radial direct-S mode propagating away from source station 5.

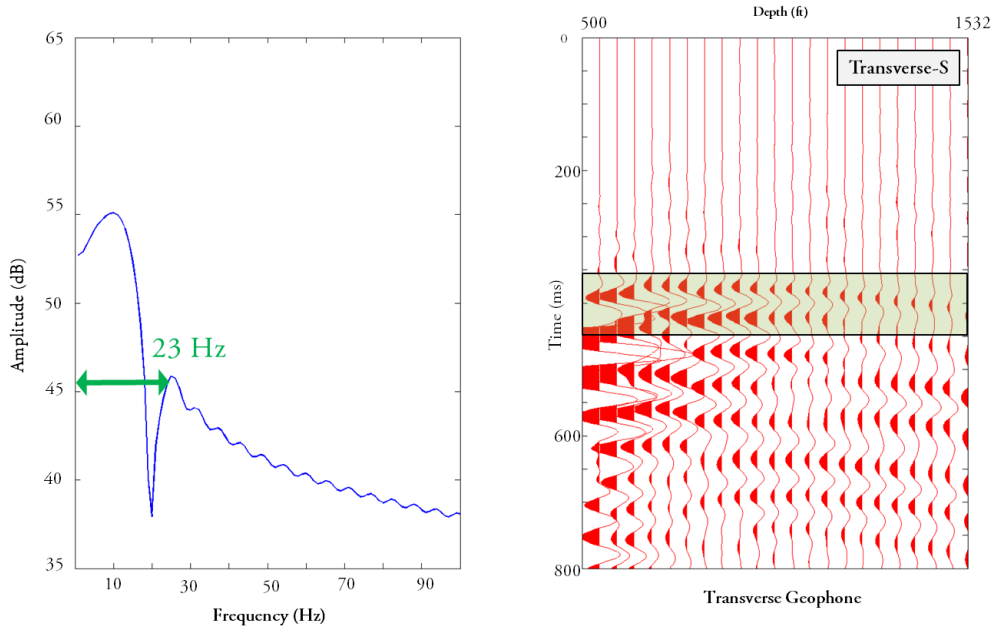

Figure 4.47: Frequency analysis of transverse-S modes produced by a vertical-impact source applied at source station 5. Amplitudes of the frequency spectra define relative strengths of the transverse direct-S mode propagating away from source station 5.

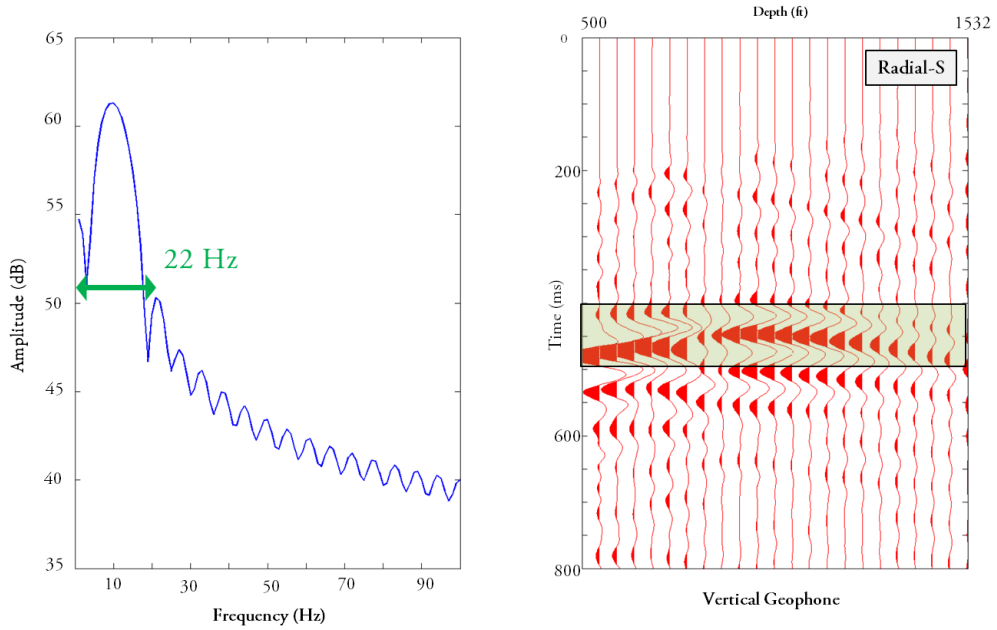

Figure 4.48: Frequency analysis of radial-S modes produced by a vertical-impact source applied at source station 5. Amplitudes of the frequency spectra define relative strengths of the radial direct-S mode propagating away from source station 5.

Frequency and amplitude-level characteristics of direct-S modes produced by impact sources and measured by the downhole vertical-receiver array are displayed on Table-4.2. On this table, calculated amplitudes are listed as "order of magnitude" quantities instead of listing as specific numerical values. These listed amplitudes and frequency characteristics define some important principles which are;

a. All three impact sources produce radial and transverse shear wave modes having the same amplitudes.

b. Frequency content of direct-S modes produced by a shot-hole explosive, vertical-impact source, and inclined-impact sources differ only slightly.

c. Frequency analysis of transverse-S modes produced by a vertical impact source shows that an obvious spectral notch appears around 20-Hz. This

phenomenon should be taken into account in the selection of seismic sources for geological layering where that frequency plays a key role in distinguishing one formation from another.

Amplitude (RMS)	Shot-Hole Explosive	Vertical-Impact	Inclined-Impact
Radial Shear	10^4	10^4	10^4
Transverse Shear	10^4	10^4	10^4
Frequency Contents (Hz)	Shot-Hole Explosive	Vertical-Impact	Inclined-Impact
Radial Shear	23	25	24-29
Transverse Shear	19	24	22-27

Table 4.2: Amplitude and frequency attributes of direct-S wave modes measured by downhole sensors. Amplitudes and frequency bandwidths were calculated from Figures 4.39 - 4.48 for shot station 5.

4.2.3. Comparison of Direct-S modes Produced by Vertical and Horizontal Vibrators

A seismic source that generates strong direct-S modes and zero direct-P modes can be considered as a perfect S-wave source. Because P-SV reflections from a deep interface may contaminate S-S reflections from a shallow interface, possessing a "perfect S-wave source" is always desired in seismic exploration that aims to produce S-imaging of targets. Recent technology provides only two operational seismic sources that produce robust direct-S modes and simultaneously create small amplitude direct-P modes: an inclined-impact source and a horizontal vibrator.

Radiation patterns of shear waves produced by a horizontal vibrator have been studied and compared by various scientists (Robertson and Corrigan, 1983; Dankbaar,

1983; Easley 1992; Sun and Jones 1993; Alkan, 2012). To visually compare wavefields produced by horizontal and vertical vibrator sources, a convenient and basic method that overlays wiggle traces displays of direct-S modes was used in this project so that arrival times and wavelet attributes of the modes can be easily compared. These wavefield comparisons are illustrated on Figure 4.49.

Because the horizontal vibrator was mistakenly oriented in the wrong direction during the field test, an opposite polarity appeared between the direct-S radial mode propagating from the horizontal vibrator and the vertical vibrator. In other words, the direction of the radial-S vector produced by the horizontal vibrator was away from receiver well, but the radial-S vector generated by the vertical vibrator was pointing at the receiver well.

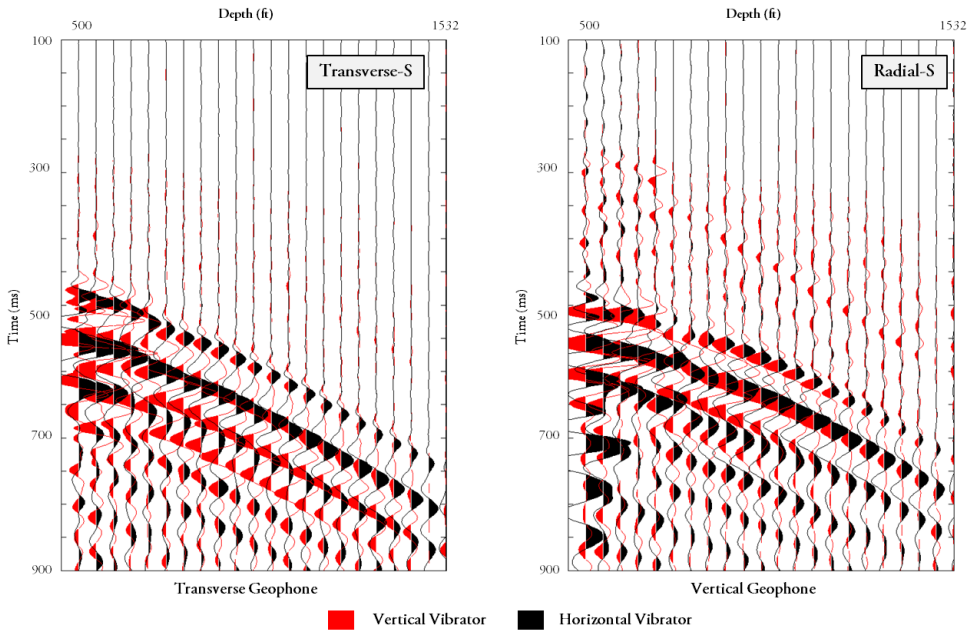

Figure 4.49: Radial and transverse direct-S wavefields produced by a vertical vibrator (red traces) and horizontal vibrator (black traces). Vibrators were located at the same shot location.

Rather than reverse the polarity of one of the direct-S radial modes on Figure 4.49, I left them as shown because a dual-color display of opposite polarity helps in the comparison of direct-S wavefields. For transverse-S wavefields, polarities and wavelet attributes are almost identical and support the concept that the direct-S modes produced by a vertical vibrator are equivalent to the direct-S modes generated by a horizontal vibrator.

In the Devine Test Study, a horizontal vibrator was used in both the inline and the crossline direction as displayed in Figure 1.10 in Chapter 1. A wavelet attribute comparison of wave modes produced by inline and crossline horizontal vibrators is displayed in Figure 4.50. The perfect match in the wavelet attributes with opposite polarity confirms the equivalence of direct-S modes produced by an inline and crossline horizontal vibrator.

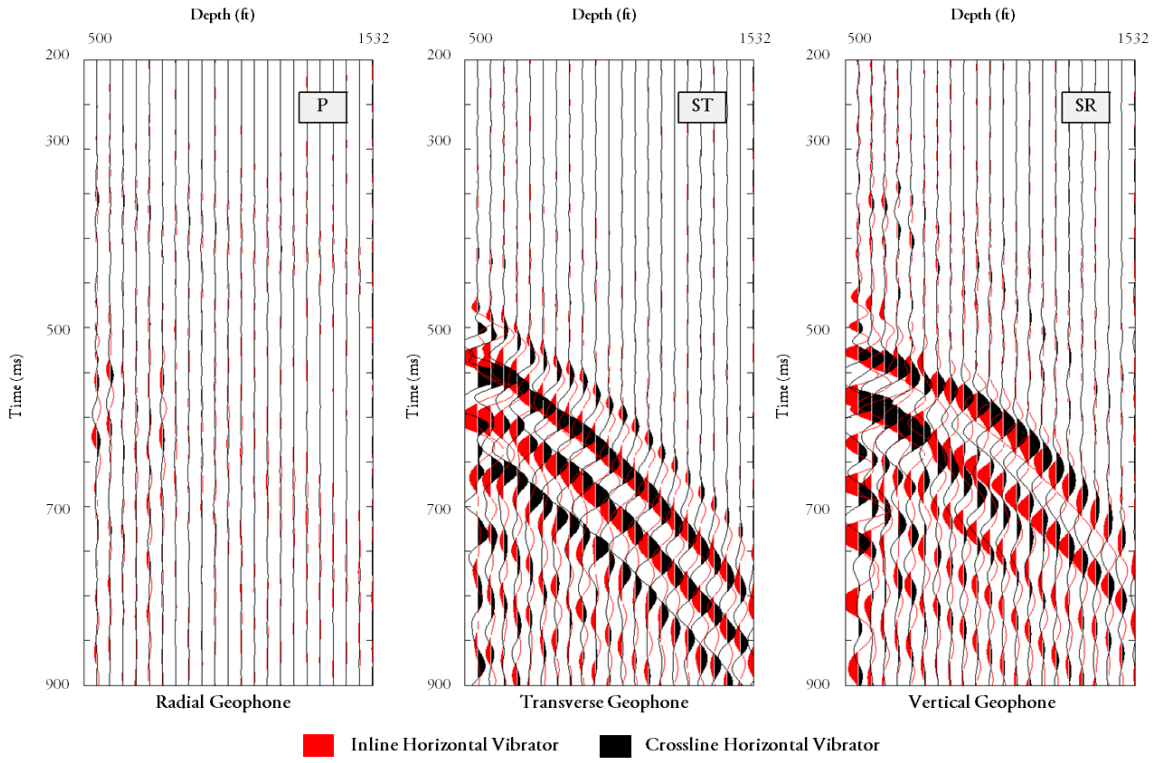

Figure 4.50: Comparison of wavefields produced by an inline horizontal vibrator (red traces) and crossline horizontal vibrator (black traces). Vibrators were located at the same shot location.

RMS amplitudes of direct-S first arrivals produced by a horizontal vibrator (inline and crossline) and a vertical vibrator are analyzed and compared in Figures 4.51 and 4.52. Wavelet amplitudes were analyzed and calculated in 90-ms windows starting at the first-break times of each arriving direct-S mode. For each wave mode, wiggles captured by the same window represent the downgoing illuminating wavefield.

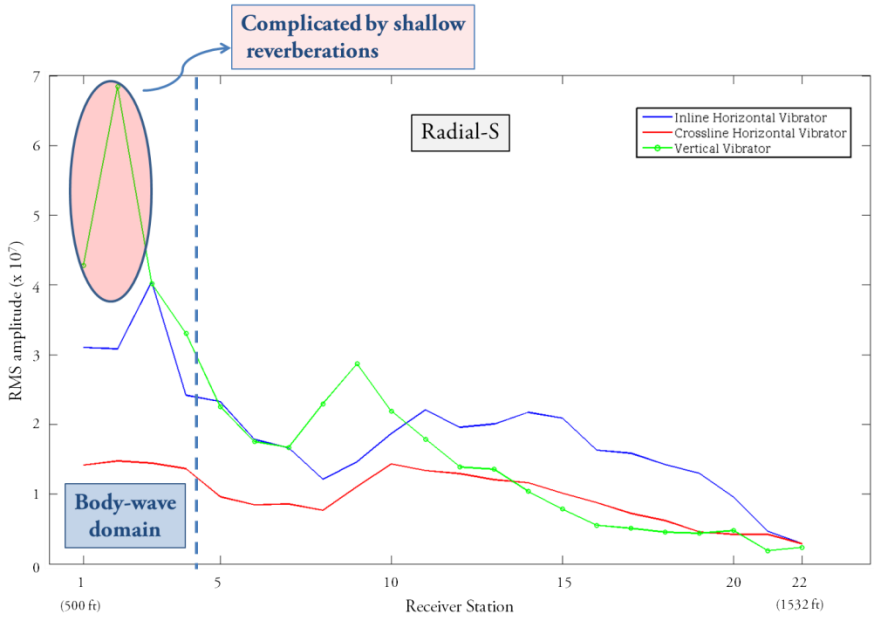

Figure 4.51: Comparison of the amplitude strengths of radial-S direct modes generated by a vertical vibrator and a horizontal vibrator applied in inline and crossline directions.

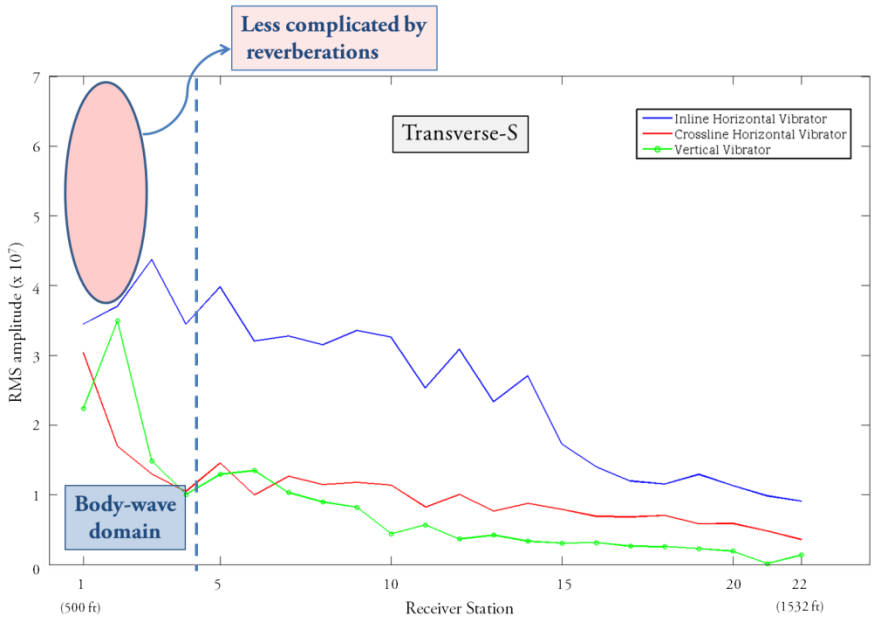

Figure 4.52: Comparison of the amplitude strengths of transverse-S direct modes generated by a vertical vibrator and a horizontal vibrator applied in inline and crossline directions.

Figures 4.51 and 4.52 show that P-wave energy radiated by a vertical vibrator causes complicated amplitude variations in radial-S data due to reverberations between shallow interfaces (Fig. 4.51). On the other hand, these amplitude variations are less complicated for transverse-S mode (Fig.4.52). In calculating the energy of first arrivals at downhole receiver stations, raypaths from source to receivers were assumed to be straight lines. Thus the raypath lengths were the same for all seismic sources tested (Figure 1.12). Energy variations caused by differences in the directivity of S-waves (Figure 4.52) were not considered.

Quantifications of the similarities and differences in frequency content of direct-S modes produced by vertical-force and horizontal-force vibrators are displayed on Figures 4.53 through 4.55. During the frequency analyses of vibrators sources, the same principles applied to impact-force sources were followed. However, for vibrator data, amplitudes that are more than 5 dB below the peak of an amplitude spectrum are considered to be too small to make a significant contribution and are ignored to obtain a reasonable indication of the signal-frequency content for each downgoing illumination wavefield.

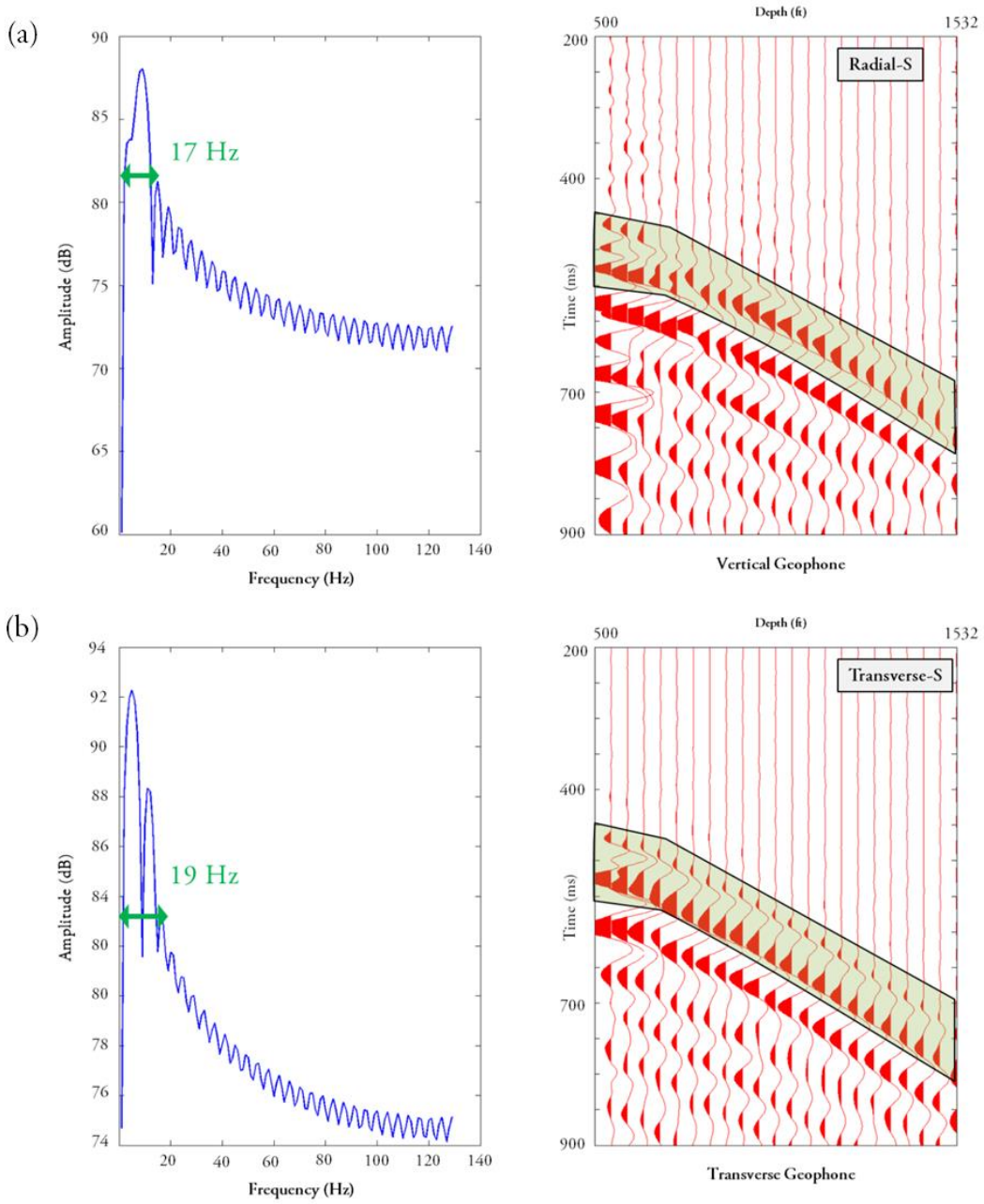

Figure 4.53: Frequency analysis of radial-S (a) and transverse-S (b) modes produced by a horizontal vibrator applied in the inline direction. Amplitudes of the frequency spectra define relative strengths of the radial and transverse direct-S mode propagating away from source station 5.

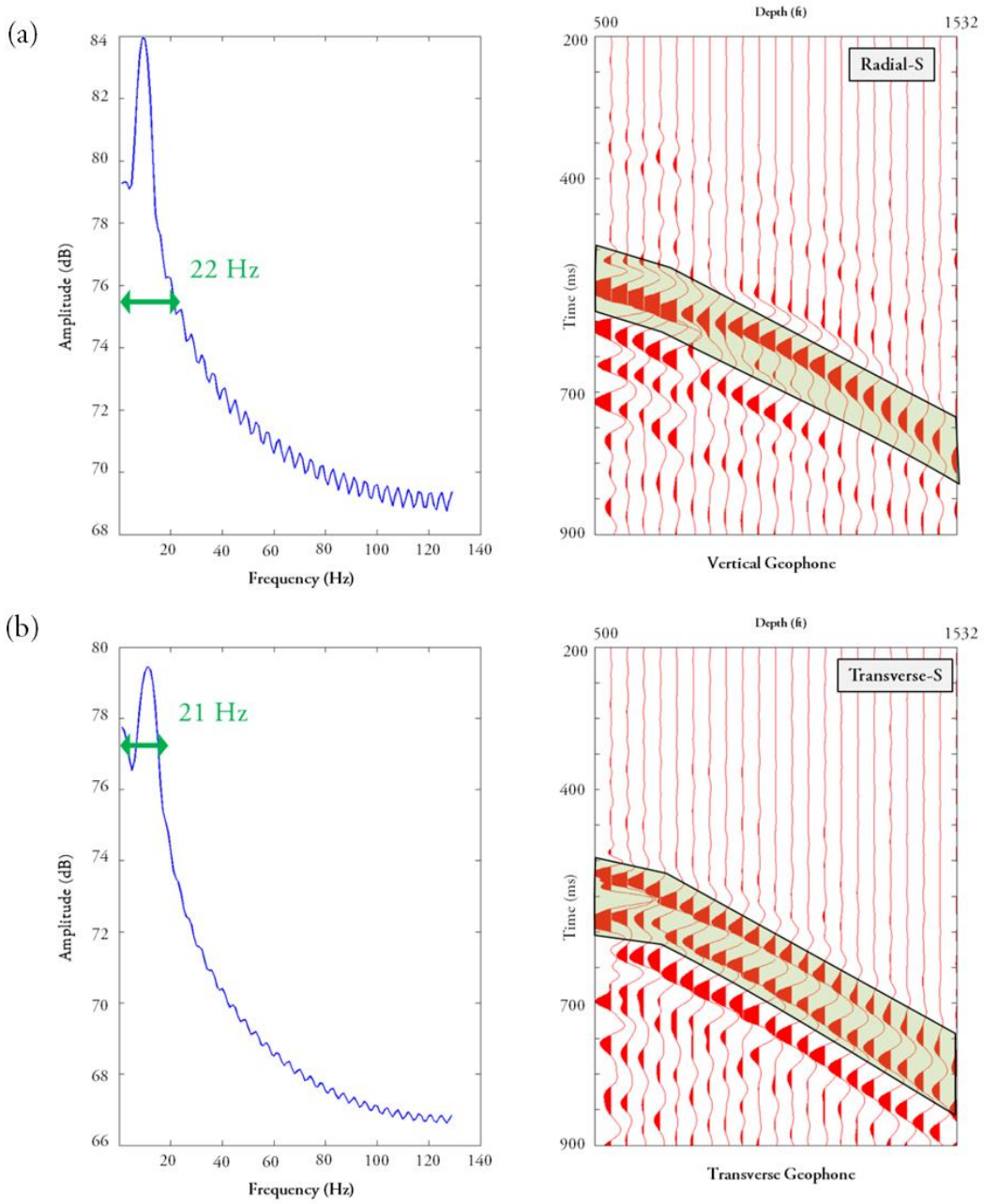

Figure 4.54: Frequency analysis of radial-S (a) and transverse-S (b) modes produced by a horizontal vibrator applied in the crossline direction. Amplitudes of the frequency spectra define relative strengths of the radial and transverse direct-S mode propagating away from source station 5.

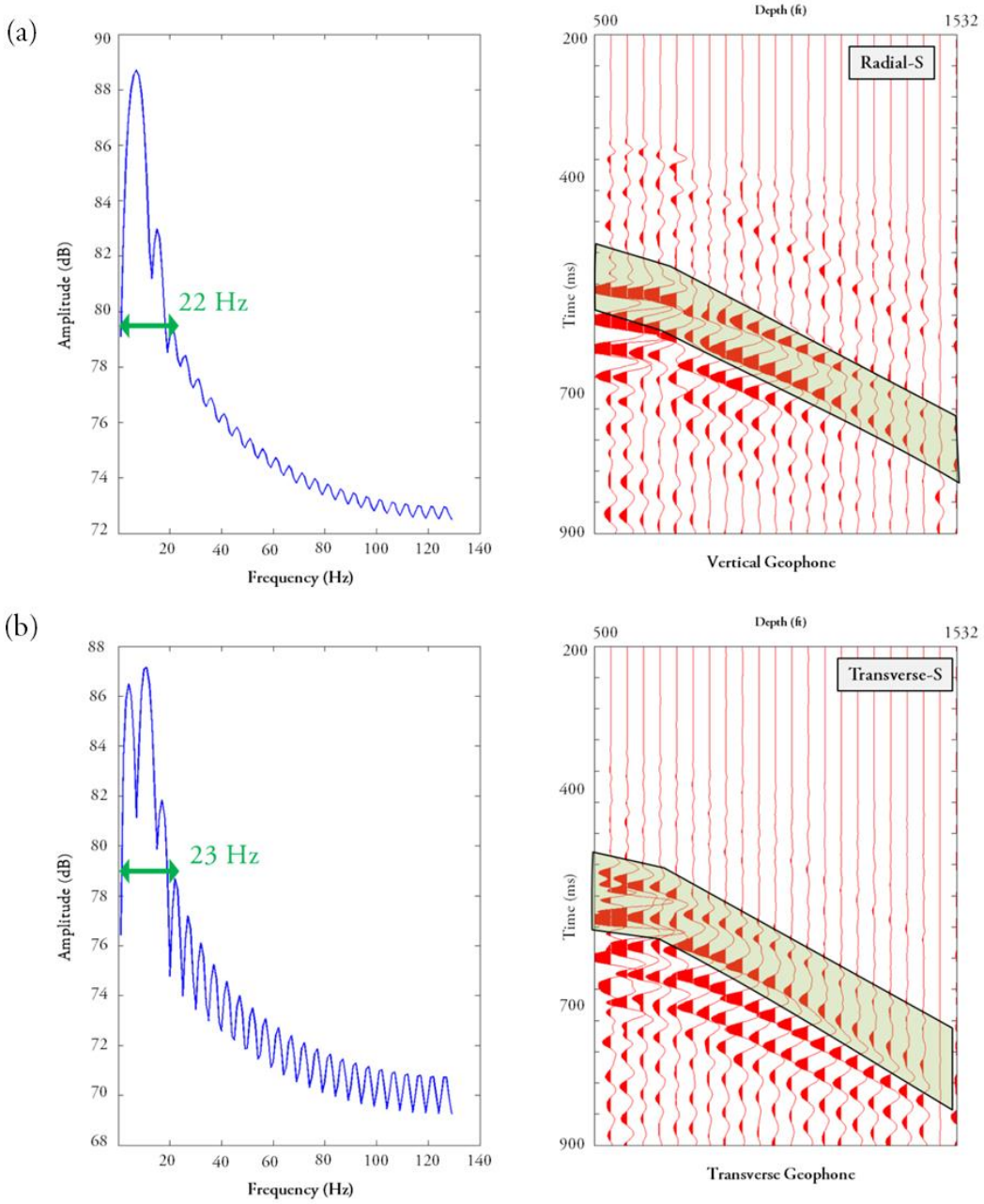

Figure 4.55: Frequency analysis of radial-S (a) and transverse-S (b) modes produced by a vertical-vibrator source. Amplitudes of the frequency spectra define relative strengths of the radial and transverse direct-S mode propagating away from source station 5.

Frequency and amplitude-level characteristics of direct-S modes produced by vibrator sources are summarized on Table-4.3.

Amplitude (RMS)	Horizontal Vibrator	Vertical Vibrator
Radial Shear	10^7	10^7
Transverse Shear	10^7	10^7
Frequency Contents (Hz)	Horizontal Vibrator	Vertical Vibrator
Radial Shear	17-22	22
Transverse Shear	19-21	23

Table 4.3: Amplitude and frequency attributes of direct-S wave modes produced by horizontal and vertical vibrator sources. Amplitudes and frequency bandwidths were calculated from Figures 4.53 - 4.55 for shot station 5.

Similar to previous analyses, calculated energy levels are tabulated as "order of magnitude" quantities instead of listing them as specific numerical values. Some key principles can be reached from these energy levels and frequency characteristics:

a. The signal frequency of SR and ST wave modes produced by a horizontal vibrator are almost the same signal frequency generated by a vertical vibrator.
b. Horizontal vibrators produce shear wave energy equivalent to shear wave energy produced by vertical vibrator.
c. Vibrator sources produce shear wave energy having amplitudes 1000 times bigger than the amplitudes produced by impact sources (Table 4.2).

Chapter 5: Conclusions

The main goal of my thesis project was to analyze direct-S wave modes generated by different types of seismic sources and document the differences and similarities among these seismic sources. Data captured by a vertical sensor array at the Devine Test Site from various seismic sources have been analyzed in terms of their amplitude strengths and frequency contents. In the VSP data acquisition phase, the orientation of horizontal geophones is unknown because a borehole geophone rotates horizontally as it is lowered into the well, causing azimuthal inconsistency between geophones. To study body waves, multi-component VSP sensors were mathematically rotated to change them from the inconsistent orientation they had at the time of recording to user-defined, consistent-azimuth coordinate system. This geophone rotation allowed SH and SR wave modes to be identified.

Direct-S amplitude strengths were calculated by using a basic procedure of calculating RMS amplitudes in a 90-ms windows starting at the first-break times of each arriving direct-S mode. Analysis of rotated data shows that amplitudes of radial and transverse direct-S modes produced by a vertical impact source, a shot-hole explosive and an inclined-impact source differ only slightly. This outcome is confirmed by the receiver stations deployed in the deeper half of the vertical geophone array because true body waves are captured by these deeper receiver stations; whereas shallow receivers record body waves as well as refractions and reverberations from shallow interfaces. The signal frequency and energy strength of radial direct-S and transverse direct-S modes produced by horizontal-force shear wave sources are essentially the same as the frequency and energy strength of radial direct-S and transverse direct-S modes propagating from a vertical-impact source.

Although there are similarities between horizontal-force shear wave sources and vertical impact sources, an obvious spectral notch at approximately 20-Hz in transverse-S data when the source is a vertical-impact should be taken into account before deciding which seismic source should be used. Another point to be considered is that shear wave energy produced by a shot-hole explosive decays faster than S energy created by an inclined-impact or a vertical impact source and is less energetic for receivers deployed in the deeper region of the body-wave domain. Also, while reverberations from shallow interfaces cause complicated amplitude variations for radial-S mode data, these amplitude variations are less complicated for transverse-S mode data.

The analysis of VSP data produced by horizontal and vertical vibrators confirms that vertical and horizontal vibrator sources generate shear wave modes having amplitudes 1000 times stronger than the other energy sources we tested. As a conclusion, the work presented in this project demonstrated that it is possible to obtain direct-S data of the same quality by using only a vertical-impact source or a shot-hole explosive. The arguments given above confirm the idea that it is not necessary to use inclined-impact sources or horizontal vibrators to generate shear wave data. S-wave data of the same quality produced by a horizontal-force source are provided by simple vertical vibrators, vertical-impact sources, and shot-hole explosives.

References

Alkan, E., 2012. Exploring hydrocarbon-bearing shale formations with multi-component seismic technology and evaluating direct shear modes produced by vertical-force sources: PhD thesis in geological sciences, University of Texas, Austin.

Cholet, J. and Pauc, A., 1981. Device for generating seismic waves by striking a mass against a target member: *The Journal of the Acoustical Society of America*, 69. doi: 10.1121/1.385903.

Dankbaar, J.W.M., (1983). The wave-field generated by two vertical vibrators in phase and in counterphase: *Geophysical prospecting*, V.31, p.873-887.

Daures R. and Tariel, P., 1985. Applying three-component records in wave field separation. SEG technical program expanded abstracts 1985: p. 61-63. doi: 10.1190/1.1892790.

DiSiena, J. P., Gaiser, J.E., and Corrigan, D., 1981. Three-component vertical seismic profiles – orientation for shear wave analysis. Paper S5.4, SEG Expanded Abstracts, 51st Annual International Meeting of SEG, 1990-2011.

DiSiena, J. P., Gaiser, J.E., and Corrigan, D., 1984. Horizontal components and shear wave analysis of three-component VSP data. in Vertical Seismic Profiling, Part B: Advanced Concepts. Toksoz and Stewart (editors). Geophysical Press, p. 177-188.

Dobrin M. B., 1976. Introduction to geophysical prospecting. 3d ed New York: McGraw-Hill.

Easley, D.T., 1992. Alternate description of wavefields generated by two vertical vibrators in counterphase: CREWES Res. Rep., 4, 2, 1-10.

Edelmann, H.A.K. (1981). Shover shear-wave generation by vibration orthogonal to the polarization. Geophy. Prospect., 29, 541-549.

Evans, B., 1997. A handbook for seismic data acquisition in exploration. Tulsa, OK: Society of Exploration Geophysicists, Geophysical monograph series, number 7.

Fertig, J., 1984. Shear waves by an explosive point-source- the Earth surface as a generator of converted P-S waves. *Geophysical prospecting*, V.32, p.1-17.

Fertig, J., and Krajewski, P., 1989. Acquisition and processing of pure and converted shear waves generated by compressional wave sources: *Surveys in Geophysics*, V.10, p.103-132.

Gaiser, J.E., 1999. Applications for vector coordinate systems of 3-D converted-wave data: *The Leading Edge*, 18(11), 1290–1300. doi: 10.1190/1.1438202.

Hardage, B. A., 2000, Vertical seismic profiling: principles: third updated and revised edition: New York, Pergamon, Seismic Exploration, v. 14, 552 p.

Hardage, B. A., DeAngelo, M. V., Murray, P. E., and Sava, D., 2011. Multicomponent seismic technology: Tulsa, Society of Exploration Geophysicists, Geophysical References Series No. 18, 318 p.

Levin, F. K. (1979). Seismic velocities in transversely isotropic media: *Geophysics*, V.44, p.918-936.

Levin, F. K. (1980). Seismic velocities in transversely isotropic media II: *Geophysics*, V.45, p.3-17.

Lynn, H.B., and McCardle, M., 1990. Four 3-component VSPs from South Texas onshore – S-wave velocities for AVO and discussion of acquisition parameters. SEG Technical Program Expanded Abstracts 1990: p.52-55. doi: 10.1190/1.1890254.

Maercklin N., 2010. Three- Component processing and Analyzing Tools for Seismic Data in SAC format. Unpublished manual. http://unina.academia.edu/NilsMaercklin/Teaching-Documents. Viewed in Janurary 2014.

Miller, G. and Pursey H., 1954. The field and radiation impedance of mechanical vibrators on the free surface of a semi-infinite isotropic solid. *Proceedings of the Royal Society of London*, Series A, 223, no. 1155, 521–541.

Robertson, J.D. and Corrigan, D., 1983. Radiation patterns of a shear-wave vibrator in near-surface shale. *Geophysics*, V.48, p.19–26.

Sun, Z., and Jones, M. J., 1993. Seismic wavefields recorded at near-vertical incidence from a counterphase source: CREWES Res. Rep., 4, 2, 1-10.

Tatham R.T. and McCormack M.D., 1991. Multicomponent seismology in petroleum exploration. Tulsa, OK: Society of Exploration Geophysicists. Edited by E. B. Neitzel and D. F. Winterstein, Tulsa, 248 p.

Telford, W.M., Geldart, L.P. and Sheriff, R.E., 1990. Applied Geophysics. 2nd Edition, Cambridge University Press, Cambridge. doi: 10.1017/CBO9781139167932.

White, J. E., 1983. Underground sound—applications of seismic waves. Amsterdam: Elsevier Science Publishers.

Wright, J.K., and Carpenter, E.W., 1962. The generation of horizontally polarized shear waves by underground explosions. *Journal of Geophysical Research*. V.67, no. 5, p. 1957-1963. doi:10.1029/JZ067i005p01957.

Yang, L., Zhang, Q., Bao, L., and Wei, X., 2007. Pure S-waves in land P-wave source VSP data. *Applied Geophysics*. V.4, no.3, p.173-182.

Zhou, R., Zhao, X., and Dushman, D. (2005). Shear-wave anisotropy from far-offset VSP. SEG Technical Program Expanded Abstracts 2005: p.971-974. doi: 10.1190/1.2148323.

Vita

Nurtac Erturk received a degree of Bachelor of Science from the Engineering Department at the Dokuz Eylul University in Izmir in 2008. After completing his mandatory military service and working in industry for several months, he was awarded a scholarship by the Turkish Petroleum Corporation. When Erturk completes his Master's degree at the University of Texas at Austin, he will return to Turkey and work for the Turkish Petroleum Corporation.

Permanent address: nurtacerturk@utexas.edu

This thesis was typed by Nurtac Erturk.